THE THEORY OF STATISTICS OF EXTREMES AND EL NIÑO PHENOMENA - A STOCHASTIC APPROACH

by

Rui Vasques de Melo Ponte

B.S., University of Rhode Island
(1982)

Submitted to the Department of Earth,
Atmospheric and Planetary Sciences
in Partial Fulfillment of the
Requirements for the Degree

MASTER OF SCIENCE

at the

MASSACHUSETTS INSTITUTE OF TECHNOLOGY

August 1985

Signature of Author: _____

Certified by: _____
Thesis Supervisor

Accepted by: _____
Chairman, Department of Earth, Atmospheric and Planetary Sciences

THE THEORY OF STATISTICS OF EXTREMES AND EL NINO PHENOMENA - A STOCHASTIC APPROACH

by

Rui Vasques de Melo Ponte

Submitted to the Department of Earth, Atmospheric and Planetary Sciences on August 5, 1985 in partial fulfillment of the requirements for the degree of Master of Science

ABSTRACT

The possibility of El Niño being a result of the random superposition of stochastically forced equatorial Kelvin waves is investigated, with the help of the theory of statistics of extremes, which provides us with the tools to evaluate the threshold crossing statistics of the sea level (SL) and sea surface temperature (SST) anomaly fields. A comprehensive review of this theory is given, since it might be relevant to other oceanographic problems. A linear, stratified, equatorial β-plane Kelvin wave ocean model is forced by stochastic zonal winds. The zonal velocity field is used to advect mean zonal temperature gradients to produce SST anomalies. Solutions are obtained in terms of the zonal wavenumber-frequency spectra of SL and SST. These spectra are used to compute the threshold crossing statistics of the respective fields. The time and space scales for the SL and SST excursions above 2 standard deviations are found to be small, when compared with observed El Nino scales. The stochastic assumption is reinterpreted as a possible triggering mechanism, rather than as a full explanation, for El Nino occurrences. Better knowledge of the wind stress forcing spectrum (zonal wavenumber and frequency) is needed in order to test the plausibility of the stochastic argument in a more conclusive way.

Thesis Supervisor: Dr. Carl Wunsch

Title: Professor of Physical Oceanography

Acknowledgments

I would like to express my sincere gratitude to my advisor, Professor Carl Wunsch, for suggesting this problem and for providing the resources and critical guidance without which this thesis could not have been completed.

The computer assistance of Charmaine King during various stages of this work is also deeply appreciated. Also a word of thanks to Eli, for helping me change my mind about computers. We can't live without them, so we might as well like them. He was always there with his easy to use written computer menus whenever I needed to be rescued from trouble.

This research was partly supported by the NSF grant OCE-8018514.

I would like to thank Dorothy Frank for her patience and skill in typing this thesis.

Table of Contents

CHAPTER 1

INTRODUCTION

Nature confronts us, almost daily, with occurrences of extreme phenomena of some sort. Whether it is a diluvial rainfall, a sharp rise in the price of gold on the international market or a strong earthquake, these extreme events are seen as drastic departures from the usual pattern of variation of these variables. They can be treated with the use of deterministic or probabilistic models, depending on the degree of disorder underlying those fields or, in other words, depending on how much we think we know about them.

The ocean also exhibits extreme variations in some of the fields which characterize its physical state. The most prominent extreme phenomenon which has been observed in the ocean is undoubtedly what is known as El Niño in the oceanographic literature. As a simple definition, El Niño events are associated with extreme sea surface temperature (SST) and sea level (SL) conditions in the equatorial Pacific. Positive anomalies are found in the eastern Pacific, while negative anomalies are generally confined to the western Pacific Ocean. Anomalous atmospheric conditions are also present in the tropical Pacific, during El Niño. The Southern Oscillation Index (SOI), being defined as the difference in surface pressure at Darwin, Australia and Easter Island, hits its highest values. In fact, the initials ENSO, standing for El Niño/Southern Oscillation, are commonly used to identify the highly correlated nature of the atmospheric and oceanic events. The usual trade wind system exhibits strong anomalies (first easterly and then westerly) and the Intertropical Convergence Zone (ITCZ) moves southward, carrying along the band of heavy precipitation normally centered north of 5°N. The whole tropical atmosphere-ocean system

changes dramatically in the region, during El Niño events, and there has been enough evidence to say that the phenomena is really a coupled ocean-atmosphere process.

As often occurs with natural extreme phenomena, El Niño has a lot of social and economical implications, especially in countries like Peru and Ecuador. When the usually cold waters off their South American coasts are replaced by anomalously warm waters, the resulting migration of fish away from the area, delivers devastating blows to the important fishery industries of those countries. In a more indirect and subtle way, there have been attempts to link the interannual atmospheric and oceanic variability associated with El Niño, with severe droughts or floodings in different regions of the globe, occurring in El Niño years. Major influences of these tropical events on the global earth climate are certainly a possibility.

In addition to its social, economical and ecological importance, for the meteorologist or the oceanographer, El Niño is the only large scale interannual phenomena which couples the ocean-atmosphere system in a dramatic, observable way. It is, therefore, not surprising, that El Niño events have been the object of numerous studies and publications, constituting one of the most active research areas in the field of oceanography.

Extensive descriptive literature exists on almost every aspect of El Niño. Wyrtki (1977, 1979, 1984) documents the changes in SL in the tropical Pacific for the latest El Niño events of 1972, 1976 and 1982/83. The patterns of SST anomalies and wind stress changes in El Niño years are analyzed in Rasmusson and Carpenter (1982). The latest ENSO event occurring in 82/83 was the strongest to be recorded in this century and, by

far, one of the best observed. A collection of papers on the 82/83 ENSO can be found in Witte (1983). A comparison between the 82/83 event and previous events is given by Cane (1983), for the oceanographic component, while Rasmusson and Wallace (1983) provide the atmospheric comparison. The global changes in the atmospheric patterns of circulation is well presented in Horel and Wallace (1981).

An intensive theoretical modeling effort has taken place in the last few years, in an attempt to better understand the mechanisms causing the onset of ENSO events. Several paths have been taken, but no fully satisfactory picture has emerged. However, several aspects of the extreme phenomena have been successfully modeled.

Wyrtki (1975) mentioned, for the first time, the importance of equatorial oceanic Kelvin waves in carrying the sea level signal from the western to the eastern Pacific. Relatively simple reduced gravity models, using realistic winds over the equator, have been able to simulate the sea level signature of El Niño events (see, for example, Busalacchi and O'Brien 1980, O'Brien et al. 1981). The importance of remotely forced equatorial Kelvin and Rossby waves in explaining SL anomalies in the equatorial Pacific is well established.

The other important signal associated with El Niño is SST anomaly. The inclusion of thermodynamics, as well as dynamics, in theoretical models, permits a better understanding of the SST anomaly patterns occurring during ENSO events. For example, advective effects associated with the passage of wave fronts are seen to be important (Schopf and Harrison 1983) and may explain the difference observed in SST anomaly patterns between the 82/83 event and the previous ones (Harrison and Schopf 1984). Changes in wind patterns over the tropical Pacific are believed to

be connected with anomalies in SST and have been simulated quite successfully, by forcing a simple atmosphere model with anomalous heating at the sea surface (Gill 1980, Zebiak 1982).

Some of the more sophisticated modeling attempts have been aimed at describing the air-sea interaction processes which probably control the evolution and decay of ENSO events. Rather than prescribing some conditions in one medium and looking for the reaction to this forcing in the other medium, ocean-atmosphere coupled models let the full system evolve on its own, after some initial state and mean conditions have been given (see, for example, Zebiak 1984).

All of the models developed until now, are able to capture some of the dynamics and thermodynamics involved in El Niño events. However, no complete picture has been provided. There are still a lot of unanswered questions about what makes El Niño occur. Sounding a bit like the "chicken and egg" problem, SST anomalies are invoked as causes for the wind anomalies, which in turn are held responsible for excitation of equatorial waves, anomalous currents and, consequently, production of SST anomalies through anomalous advection. What process comes first, is still unclear. Why the aperiodicity of El Niño events? Although we usually talk about a rough 3-4 year period for recurrence of extreme conditions in the tropical Pacific region, periods as long as 10 years and as short as 2 years have been observed. Despite enough similarity between events, permitting Rasmusson and Carpenter (1982) to talk about the composite El Niño, either the amplitude (defined by the size of SST and SL anomalies) or the timing of the events exhibit strong differences over the years. The best example of an extremely strong event was the 82/83 El Niño, which also started at the "wrong" time (see Cane 1983). Even aborted events, like the one in

1975, have been spotted (Busalacchi et al. 1983).

The quest for the ability to predict the occurrence of El Niño has been a driving force behind the theoretical modeling effort going on during the last decade. Despite the variability and aperiodicity of events, predictability, in its deterministic sense, is still one of the goals El Niño modelers would like to achieve. Forecasting schemes using different advanced statistical ideas, have been tried with some success, using the zonal winds over the western and central Pacific as predictors and SST (as in Barnett (1983)) or SL (as in Inoue and O'Brien (1983)) as predictands. However, this ability to forecast anomalous conditions off the South American coast 3 to 4 months ahead, does not imply more than the notion that one are present over some region of the Pacific, a favorable anomalous wind conditions signal is generated and propagates in the form of a Kelvin wave towards the east. What triggers the anomalous winds remains unknown, and hence, does not enter the forecast. The winds are still the best predictor to be used in forecasting schemes of the kind mentioned above.

If one could pinpoint the ultimate cause which sets off the ENSO events, real predictability, in a deterministic sense, would have been gained. Unfortunately, the complexity of dynamical and thermodynamical processes has proven to be an unsurpassable barrier and there is probably no simple cause, but rather some sort of complicated feedback or instability mechanism, behind the occurrence of ENSO events.

Given this much uncertainty, in the search for the ultimate mechanism behind the ENSO cycle, as some like to call it, and even though some of the odd characteristics of the equatorial phenomena like the aperiodicity can be accounted by relatively simple coupled atmosphere-ocean models (see Cane

and Zebiak 1985), we thought there was enough room to investigate the extent to which purely stochastic processes could be a factor in describing such important events. The specter of unpredictability should not prevent us from exploring this possibility. The appeal of this stochastic approach is basically two-fold: the responsibility for the start of an event is delegated to the random components of the forcing; and the variability and aperiodicity of events stem from the randomness, inherent to the process.

Atmospheric stochastic forcing, at short space and time scales, has been used to produce a predominantly red response (low frequency and wavenumber) in the ocean, which acts as an integrator of the random atmospheric forcing. Frankignoul and Hasselman (1977) produced some realistic, red SST spectrum from white noise atmospheric forcing. Frankignoul and Müller (1979) use the same concept to suggest that stochastic wind forcing could explain some of the eddy variability, in regions away from boundaries or strong currents, despite the discrepancy between the dominant time-space scales of the atmospheric and oceanic disturbances. For similar reasons, the long scales associated with El Niño signals do not necessarily require atmospheric forcing at those scales.

Bringing the random forcing element into the El Niño scenario eliminates the need for a deterministic cause for the onset of such events. There are obvious aspects of the phenomena which are best treated in a deterministic way. The massive collapse of the Trades over the region west of the dateline, for example, is certainly caused by SST anomalies which develop in that area, after the onset phase. Still, these SST anomalies could be the result of stochastically forced Kelvin waves and the consequent advection of warm waters from the west.

If the random hypothesis is a plausible mechanism of generation of ENSO events, it should produce the anomalous oceanic conditions with a frequency resembling observed records, in the mean sense. Obviously, the stochastic assumption only allows us to talk about El Niño occurrences in a probabilistic way (i.e., involving some averaging operation).

Considering equatorial Kelvin waves as an important part of the ocean's response to the wind, and in light of the stochastic forcing assumption, we may imagine the random winds constantly exciting Kelvin waves in the ocean. Then, the occurrence of an El Niño event could be interpreted as a result of the superposition of randomly forced Kelvin waves, in such a way as to produce a big Kelvin wave which is normally associated with El Niño signals. Once in a while, the timing and strength of the random wind events over the tropical Pacific could be such as to generate extreme responses in the ocean by the superposition of the individually excited waves (implied in this idea is the notion that there is no need for a single strong wind event in order to generate an El Niño). Could the stochastic winds force the ocean in a way as to produce the extreme sea level signals observed during El Niño? Could the strong anomalies in the equatorial SST field be the ocean response to those winds? Could the duration and spatial extent of these extreme ocean signals be accounted for solely by the stochastic superposition argument? In essence, the motivation behind this study lies in trying to answer these questions.

In the process of trying to investigate the plausibility of our stochastic forcing hypothesis of El Niño, we were led to learn about the theory of statistics of extremes, in the context of random field theory, described in the classical work of Rice (1945), the more recent work of Vanmarcke (1983) and many others. The theory essentially relates the

spectral density function of a given process and its probability density function, to the statistics of threshold crossings above high levels. A brief review and discussion of this theory is presented in Chapters 2 and 3. Chapter 2 treats the case of 1-D process, while Chapter 3 extends the same theoretical concepts to 2-D processes. Expressions for the mean time or length between two successive upcrossings of some threshold level by a given process, and for the mean time or length that the process will stay above this threshold are presented in Chapter 2, as well as an expression for the probability of having a threshold crossing during some period of time or over some distance (we are obviously considering either time or space processes here). Similar expressions are given in Chapter 3 for the case of 2-D processes, with threshold crossings here occurring over some area of parameter space (usually time and space).

The possibilities for the useful application of this theory of statistics of extremes to the field of oceanography are not restricted to the particular case of this study. The transport of sediment in the ocean constitutes an example of a process which is critically dependent on the threshold statistics of the flow field. If the velocity over the ocean bed does not exceed a certain threshold value, no transport of sediment along the bottom takes place (Shepard 1963). Therefore, knowledge of the threshold crossing statistics of the velocity field near the ocean bottom could be useful in studying sediment transport. The statistical analysis of sea surface waves is another example of a field in which extreme value theory could be applied. In this work, the theory is applied to studying the temporal and spatial scales of SL and SST extremes directly associated with El Niño events.

Chapter 4 is devoted to developing an analytical model of an idealized equatorial ocean. We consider the linear response of a continuously stratified equatorial β-plane ocean to zonal wind stress stochastic forcing. Only Kelvin waves are permitted in our model. The very simple dynamics yield a zonal wavenumber-frequency spectrum of SL. Using the anomalous Kelvin wave zonal velocities to advect existing mean zonal temperature gradients leads to the generation of SST anomalies. From the simple thermodynamics, we obtain an SST zonal wavenumber-frequency spectrum. The particular forms of these spectra are dependent on the choice of the forcing spectrum.

In Chapter 5, the analytical SL and SST zonal wavenumber-frequency spectra obtained before are used to compute the statistics of extremes associated with the respective fields, according to the theory of Chapters 2 and 3. We find that, for reasonable forms of the zonal wind stress spectrum, the zonal space and time scales of excursions above the 2 standard deviation threshold for SL and SST are somewhat smaller than the observed El Niño scales. The computed mean period between consecutive upcrossings of that threshold is shorter than the 3 to 4 year period for ENSO events, but the reliability of this result is weak due to its extreme sensitivity to some of our assumptions. A discussion of our results is given and the importance of some of our model assumptions and simplifications is examined. A reinterpretation of our results for the scales of SST anomalies leads to the possibility of the stochastically forced waves being a triggering mechanism for El Niño (rather than its full description). Feedback processes between the ocean and the atmosphere are invoked as a possible way to prolong and extend the anomalous oceanic

conditions resulting from the stochastic model. A brief summary and some conclusions from our study are left for the last chapter.

The material covered in this work is arranged in a way as to fit the interests of two potential different readers. For the oceanographer mainly interested in applying the theory of statistics of extremes to his research problem, Chapters 2 and 3 offer a concise and comprehensive review of that theory, as well as a list of references which may be needed for further details on the theory. For the reader primarily interested in the particular application of extreme value theory to the El Niño phenomena, he may want to skip the technical details of Chapters 2 and 3 and concentrate his attention on the remaining chapters, since a brief summary of the statistical expressions needed to follow that part of the study is included in Chapter 4.

CHAPTER 2

STATISTICS OF EXTREMES FOR 1-D RANDOM PROCESSES

It is always much easier to think about and rationalize results which are obtained in the context of one dimensional problems than to deal with the complexities of an N-dimensional problem. This is why we first shall pursue here the theory of statistics of extremes for only one dimensional stationary process. Higher dimensional analysis is left for Chapter 3.

The theory of statistics of extremes for 1-D processes has been worked out for some time, primarily by Rice (1944, 1945). We shall follow here Rice's work and also Vanmarcke (1983), which not only reviews Rice's papers, but also extends the statistical analysis to other parameters not discussed by Rice.

We hope that, by the end of this chapter, we will be able to answer questions such as the ones mentioned in the introductory section, which are the motivation behind this study.

2.1 RICE'S CLASSICAL FORMULA

Consider a stationary random process X(t), where the independent variable t can be taken as time for the purpose of this section. By stationary we mean that the autocorrelation function of the process X(t) only depends on $\tau_\ell = t - t'$.

We are interested in finding an expression for the mean rate of crossings of some threshold b by process X(t). Rice (1945), in his work on random noise in electrical circuits, came up with a classical formula for the rate of crossings of level b for some random field. We shall derive this important result from which most of the theory presented here naturally follows.

Consider the picture represented in Figure 1. We want to find the probability of having X(t) cross the level b in the interval $[t',t'+dt]$. The element dt is taken to be small enough so that we can make the slope s constant over this interval of time. The equation for the line in this infinitesimal domain is

$$x=s(t-t')+x_o \tag{2.1}$$

where

$$s = \frac{dX}{dt}(t=t'), \quad x_o = X(t') \tag{2.2}$$

Solving for the independent variable t and putting x=b gives

$$t = (b-x_o)/s+t' \tag{2.3}$$

In order to have X(t) crossing the threshold b with positive slope s in the interval considered, t has to be contained in the interval [t', t'+dt]. Hence, the following inequality has to hold

$$t' < (b-x_o)/s+t' < t'+dt$$

or simplifying it

$$b-s\cdot dt < x_o < b \tag{2.4}$$

This simply says that for positive slope s (i.e., only upcrossings considered), to have X(t) = b, the slope s has to be greater than $(b-x_o)/dt$. If s,x_o satisfy inequality (2.4), we have one b upcrossing. The probability of s,x_o satisfying this inequality is

$$\int_0^\infty dx' \int_{b-x'dt}^{b} f(x,x')dx \tag{2.5}$$

where f(x,x') is the joint probability density function (abbreviated as pdf hereafter) of the random variables X and its derivative X'.

For dt sufficiently small in (2.5), we may take

$$f(x,x') \simeq f(b,x')$$

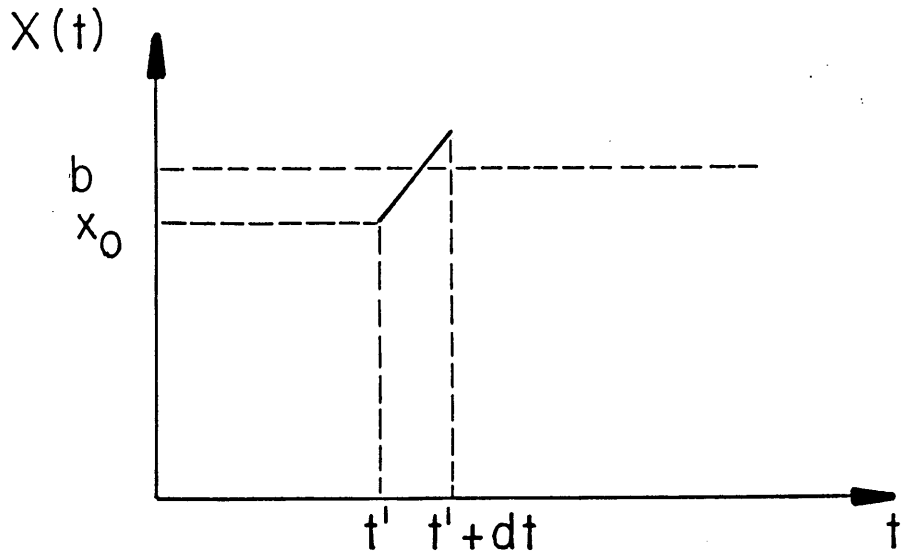

Figure 1. Crossing of threshold b by random process X(t). The element dt is small enough so that the slope of X(t) can be taken as a constant in the interval [t',t'+dt].

The probability integral over x is then straightforward and (2.5) reduces to

$$dt \int_0^{\infty} x' f(b,x') dx' \tag{2.6}$$

Similarly, we can do the same derivation for downcrossings (i.e., crossings with negative slope s). The probability of having a threshold crossing with negative slope is then

$$-dt \int_{-\infty}^{0} x' f(b,x') dx' \tag{2.7}$$

Adding the two results and dividing by dt yields

$$\nu_b = \int_{-\infty}^{\infty} |x'| f(b,x') dx' \tag{2.8}$$

This is Rice's classical formula. It gives us the probability that X(t) will cross the level b (either up or down) in one unit of time. ν_b is then the expected value of the rate of crossing of the threshold b by the random process X(t).

The mean rate of upcrossings or downcrossings given by expressions (2.6) and (2.7) respectively after dividing by dt, are easily shown to be equal (Cramer and Leadbetter 1967). We may simply realize that, even though on a finite region the number of upcrossings may differ by ±1 from the number of downcrossings, in the mean they should be equal. Then we may write

$$\nu_b^- = \nu_b^+ = \frac{\nu_b}{2} \tag{2.9}$$

where the superscripts + and - relate to up and downcrossings respectively.

The relations given in (2.8) and (2.9) imply that, by knowing the joint pdf of a random process X(t) and its derivative X'(t), we can define

what the threshold crossing statistics are. It is important to notice the dependence of the level crossing statistics on the derivative process X'(t), a result which we could expect intuitively. We might therefore anticipate that threshold crossing statistics of the process X'(t), intimately related to maximum value statistics (X'(t) = 0 at places where X(t) has a maximum or minimum), will depend on the statistics of the second derivative process X"(t). This will be seen more clearly in the following section, where we concern ourselves with the special case of a normally distributed process, for which the integral in (2.8) can be evaluated easily.

2.2 THRESHOLD CROSSING STATISTICS FOR THE CASE OF A GAUSSIAN DISTRIBUTED PROCESS

We now focus our discussion on the extreme value statistics of a normally distributed process X(t), whose pdf is given by

$$f(x) = (\sqrt{2\pi}\ \sigma)^{-1}\exp\{-x^2/2\sigma^2\} \tag{2.10}$$

where σ is the standard deviation. The mean of X(t) is taken to be zero here, without loss of generality.

Since X(t) is stationary, we can write

$$B(\tau_\ell) = B(-\tau_\ell) \tag{2.11}$$

where $B(\tau_\ell)$ is the autocorrelation function of the process. We rewrite (2.11) as

$$\int_0^\infty X(t)[X(t+\tau_\ell)-X(t-\tau_\ell)]dt = 0 \tag{2.12}$$

and divide it by $2\tau_\ell$, before letting $\tau_\ell \to 0$ to obtain

$$\int_0^\infty X(t)X'(t)dt = 0 \tag{2.13}$$

which just tells us that the correlation at zero lag of X(t) and X'(t) is zero. Since this correlation is a maximum for $\tau_\ell=0$, we deduce that X(t) and X'(t) are uncorrelated.† Normality then implies that X(t) and X'(t) are independent and (2.8) becomes

$$\nu_b = f_X(b) \int_{-\infty}^{\infty} |x'| f_{X'}(x')dx' = f_X(b)\langle|x'|\rangle \tag{2.14}$$

where $\langle|x'|\rangle$ is the expected value of the absolute value of the process X'(t) and $f_{X'}(x)$ is its pdf (I shall use subscripts in pdf's whenever it is not clear what process I am referring to).

For a general Gaussian field X(t), its derivative X'(t) is also normally distributed with mean zero, since differentiation is a linear operation. The integral in (2.14) is easily computed to give

$$\langle|x'|\rangle = \int_{-\infty}^{\infty} \frac{x'}{\sqrt{2\pi\sigma_{x'}}} \exp\{-\frac{x'^2}{2\sigma_{x'}^2}\}dx' = \sqrt{\frac{2}{\pi}}\,\sigma_{x'} \tag{2.15}$$

Substituting (2.15) and (2.10) in the expression for ν_b yields

$$\nu_b = \sigma_{x'}\,(\pi\sigma)^{-1} \exp\{-b^2/2\sigma^2\} \tag{2.16a}$$

or by (2.9)

$$\nu_b^- = \nu_b^+ = \sigma_{x'}\,(2\pi\sigma)^{-1}\exp\{-b^2/2\sigma^2\} \tag{2.16b}$$

where $\sigma_{x'}$ is the standard deviation for the process X'(t) (when no subscript is used, I am referring to the standard deviation of X(t)).

We now turn our attention to the question of finding the expected values for the times T_b and T_b' the process X(t) actually spends above and below a given threshold b, respectively (see Figure 2).

---

†This is not actually true for discrete processes because the derivative (i.e., its finite difference approximation) depends on two points. However, we may still take the continuous underlying processes X(t) and X'(t) to be uncorrelated.

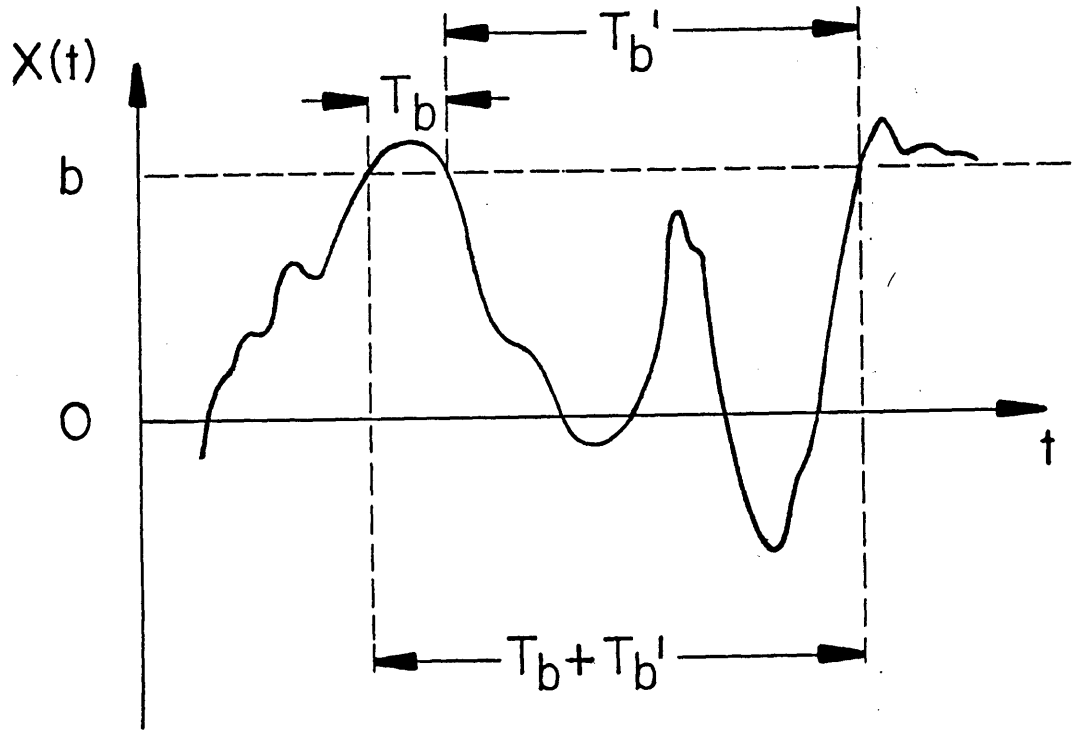

Figure 2. Time spent above and below a fixed threshold b by random process X(t).

The expected value for the time between two successive upcrossings of level b, is just the inverse of the mean rate of upcrossings of level b, (Vanmarcke 1969, 1975)

$$\langle T_b+T_b'\rangle = 1/\nu_b^+ \tag{2.17}$$

This is the quantity usually known as the return time, so relevant in extreme value problems (Gumbel 1958).

The fraction of time T_b spent above level b for each period T_b+T_b' is proportional to the cumulative distribution function (abbreviated as cdf hereafter)

$$\frac{\langle T_b\rangle}{\langle T_b+T_b'\rangle} = \int_b^\infty f(x)dx = F^c(b) \tag{2.18}$$

where F(x) is the cdf of X(t) and superscript c stands for complementary.

We now can solve for $\langle T_b\rangle$ and $\langle T_b'\rangle$, using the last two equations, to get

$$\langle T_b\rangle = \frac{2F^c(b)}{\langle|x'|\rangle f(b)} \tag{2.19}$$

and

$$\langle T_b'\rangle = \frac{2F(b)}{\langle|x'|\rangle f(b)} \tag{2.20}$$

The values for the standard (i.e., σ=1, mean m=0) normal cdf $F_U(u)$ are widely tabulated, permitting thus the evaluation of $F^c(x)$ and F(x) for any random variable x. For the case of large values of x (i.e., $x/\sigma >>1$), then we may use the approximation

$$F_U(u) = 1-(\sqrt{2\pi}\,u)^{-1}\exp\{-u^2/2\}g(u) \tag{2.21a}$$

where

$$g(u)\simeq 1 - \frac{1}{u^2} + \frac{3}{u^4} - \frac{1\cdot3\cdot5}{u^6} + \ldots\ldots \tag{2.21b}$$

With this approximation, (2.19) can be simplified (Vanmarcke 1983) to give an asymptotically exact expression for the mean excursion time

$$\langle T_b \rangle = (\sigma/\sqrt{2\pi}\ b\nu_o^+)g(b/\sigma) \tag{2.22}$$

where ν_o^+ is given by setting b equal to zero in (2.16b). The function g(u) is tabulated in Vanmarcke (1983).

Consider now the process X'(t) and its derivative X"(t), with respective variances $\sigma_{X'}^2$ and $\sigma_{X''}^2$, instead of X(t) and X'(t) as before. In this case, (2.16b) becomes

$$\nu_{b'}^+ = \nu_{b'}^- = \sigma_{X''}/(2\pi\sigma_{X'})^{-1}\exp\{-b'^2/2\sigma_{X'}^2\} \tag{2.23}$$

Here, b' is a threshold in the X'(t) vs. t plot. If we realize that for X'(t) = 0 and X"(t)<0, X(t) has a local maximum, then the zero crossings of process X'(t) with negative slope gain some significance. We have

$$\nu_m = \nu_o^- = \sigma_{X''}/(2\pi\sigma_{X'}) \tag{2.24}$$

where ν_m is the mean rate of occurrence of local maxima for process X(t).

The expressions so far obtained here are given in terms of the variances of X(t), X'(t) and X"(t). In fact, there is a correspondence between these variances and the different spectral moments of X(t). A derivation of these relations is given in Appendix A. Here, it suffices to accept the validity of the derived results, listed below

$$\begin{aligned} \lambda_o &= \sigma^2 \\ \lambda_2 &= \sigma_{X'}^2 \\ \lambda_4 &= \sigma_{X''}^2 \end{aligned} \tag{2.25}$$

where λ is the symbol used for the spectral moments, defined as

$$\lambda_j = \int_0^\infty \omega^j \Phi(\omega) d\omega \tag{2.26}$$

Here, $\Phi(\omega)$ is the one sided power density function.

It is useful to introduce, in relation to the spectral moments λ_j, two dimensionless spectral parameters. Vanmarcke (1983) defines a quantity δ in terms of the zeroth, first and second moments as follows

$$\delta = \left(1 - \frac{\lambda_1^2}{\lambda_0 \lambda_2}\right)^{1/2} \tag{2.27}$$

A clear interpretation of parameter δ is best achieved by defining a characteristic frequency Ω_j for each moment λ_j

$$\Omega_j = (\lambda_j/\lambda_0)^{1/j} \tag{2.28}$$

The spectral density function being analogous to a pdf, we can think of Ω_1 and Ω_2, for example, as being the mean and the root mean square frequencies, respectively. In terms of these characteristic frequencies, (2.27) becomes

$$\delta = \frac{(\Omega_2^2 - \Omega_1^2)^{1/2}}{\Omega_2} \tag{2.29}$$

The factor δ, being a ratio of the frequency standard deviation to the root mean square frequency, can now be viewed as a measure of dispersion or bandwidth of the spectral density function, and can only take on values between 0 and 1 ($0 < \lambda_1^2/\lambda_0\lambda_2 < 1$ by Schwartz's inequality).

Another measure of bandwidth involving the zeroth, second and fourth moments is defined as follows (Longuet-Higgins 1952)

$$\Gamma = \sqrt{(1-\lambda_2^2/\lambda_4\lambda_0)} = \sqrt{[1-(\Omega_2/\Omega_4)^4]} \tag{2.30}$$

This parameter is much more dependent on the high frequencies than parameter δ but may be interpreted in a similar way. The dependence on moment λ_4, which is analogous to the fourth moment of a pdf, makes the concept of kurtosis useful in the interpretation of Γ.

For an extremely narrow band process (the most extreme case would be if $\Phi(\omega)$ were a Dirac delta function), both parameters δ and Γ approach zero.

Now, using relations (2.25) in the expressions for the mean rate of crossings (2.16a,b) and mean rate of occurrence of local maxima (2.24), we obtain

$$\nu_b^- = \nu_b^+ = (2\pi)^{-1}\sqrt{(\lambda_2/\lambda_0)}\ \exp\{-b^2/2\lambda_0\} \tag{2.31}$$

and

$$\nu_m = (2\pi)^{-1}\sqrt{(\lambda_4/\lambda_2)} \tag{2.32}$$

respectively. We can in turn express ν_m in terms of the dimensionless parameter Γ. Solving (2.30) for λ_4, plugging it in (2.32) and using (2.31) gives

$$\nu_m = \nu_0^+/\sqrt{(1-\Gamma^2)} \tag{2.33}$$

For Γ approaching zero (for an extremely narrow band process), ν_m is nearly equal to ν_0^+, meaning that there is one local maximum for each zero crossing, as we intuitively expect from a narrow band process. This implies that all local maxima are positive. The complementary cdf of the local maxima M (defined as $M=X(t_m)$ where t_m is the time when $X'(t) = 0$ and $X''(t)<0$), is just the number of maxima occurring above b, $\nu_b^+ \cdot \Delta t$, over the total number of maxima, which in the special case of $\Gamma=0$, is just the number of zero crossings, $\nu_0^+ \cdot \Delta t$. Thus

$$F_M^c(b) = \nu_b^+/\nu_0^+ = \exp\{-b^2/2\sigma^2\} \tag{2.34}$$

for $\Gamma=0$ and $b \geq 0$.

The pdf of M is easily obtained by differentiating (2.34) above

$$f_M(b) = (b/\sigma^2)\exp\{-b^2/2\sigma^2\} \tag{2.35}$$

The local maxima are Rayleigh distributed for the extreme case of $\Gamma=0$. The more general expression for the pdf of local maxima of a stationary Gaussian process is given in Vanmarcke (1983).

The mean rate of occurrence of local maxima above a threshold b, $\nu_{b,m}$, is then just the rate of occurrence of local maxima multiplied by the

probability of having M > b, or

$$\nu_{b,m} = \nu_m F_M^c(b) \tag{2.36}$$

It is easy to prove (Vanmarcke 1983) that only for processes with $\Gamma > 0.98$, we can have more than one local maximum per crossing of high threshold b. Only for extremely wide band processes will the ratio $\nu_{b,m}$ over ν_b^+ (always bigger than or equal to one) significantly differ from one.

Having derived until now a number of statistically important parameters in the analysis of extreme values of a random process, we should keep in mind that these formulas were derived specifically for normally distributed one dimensional stationary processes. Furthermore, it is clear that the validity of these formulas holds, as long as the moments λ_j (or conversely the variances) are finite. In terms of the derivatives of the autocorrelation function (see Appendix A), we can generally say that expression (2.16a) is valid if the second derivative of the autocorrelation function is finite at $\tau_\ell=0$.

Finiteness of $\sigma_{X'}$ is equivalent to saying that the process X(t) is mean square differentiable. The necessary and sufficient condition for mean square differentiability is that the first derivative of the autocorrelation function evaluated at zero lag is zero (Vanmarcke 1983). An ideal white noise process (i.e., $\Phi(\omega)$=constant), to cite a well known example, is not mean square differentiable and its spectral moments are not finite. In some cases, the use of an upper frequency cutoff will be needed if we want to have finite moments λ_j.

The statistical expressions derived for local maxima of X(t), which depend on second order statistics (i.e., depend on the variance of X"(t)) are valid if also the fourth derivative of the autocorrelation function

evaluated at zero lag is well defined.

In computing quantities such as ν_b^+ and ν_m from a power spectrum, it is particularly important to notice the dependence of these parameters on both the low and the high frequency parts of the spectrum. Reasonable resolution on the two frequency regions is required, if we are to have reliable statistical information on the extreme values of the process under consideration. Most of the variance of X'(t) is contained in the high frequencies. The importance of the process X'(t) on the statistics of extremes, well expressed in Rice's formula, then renders extreme value statistics sensitive to high frequencies, as well as to low frequencies.

2.3 ENVELOPE STATISTICS AND THE PROBLEM OF CLUSTERING OF LEVEL CROSSINGS

The concept of an envelope R(t) of a random process X(t) is intimately related, in the field of extreme value statistics, to the problem of clustering of threshold crossings which can especially occur in narrow band processes.

When talking about group velocity and phase velocity in wave theory, the concept of envelope arises naturally in relation to the wave group velocity. The usual example illustrating what an envelope function is, considers a process composed of two sinusoids of nearly the same frequencies ω_o and ω_1. The addition of these two sine waves produces a rapidly oscillating sinusoid of frequency $\omega_o+\omega_1$, modulated by a slowly varying function, oscillating at frequency $\omega_o-\omega_1$ (Fig. 3). This modulation function, whose propagation characteristics closely describe the propagation of the wave energy (hence the relation to group velocity), may be thought of as the envelope R(t) of the more rapidly oscillating sinusoid. It is easily seen, by looking at fig. 3, that crossings of a level b by the underlying high frequency process will occur in clusters,

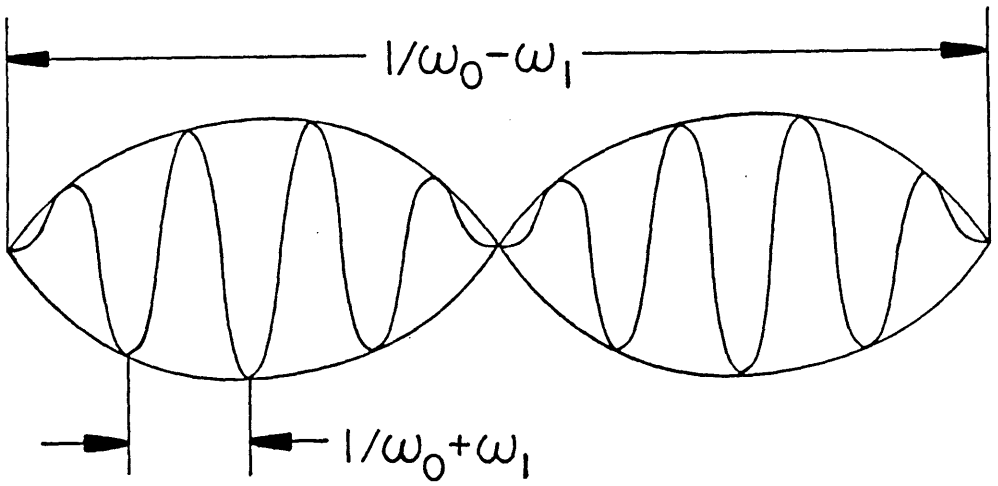

Figure 3. The result of adding two sine waves of nearly the same frequencies ω_0, ω_1. The amplitude of the resulting wave of period $(\omega_0+\omega_1)^{-1}$ is modulated by the envelope wave of period $(\omega_0-\omega_1)^{-1}$.

with an apparent period which is smaller than the expected value. This clustering effect is specially prominent in narrow band processes, such as the simple example used here. It is important to be aware of this effect and to try to somehow obtain a quantitative measure of it, in terms of a mathematical definition of the envelope function R(t).

The envelope R(t) of a process X(t) may be thought of as a slowly varying function satisfying $R(t) \geq |X(t)|$ at all times and $R(t) = |X(t)|$ near the maxima of X(t). The stationary process X(t) may be represented as

$$X(t) = \sum_{n=1}^{N} c_n \cos(\omega_n t + \phi_n) \tag{2.37}$$

where ϕ_n is a random phase angle. Rice (1944) assumed the existence of a representative mid-band frequency ω_m, writing X(t) as

$$X(t) = \sum_{n=1}^{N} c_n \cos(\omega_n t + \omega_m + \phi_n - \omega_m t) =$$

$$= I_c(t) \cos \omega_m t - I_s(t) \sin \omega_m t \tag{2.38}$$

where I_c and I_s are given by

$$I_c(t) = \sum_{n=1}^{N} c_n \cos\{(\omega_n - \omega_m)t + \phi_n\} \tag{2.39a}$$

and

$$I_s(t) = \sum_{n=1}^{N} c_n \sin\{(\omega_n - \omega_m)t + \phi_n\} \tag{2.39b}$$

He then proceeded to define the envelope of process X(t) by the expression

$$R(t) = \{I_c^2(t) + I_s^2(t)\}^{1/2} \tag{2.40}$$

Vanmarcke (1983) chooses ω_m to be zero in computing the one dimensional envelope statistics. The choice of $\omega_m = 0$ is very convenient for the analytical manipulation done in computing the statistics of R(t), even though these statistics do not depend on the specific choice of ω_m. With

$\omega_m = 0$, (2.39a,b) become

$$X_c(t) = I_c(t)(\omega_m=0) = \sum_{n=1}^{N} c_n \cos(\omega_n t+\phi_n) = X(t) \qquad (2.41a)$$

and

$$X_s(t) = I_s(t)(\omega_m=0) = \sum_{n=1}^{N} c_n \sin(\omega_n t+\phi_n) \qquad (2.41b)$$

The component $X_c(t)$ is identically equal to the process itself. The expression for the envelope is now

$$R(t) = \{X_c^2(t) + X_s^2(t)\}^{1/2} \qquad (2.42)$$

We are now interested in expressing the statistics of R(t) in terms of the statistics of X(t). The statistical properties of X_c are the same as those of X(t). Since X_c and X_s only differ by the random phase factor ϕ_n, we should expect their statistics to be the same. Having said this, the variance of R(t), σ_r^2, can easily be written in terms of σ, the variance of X(t), by taking the expectation on both sides of (2.42)

$$\sigma_r^2 = \langle R^2(t)\rangle = \langle X_c^2\rangle + \langle X_s^2\rangle = 2\sigma^2 \qquad (2.43)$$

The variance of R'(t) is also important in the context of extreme value statistics, as we have previously seen. Vanmarcke (1983) derives an expression for $\sigma_{r'}$ in terms of $\sigma_{x'}$ for the case of a Gaussian process X(t)

$$\sigma_{r'}^2 = \langle R'^2(t)\rangle = \delta^2 \sigma_{x'}^2 \qquad (2.44)$$

The parameter δ, described in the last section, becomes relevant when talking about envelope statistics. Relation (2.44) merely says that for narrow band processes (i.e., δ small), the slope of R(t) oscillates much less than the slope of X(t) (see, for example, fig. 3).

The envelope R(t) of a Gaussian process is Rayleigh distributed (see equation (2.35)) with mean square given by (2.43), i.e.,

$$f_R(r) = (r/\sigma^2) \exp\{-r^2/2\sigma^2\} \qquad (2.45)$$

Knowing $f_R(r)$ quickly leads to expressions for the mean rate of occurrence of crossings of level b by envelope R(t), $\nu_{b,R}$, and the mean time spent above it, $\langle T_{b,R}\rangle$. The derivative R'(t) is normally distributed with mean zero and variance given by (2.44). Expression (2.14) in terms of R(t) becomes

$$\nu_{b,R} = f_R(r)\langle R'(t)\rangle \tag{2.46}$$

The expected value $\langle R'(t)\rangle$ is given by (see equation (2.15))

$$\langle R'(t)\rangle = \sqrt{2/\pi}\ \sigma_{r'} = \sqrt{2/\pi}\ \ \delta\sigma_{x'} = \delta\langle|x'|\rangle \tag{2.47}$$

Using (2.16b), (2.45) and (2.47) in relation (2.46) yields

$$\nu_{b,R}^{+} = (b/\sigma)\sqrt{2\pi}\ \delta\nu_b^{+} \tag{2.48}$$

This is the expression for the mean rate of upcrossings of a level b by the envelope process R(t).

Expression for the mean time spent above b by R(t) may be found by computing $F_R^c(b)$ from (2.45) and use the result together with (2.47) in expression (2.19) to simply get

$$\langle T_{b,R}\rangle = F_R^c(b)/(\langle R'(t)\rangle f_R(b)) = \sigma/(\sqrt{2\pi}\ b\delta\nu_o^{+}) \tag{2.49}$$

For the case $b>>\sigma$, dividing (2.22) by (2.49), with $g(b/\sigma)=1$, we obtain

$$\frac{\langle T_b\rangle}{\langle T_{b,R}\rangle} \simeq \delta \qquad \text{for} \quad b>>\sigma \tag{2.50}$$

The ratio between the two mean periods at high thresholds approaches the value of the spectral parameter δ. It is very small in the case of narrow band processes and becomes close to one for wide band processes.

Turning to the clustering problem mentioned in the beginning of this section, we hope now to get an estimate of what Vanmarcke (1983) defines as the mean clump size, i.e., the mean number of crossings of X(t) for each crossing of R(t), at a given level b. Lyon (1961) defines the ratio

$$r_b = \frac{\nu_b^+}{\nu_{b,R}^+} = \frac{\sigma}{\sqrt{2\pi}\ \delta b} \tag{2.51}$$

to be a measure of the mean clump size. This is a good estimate when we are considering narrow band processes which tend to have the mean excursion time of the envelope much larger than the mean excursion time of the process itself. However, for significantly wide band processes we may actually have more R-crossings than X-crossings (wiggly wide band process may send the envelope jumping above threshold b without having an X-crossing within the next cycle). This fact led Vanmarcke (1969, 1975) to provide a better estimate of the expected value of the clump size N_b

$$\langle N_b \rangle \simeq (1-\exp\{-r_b^{-1}\})^{-1} \tag{2.52}$$

This expression is consistent with Lyon's estimate of clump size (2.51) for narrow band processes for which $\delta b/\sigma$ is fairly small. We may then expand the exponent in (2.52) as

$$\exp\{-1/r_b\} \simeq 1-1/r_b+ \ldots\ldots$$

to obtain (2.51). The two expressions differ, however, for the wide band case for which $\delta b/\sigma$ is fairly large.

The concept of clustering and the mathematical expressions given here are important in inferring whether regions of tightly packed crossings of some level b may be expected or not. It is helpful to keep in mind that the expected value for the rate of X-crossings above b may be deceiving, since these crossings may occur in fairly small regions, with much smaller "apparent" periods, especially if X(t) is narrow band.

2.4 LOCAL AVERAGING AND THE CASE OF NON-GAUSSIAN STATIONARY PROCESSES

The theory discussed in the preceding sections is well developed for the case of Gaussian random fields. Under the assumption of normality, Rice's formula (2.8) is very easy to evaluate analytically and the rest of the theory follows beautifully. However, unfortunately not all processes in nature are normally distributed. We have to deal with other distributions and we would still like to be able to say something about the extreme value statistics of such distributions.

Let X(t) now be a non-Gaussian stationary process. One might hope that the joint pdf of X(t) and X'(t) is fully defined either from theoretical or experimental considerations. Obtaining the mean rate of occurrence of threshold crossings is then just a matter of doing the integral in (2.8), numerically or analytically. We would not necessarily know anything about the statistics of local maxima since that implies information on the second order statistics of the process (i.e., information about X"(t)), which we don't have from only the joint pdf of X(t) and X'(t). Nevertheless, the mean time between two successive b upcrossings $\langle T_b+T_b' \rangle$ and the mean time spent above and below b, $\langle T_b \rangle$ and $\langle T_b' \rangle$, could still be easily computed.

Having complete knowledge of the joint pdf of X(t) and X'(t) is very seldom the case. Even in the case of theoretical derived distributions, quantities such as the mean and the standard deviation are most likely to be involved and they have to be roughly estimated, probably from the data available on the process.

If we either know or assume the form of $f_X(x)$ in some region, and X(t) and X'(t) are still independent random variables, we could try to determine empirically the constant of proportionality $\langle |x'| \rangle$, which comes up in the

linear relations (2.14) and (2.19), without having to know anything about the pdf of the derivative process. Deducing $\langle|x'|\rangle$ from a record by numerically computing derivatives is a very noisy procedure. On the other hand, we can use the linear relations (2.14) or (2.19) to estimate the proportionality constant $\langle|x'|\rangle$, provided we have enough information about ν_b or $\langle T_b\rangle$ and $f_x(b)$ in some region or regions. Once $\langle|x'|\rangle$ had been estimated, we could then assume a general, more arbitrary form for the pdf to compute values for ν_b or $\langle T_b\rangle$ at regions where information on ν_b or $\langle T_b\rangle$ is scarce or not at all available.

This question of empirical estimation gains more relevance when we are dealing with processes in higher dimensions, where the proportionality constants which arise, are more difficult to solve for, analytically, even in the case of a Gaussian process. We will get back to this question in Chapter 3 of this thesis.

In dealing with non-Gaussian processes and their extreme value statistics, the concept of local averaging emerges as an important one. A form of the central limit theorem, well known in statistical theory, establishes that the sum of N independent variables, tends to become normally distributed for N large (it becomes Gaussian in the limit $N \to \infty$). An immediate conclusion from this theorem is that local integration or averaging over some period of time T can force an originally non-Gaussian process closer to a Gaussian one. The requirement of independence between the averaged variables is not usually met by any real random field. However, it is well known that the central limit theorem only requires that the averaging involves many weakly correlated random effects (Vanmarcke 1983). The averaging window should be reasonably large compared with the typical correlation distance of the process under consideration, to assure

the validity of the central limit theorem.

If by doing a certain amount of local averaging on the non-Gaussian process X(t), we arrive at a Gaussian process $X_T(t)$, we may then plow ahead and use the theoretical expressions derived in the previous sections to obtain the extreme value statistics of $X_T(t)$. The disadvantage of local averaging a field is certainly the loss of information about the high frequency components of the original field.

In practice, any real field will lack resolution at high frequencies due to the usual sparse data the experimentalist is able to get. Hence, when modeling stochastic processes, sometimes it is convenient to introduce some local integration in the model. This will smooth out the unnecessary fine scale details present in the model and therefore allow for a better comparison between the model and the data. Vanmarcke (1983) gives expressions for $\nu_{b,T}^{+}$ and $\langle T_{b,T} \rangle$ (where subscript T refers to the process $X_T(t)$) in terms of the original process parameters, the averaging interval T, and the variance function $\gamma(T)$ and the scale of fluctuation θ defined as

$$\gamma(T) = \sigma_T^2/\sigma^2 \tag{2.53}$$

and

$$\theta = \lim_{T\to\infty} T\gamma(T) \tag{2.54}$$

where σ_T^2 is the variance of $X_T(t)$. I shall not go into the details of these expressions, which can be found in Chapter 5 of Vanmarcke's book. The local averaging concept is introduced here, primarily for the purpose of identifying one way of dealing with a non-Gaussian random field.

2.5 EXTREME VALUE DISTRIBUTIONS

A relevant question when trying to analyze a random field for its extreme value statistics is "what is the probability that the process will cross a level b in a certain period of time t_o?". Since extremes are usually connected to safety issues (extreme floods in safety dam construction, for example), this question is very important and it has certainly been part of the motivation for studying extreme value statistics.

In considering X(t) crossings above some threshold b, we may define a counting process N(t) as

$$N(t) = \sum_{k=0}^{t} Z(k) \qquad t = 0,1,2... \tag{2.55}$$

where Z(k) is a two-valued random variable, usually called a Bernoulli variable, defined by

$$Z(t) = \begin{cases} 0, & \text{if} \quad X(t) \leq b \\ 1, & \text{if} \quad X(t) > b \end{cases} \tag{2.56}$$

N(t) gives the number of crossings above b which have occurred during a time t. Elementary probability theory can be used to show that N(t) has the binomial distribution

$$P_N(n) = P[N(t)=n] = \frac{t!}{n!(t-n)!} p^n (1-p)^{t-n} \tag{2.57}$$

for n = 0,1,2,...,t and t = 0,1,..., where p = P[X(t)>b]. For the case of high thresholds ($b \to \infty$), p is very small ($p \ll 1$) and we can in this limit, say that p is equal to the mean number of crossings of X(t) per unit time, ν_b^+, since the excursions above b occur very rarely.

Since it is well known that the binomial distribution (2.57) converges toward the Poisson distribution, for t sufficiently large (see, for example, Feller 1957), we may assume that crossings of high threshold b are

independent events which obey the Poisson distribution, with mean rate ν_b^+,

$$p(N) = \exp -\{\nu_b^+ t\}\ (\nu_b^+ t)^N/N! \qquad (2.58)$$

then, the probability L_b that the first crossing of b will occur after time t_o is

$$L_b(t_o) = \text{Prob}\{\max_{t_o} X \leq b\} = \text{Prob}\{N(t_o) = 0\} = \exp-\{\nu_b^+ t_o\} \qquad (2.59)$$

from (2.58). This function is usually called the reliability function. Cramer (1966) showed that the Poisson assumption is asymptotically exact in the limit $b \to \infty$, for a stationary Gaussian process. The error resulting from making this assumption for finite b is negligible for narrow band processes and slightly on the unsafe side for wide band processes (Vanmarcke 1983).

The Poisson assumption leads to two unsatisfactory effects. The crossings are not really independent, especially in narrow band processes where they tend to occur in clusters, as we have seen. Also, it does not take into consideration the finite time X(t) spends above b once it crosses it.

To deal with these problems, Vanmarcke (1983) starts with an estimate

$$L_b(t_o) = L_b(0)\exp-\{a_b t_o\} \qquad t_o \geq 0 \qquad (2.60)$$

where $L_b(0)$ is the probability of having $X(t)<b$ at the starting time and a_b is the constant determining the rate of decay of that probability. For $b \to \infty$, we should have asymptotically

$$L_b(0) \to 1 \qquad (2.61a)$$

$$a_b \to \nu_b^+ \qquad (2.61b)$$

so that (2.60) becomes equal to (2.59).

Now, correcting for finite duration of excursions, we have

$$L_b(0) = F_x(b) \tag{2.62a}$$

$$a_b = 1/\langle T_b' \rangle = \nu_b^+/F_x(b) \tag{2.62b}$$

The probability $L_b(0)$ will decay in a time scale equal to the expected value for the time X(t) will spend below b.

The other correction applied by Vanmarcke for narrow band processes takes into account the clump size. The counting process is still a Poisson process, with reduced mean rate $\nu_b^+/\langle N_b \rangle$ ($\langle N_b \rangle/\nu_b^+$ is roughly equal to the mean time between clump occurrences). Therefore, we have

$$a_b = \nu_b^+/\langle N_b \rangle = \nu_b^+(1-\exp\{-1/r_b\}) \tag{2.63}$$

where we have used (2.52).

In his book, Vanmarcke puts the two corrections together to get finally

$$L_b(0) = F_x(b) \tag{2.64a}$$

$$a_b = \nu_b^+(1-\exp\{-1/r_b\})/F_x(b) \tag{2.64b}$$

The clustering effect does not affect $L_b(0)$, so that (2.62a) is valid, while in (2.62b), ν_b^+ is replaced by its reduced value in (2.63).

The probability that X(t) will stay below level b during time t_o, corrected for the clustering effect and taking into consideration the finite probability of that occurring for t_o=0, is

$$L_b(t_o) = F_x(b) \exp - \{\frac{\nu_b^+(1-\exp -\{1/r_b\})}{F_x(b)} t_o\} \tag{2.65}$$

As $b \to \infty$, (2.65) is in fact seen to equal (2.59).

A different approach in arriving at largest values distributions can be taken. Let's suppose we have a set A of N independent and identically distributed variables $A = \{X_1, \ldots\ldots, X_N\}$. We define the variable S to be the maximum value of the above set. The probability of $S \leq s$ is

$$\text{Prob}\{S \leq s\} = F_A(s, s, \ldots, s)$$

or

$$\text{Prob}\{S \leq s\} = F_S(s) = \{F_X(x)\}^N \tag{2.66}$$

Gumbel (1958), among others, has shown that for most (but not all) cdf's $F_X(x)$, and in the limit $N \to \infty$, the cdf $F_S(s)$ falls into one of the three following categories

$$\text{(I)}\quad F_S(s) = \exp\{-\exp(-s)\} \qquad -\infty < s < \infty$$

$$\text{(II)}\quad F_S(s) = \begin{cases} \exp\{-s^{-j}\} & s \geq 0,\ j \geq 0 \\ 0 & s < 0 \end{cases} \tag{2.67}$$

$$\text{(III)}\quad F_S(s) = \begin{cases} 1 & s \geq 0 \\ \exp\{-(-s)^j\} & s < 0,\ j > 0 \end{cases}$$

where j is a parameter defined for the initial distribution $F_X(x)$.

These are the three classical asymptotic Gumbel distributions. The last one is a distribution of minimum values. The normal, exponential and Gamma distributions all fall in the Type I Gumbel distribution. A look at expression (2.65) will reveal that, for a Gaussian process, the extreme value distribution derived using random field theory is consistent with the classical asymptotic theory of Gumbel and falls in the Type I Gumbel distribution in (2.67).

CHAPTER 3

STATISTICS OF EXTREMES FOR 2-D RANDOM PROCESSES

The statistical theory for the extreme values of a one-dimensional process is easily extended to higher dimensional random processes. The ability to deal with higher dimensions lends this statistical theory of extremes a greater practical relevance, when trying to cope with random fields occurring in nature. The importance of the occurrence of extremes in the time domain is sometimes tied to the spatial extent over which these extremes occur. It is in these situations, when both the spatial and time components of excursions above some threshold are important, that higher dimensional theory of statistics of extremes becomes useful to the analyst.

The classical extreme value theory dealt almost exclusively with 1-D random processes. We shall continue here to follow Vanmarcke (1983), where the theory is expanded to encompass higher dimensional analysis. The presentation given in this chapter will be more sketchy than the one in Chapter 2, mainly because the same ideas and arguments invoked before are again used here. Treatment of the 2-D case is given in detail. The more general N-dimensional statistical relations can be found in Vanmarcke's book.

3.1 THRESHOLD CROSSING STATISTICS FOR THE CASE OF A 2-D GAUSSIAN DISTRIBUTED PROCESS

Most of the concepts and parameter definitions used in Chapter 2, for dealing with 1-D processes, can be easily extended to higher dimensions. We start this section by doing this, since we will need these definitions later.

We shall consider here a 2-D homogeneous process Y(x,t), where x and t can be thought as a space and time coordinate, respectively, without loss of generality. These will actually be the physical coordinates, when we try to apply this theory to El Niño phenomena, later on this study. Homogeneity here is simply the extension of the concept of stationarity to higher dimensions. It means that the covariance function of Y(x,t) will only depend on the lag vector $\vec{\tau}_L$, i.e., on the differences t-t', x-x' for the 2-D case.

The spectral moments of this process Y(x,t) can be defined, in their most general form, as in Vanmarcke (1983)

$$\lambda_{jn} = \int_{-\infty}^{\infty}\int_{-\infty}^{\infty} \omega^j k^n \psi(\omega,k)\,d\omega\,dk \qquad \begin{matrix} j=0,1,2\ldots \\ n=0,1,2\ldots \\ j+n \text{ even} \end{matrix} \qquad (3.1)$$

where $\psi(\omega,k)$ is the two-sided spectral density of Y(x,t). The moments λ_{jn} are referred to as being order j with respect to the frequency ω and order n with respect to the wavenumber k. Homogeneity of Y(x,t) implies

$$\psi(\omega,k) = \psi(-\omega,-k) \qquad (3.2)$$

and hence, for j+n odd the double integral (3.1) vanishes. These moments can be represented by using the one-sided spectral density function $\Phi(\omega,k)$, just as we have done in Chapter 2. For example,

$$\lambda_{on} = \lambda_n^k = \int_0^{\infty}\int_0^{\infty} k^n \Phi(\omega,k)\,d\omega\,dk = \int_0^{\infty} k^n \Phi(k)\,dk \qquad (3.3a)$$

$$n=0,1,2,\ldots$$

or

$$\lambda_{jo} = \lambda_j^{\omega} = \int_0^{\infty}\int_0^{\infty} \omega^j \Phi(\omega,k)\,d\omega\,dk = \int_0^{\infty} \omega^j \Phi(\omega)\,d\omega \qquad (3.3b)$$

$$j=0,1,2\ldots$$

where we have used the relations

$$\int_0^\infty \Phi(\omega,k)d\omega = \Phi(k) \tag{3.4a}$$

and

$$\int_0^\infty \Phi(\omega,k)dk = \Phi(\omega) \tag{3.4b}$$

Expressions (3.3) are equivalent to expression (2.26).

If $\psi(\omega,k)$ is quadrant symmetric, i.e.,

$$\psi(\omega,k) = \psi(\omega,-k) = \psi(-\omega,k) \tag{3.5}$$

then the moments λ_{jn} may be expressed as follows (Vanmarcke 1983)

$\lambda_{jn} = 0$ j,n both odd

$$\lambda_{jn} = \int_0^\infty \int_0^\infty \omega^j k^n \Phi(\omega,k)d\omega dk \tag{3.6}$$

It is convenient to arrange the second order moments in a 2-D matrix

$$\vec{\Lambda} = \begin{bmatrix} \lambda_{02} & \lambda_{11} \\ \lambda_{11} & \lambda_{20} \end{bmatrix} = \begin{bmatrix} \overset{k}{\lambda_2} & \lambda_{11} \\ \lambda_{11} & \overset{\omega}{\lambda_2} \end{bmatrix} \tag{3.7}$$

which reduces to a diagonal matrix, if $\psi(\omega,k)$ is quadrant symmetric. This property of quadrant symmetry simply means, for the 2-D case, that the partial derivatives of Y(x,t) with respect to x and t are uncorrelated, a fact which has some relevance in the statistics of Y(x,t), as we will see later on this section.

The spectral moments $\overset{k}{\lambda_2}$, $\overset{\omega}{\lambda_2}$, λ_{oo} and λ_{11} have very useful interpretations, in terms of the variances of Y(x,t) and its partial derivatives, just as for the 1-D case (see Appendix A). From relations (3.3), λ_{oo} (from now on denoted simply by λ_o) is just the variance σ^2 of the process Y(x,t), while $\overset{k}{\lambda_2}$ gives the variance σ_x^2 associated with the derivative process Y_x and $\overset{\omega}{\lambda_2}$ gives the variance σ_t^2 associated with the derivative process Y_t. The moment λ_{11} is in turn equal to the covariance of these two derivative processes.

The concept of bandwidth, defined in section 2.2 for the 1-D case, is easily extended to the 2-D case now under consideration. A nondimensional measure of bandwidth, defined in terms of the second order spectral moments of Y(x,t) is given by

$$\Delta = \frac{\lambda_{11} - \lambda_1^k \lambda_1^\omega/\lambda_o}{(\lambda_2^k \lambda_2^\omega)^{1/2}} \tag{3.8}$$

The bandwidth δ^k and δ^ω, associated with the spectral density functions $\Phi(k)$ and $\Phi(\omega)$ respectively, are obtained by letting the moments in (3.8) be with respect to either k or ω. Then, we have

$$\delta^i = [1 - \frac{(\lambda_1^i)^2}{\lambda_o \lambda_2^i}]^{1/2} \qquad i = \omega \text{ or } k \tag{3.9}$$

which is just equivalent to expression (2.27). The coefficients in (3.8) and (3.9) can be arranged in a 2 by 2 matrix

$$\vec{\Delta} = \begin{vmatrix} (\delta^k)^2 & \Delta \\ \Delta & (\delta^\omega)^2 \end{vmatrix} \tag{3.10}$$

If $\Phi(\omega,k)$ is quadrant symmetric, $\vec{\Delta}$ becomes diagonal.

The 2-D process Y(x,t) can be treated as two 1-D processes, by taking either x or t as a parameter, and allowing the other to vary. In each case, the theory presented in Chapter 2 is valid if the same assumptions hold true, namely if the second order moments are finite. Therefore, if Y(x,t) is Gaussian with pdf of the form (2.10), we can write

$$\nu_b^{i,+} = \frac{1}{2\pi} \left(\frac{\lambda_2^i}{\lambda_o}\right)^{1/2} e^{-b^2/2\lambda_o} \tag{3.11}$$

for $i = \omega$ or $i = k$. Here $\nu_b^{k,+}$ is the mean rate of upcrossings of the unidirectional process $Y(x;t_o)$, where t is taken as a parameter, while $\nu_b^{\omega,+}$ is the mean rate of upcrossings for the process $Y(t;x_o)$. We obviously have assumed independence of $Y(x,t)$ and its partial derivatives, which is true for stationary Gaussian processes.

Similarly, the mean time of excursion $\langle T_b \rangle$ above b is given by (2.19) or the approximation (2.22), for b/σ large,

$$\langle T_b \rangle = \frac{\sigma}{\sqrt{2\pi}\, b\nu_o^{\omega,+}}\, g\left(\frac{b}{\sigma}\right) \tag{3.12}$$

(superscript + relates to b upcrossings), while the mean length of excursion $\langle X_b \rangle$ is given by

$$\langle X_b \rangle = \frac{\sigma}{\sqrt{2\pi}\, b\nu_o^{k,+}}\, g\left(\frac{b}{\sigma}\right) \tag{3.13}$$

For high thresholds levels (say, $b/\sigma \geq 2$), each crossing for either unidirectional process, becomes nearly always associated with a single local maximum, provided that these 1-D processes are not extremely narrow banded (i.e., δ^k or δ^ω not very close to zero).

When analyzing a 2-D field, we are interested also in the complete 2-D statistics of extremes. We talk about regions of excursion above b, which are associated with some mean area in parameter space (here, x and t). We might expect, from what has been said about the undirectional processes, that the shapes of these regions of excursion become less complicated and irregular, as we shift our threshold b to higher levels. Each of these simple isolated regions is then associated with a single local maximum. The occurrence of local maxima obeys a 2-D Poisson distribution for $b \to \infty$,

just as the crossings of $Y(x;t_o)$ and $Y(t;x_o)$ constitute 1-D Poisson processes, as seen in Chapter 2.

We should expect that, if the partial derivatives Y_x and Y_t are uncorrelated at the points (x_m,t_m) where $Y(x,t)$ attains local maxima, then the mean area of excursion, $\langle A_b \rangle$, above b is just the product of the mean dimensions, $\langle T_b \rangle$ and $\langle X_b \rangle$. Thus, for $\lambda_{11} = 0$, we may use expressions (2.15) and (2.19) to obtain

$$\langle A_b \rangle = \langle T_b \rangle \langle X_b \rangle = \left[\frac{F^c(b)}{f(b)}\right]^2 \frac{2\pi}{(\lambda_2^k \lambda_2^\omega)^{1/2}} \tag{3.14}$$

where we have used the equivalence between spectral moments λ_2^k, λ_2^ω and variances σ_x^2, σ_t^2, respectively. Use of the approximate forms (3.12) and and (3.13) yield, in turn

$$\langle A_b \rangle = \frac{2\pi}{b^2} \frac{\lambda_o^2}{(\lambda_2^k \lambda_2^\omega)^{1/2}} [g(-)]^2_{\sigma} \quad b/\sigma \text{ - large} \tag{3.15}$$

In general, the partial derivatives are correlated and $\lambda_{11} \neq 0$. Rotation of the coordinate axes causes changes in the moments, but the value of $\langle A_b \rangle$ should be invariant with respect to coordinate rotations. The appearance of the factor $(\lambda_2^k \lambda_2^\omega)^{1/2}$, which is just equal to the square root of the determinant of matrix $\vec{\Lambda}$, with $\lambda_{11} = 0$, defined by (3.7), hints at the general form that $\langle A_b \rangle$ should take, namely

$$\langle A_b \rangle = \left[\frac{F^c(b)}{f(b)}\right]^2 2\pi |\vec{\Lambda}|^{-1/2} \tag{3.16}$$

where $|\vec{\Lambda}|$ is the determinant of $\vec{\Lambda}$. This determinant is a maximum for $\lambda_{11} = 0$ and provides the invariance to $\langle A_b \rangle$, compensating for the changes in the product $\langle T_b \rangle \langle X_b \rangle$ which occur under rotation of the coordinate axis. In the same way, (3.15) becomes for the general case $\lambda_{11} \neq 0$

$$\langle A_b \rangle = \frac{2\pi}{b^2} \frac{\lambda_o^2}{|\vec{\Lambda}|^{1/2}} [g(-)]^2 \qquad \frac{b}{\sigma} \text{ - large} \qquad (3.17)$$

This intuitive derivation of the mean area $\langle A_b \rangle$, which is followed by Vanmarcke (1983), appears to be asymptotically exact, since it leads to the correct asymptotic mean rate of occurrence of isolated regions of excursion above b, μ_b, or the mean number of local maxima above b, per unit area of parameter space. In a given area a_o, $\mu_b a_o$ is the number of crossing events. Then the total area of excursion in a_o can be expressed in two different, but equivalent, ways:

$$\langle A_b \rangle \mu_b a_o = F^c(b) a_o$$

The term on the right hand side is simply another way of writing the fraction of the area a_o over which $Y(x,t) > b$. Solving for μ_b is trivial, and with the use of (3.16)

$$\mu_b = \frac{F^c(b)}{\langle A_b \rangle} = \frac{1}{2\pi} \frac{[f(b)]^2}{F^c(b)} |\vec{\Lambda}|^{1/2} \qquad (3.18)$$

We may also use expression (3.17) for $\langle A_b \rangle$ and approximate $F^c(b)$ with the help of (2.21), to obtain a relation for μ_b, valid for b/σ large

$$\mu_b = \frac{1}{(2\pi)^{3/2}} \frac{b}{\sqrt{\lambda_o}} \frac{|\vec{\Lambda}|^{1/2}}{\lambda_o} \frac{e^{-b^2/2\lambda_o}}{g(-)\frac{b}{\sigma}} \qquad \frac{b}{\sigma} \text{ - large} \qquad (3.19)$$

If we compare expression (3.19) and its 1-D counterpart (2.16b), it becomes evident that the dependence of extreme value statistics on the correlation properties and higher order statistics of the process under consideration, gets more complicated for the 2-D case, and even more so for higher dimensions. The constant factor which captures this dependence, is

easily computed analytically for Gaussian processes of any order (see Vanmarcke 1983), but we might imagine that for non-Gaussian processes, this will not in general be true. If these non-Gaussian processes still satisfy the assumption of independence between them and their partial derivatives, then the derivation of the statistical formulas can be done by carrying the dependence on the correlation properties and higher order statistics as a constant of proportionality, to be determined empirically. Vanmarcke (1985) gives a detailed description of this alternate procedure. We will get back to this issue later on this chapter.

With the expressions developed in this section, we can now compute the mean area of excursion above b or the mean number of excursions per unit area of parameter space, from knowledge of the frequency-wavenumber spectral density function of a stationary 2-D Gaussian process.

3.2 ENVELOPE STATISTICS AND PROBLEM OF CLUSTERING OF LEVEL CROSSINGS

The concept of envelope of a process, introduced in section 2.3 in connection with the problem of clustering of level crossings, can be applied to higher dimensional processes. The envelope R(x,t) of the process Y(x,t) is defined by the expression

$$R(x,t) = [Y_c^2(x,t)+Y_s^2(x,t)]^{1/2} \tag{3.20}$$

This is the 2-D version of equation (2.42). Here, Y_c and Y_s are still given by the sums of sines and cosines (see (2.41) and (2.42)), but now with arguments being functions of x and t.

The 2-D envelope has the same physical interpretation as the one given for its 1-D counterpart in section 2.3. In fact, by fixing one of the variables in (3.20), we may treat R(x,t) as two 1-D envelopes, $R^x(x,t)$ and $R^t(x,t)$, with x or t taken as a parameter, respectively. All the relations

between the variances of the process and its envelope, developed in section 2.3, remain valid for these unidirectional fields. Thus, we have

$$\sigma_r^2 = \langle [R^x(x,t)]^2 \rangle = \langle [R^t(x,t)]^2 \rangle = 2\sigma^2 \tag{3.21}$$

and

$$\begin{aligned} \sigma_{r_x} &= \delta^k \sigma_x \\ \sigma_{r_t} &= \delta^\omega \sigma_t \end{aligned} \tag{3.22}$$

where σ_{r_x} is the standard deviation of $R_x(x,t)$ and σ_{r_t} is the standard deviation of $R_t(x,t)$. In order to completely determine the relevant second order statistics of $R(x,t)$ in terms of the statistics of $Y(x,t)$, we need an expression for $\langle R_x R_t \rangle$. A simple derivation given by Vanmarcke (1983) leads to the relation

$$\langle R_x R_t \rangle = \Delta \sigma_x \sigma_t \tag{3.23}$$

with Δ defined by (3.8).

The concept of bandwidth gains more physical significance here, appearing as a link between the statistical properties of $Y(x,t)$ and its envelope $R(x,t)$, like we had seen before.

Using expressions (3.21), (3.22) and (3.23), it is easy to obtain formulas for the mean area of excursion above b, $\langle A_{b,R} \rangle$, and mean number of crossings per unit area of parameter space, $\mu_{b,R}$, for the envelope process $R(x,t)$ in terms of the statistical parameters of $Y(x,t)$. The matrix $\vec{\Lambda}_R$, associated with $R(x,t)$ is simply

$$\vec{\Lambda}_R = \begin{bmatrix} \sigma_{r_x}^2 & \langle R_x R_t \rangle \\ \langle R_x R_t \rangle & \sigma_{r_t}^2 \end{bmatrix} \tag{3.24}$$

whose determinant can be expressed as

$$|\vec{\Delta}_R| = |\vec{\Delta}| \, \sigma_x^2 \, \sigma_t^2 \tag{3.25}$$

From relations (3.16) and (3.25), we have

$$\langle A_{b,R} \rangle = \left[\frac{F_R^c(b)}{f_R(b)}\right]^2 \frac{2\pi}{\sigma_t \sigma_x |\vec{\Delta}|^{1/2}} \tag{3.26}$$

where F_R^c and f_R are the complementary cdf and pdf of R(x,t), respectively, and are given by (2.34) and (2.35) (recall that the envelope of a Gaussian process is Rayleigh distributed). Using (2.34) and (2.35) in (3.26) yields, in terms of spectral moments

$$\langle A_{b,R} \rangle = \frac{2\pi}{b^2} \frac{\lambda_o^2}{(\lambda_2^k \lambda_2^\omega)^{1/2}} \frac{1}{|\vec{\Delta}|^{1/2}} \tag{3.27}$$

The expression for $\mu_{b,R}$ is just as easily obtained:

$$\mu_{b,R} = \frac{F_R^c(b)}{\langle A_{b,R} \rangle} = \frac{b^2}{2\pi} \frac{(\lambda_2^\omega \lambda_2^k)^{1/2}}{\lambda_o^2} |\vec{\Delta}|^{1/2} \, e^{-b^2/2\lambda_o} \tag{3.28}$$

We can turn now to the problem of clusterings of crossings. The simplest measure of the tendency for clustering, defined by (2.51) for 1-D case, becomes in its 2-D form,

$$\frac{\mu_b}{\mu_{b,R}} = \frac{1}{(2\pi)^{1/2}} \frac{\sigma}{b} \frac{1}{\sigma_x \sigma_t} \frac{|\vec{\Delta}|^{1/2}}{|\vec{\Delta}|^{1/2}} \qquad \frac{b}{\sigma} \text{ - large} \tag{3.29}$$

using (3.19) and (3.28). This is called the mean clump size as before, and gives a good estimate of the number of crossings of Y(x,t) per crossing of R(x,t), if Y(x,t) is a narrow band process. For wide band processes, a better estimate of mean clump size $\langle N_b \rangle$, which compensates for empty excursions of R(x,t), is given by (2.52) as before with r_b given by (3.29).

3.3 EXTREME VALUE DISTRIBUTIONS OF 2-D RANDOM PROCESSES

As it was already discussed in section 3.1, the pattern of crossings of high thresholds b by Y(x,t) constitute a 2-D Poisson process with mean rate μ_b, in the limit $b \to \infty$. Thus, the probability that n local maxima occur in an area a_o, as $b \to \infty$ is given by

$$P[N(a_o)=n] = \frac{(a_o\mu_b)^n}{n!} e^{-a_o\mu_b} \quad n = 0,1,2... \tag{3.30}$$

The probability of no local maxima occurring in area a_o (i.e., $P[N(a_o) = 0]$), called the reliability function $L_b(a_o)$, is simply

$$L_b(a_o) = P[\underset{a_o}{\text{Max}}\ Y(x,t)<b] = e^{-a_o\mu_b} \quad b \to \infty \tag{3.31}$$

The reliability function was seen to be related to safety issues which come up in connection with extreme natural phenomena. Here, it gives an estimate of how far and how long (for our case of space and time coordinates) it takes, to observe a crossing of very high threshold b, by process Y(x,t). However, as we decrease b, some corrections should be made to account for clustering effects and the finite size of the region of excursions, which are neglected in making the "point process" Poisson assumption. Furthermore, the probability of finding Y(x,t) below b as $a_o \to 0$ is not one, as implied by (3.31), but should equal F(b). These corrections have been discussed in some detail in section 2.5, for the case of 1-D random process. It suffices here to write the final expression for the reliability function, corrected for all the mentioned effects, derived in Vanmarcke's book:

$$L_b(a_o) = F(b)\exp\{-\frac{\mu_b a_o}{F(b)}[1-\exp(-\frac{\mu_{b,R}}{\mu_b})]\} \tag{3.32}$$

In the limit $b \to \infty$, the above expression becomes equal to (3.31).

If the alternate approach, followed by Vanmarcke (1985), is taken (i.e., to carry the dependence of extreme value statistics on the correlation structure and higher order statistics of the process as a proportionality constant), we are left with a constant to be determined empirically. In addition to the methods briefly outlined in section 2.4, another possible method is to compare the reliability function (derived in terms of the proportionality constant), with one of the Gumbel type distributions mentioned in section 2.5 (Vanmarcke, personal communication). The practical relevance of this procedure will not be tested in this study. However, it should prove to be a powerful tool, if the random process to be analyzed is not Gaussian and of high dimensionality.

CHAPTER 4

A SIMPLE ANALYTICAL MODEL FOR SST AND SL SPECTRA IN THE EQUATORIAL PACIFIC

In the previous two chapters, the theory for analyzing threshold crossing statistics of a random field was discussed in detail. We shall now apply this theory in the analysis of the SST and SL fields associated with ENSO events. For the reader who has chosen to skip the lengthy description of the theory of statistics of extremes given in the first section of this chapter. This summary may also be helpful in refreshing one's memory about the material covered in the previous two chapters.

Knowledge of the wavenumber-frequency spectral density function is necessary to define the crossing statistics of a 2-D random field. The bulk of this chapter is devoted to developing a simple equatorial ocean model, which will give us a model wavenumber-frequency spectra for the SST and SL fields, associated with ENSO events. Some relevant characteristics of the SST and SL signals, evident from the available data, are briefly discussed and the same is done for the tropical wind stress.

4.1 SUMMARY OF EXPRESSIONS DEFINING THE THRESHOLD CROSSING STATISTICS OF A GAUSSIAN RANDOM FIELD

The threshold crossing statistics of a 2-D (time and space) stationary random field are completely determined from knowledge of its one sided spectral density function, $\Phi(\omega,k)$, where k is wavenumber and ω is frequency, and of its probability density function (pdf). Here, we only consider the specific case of Gaussian random fields.

The following spectral moments of $\Phi(\omega,k)$ are important

$$\lambda_o = \int_0^\infty \int_0^\infty \Phi(\omega,k)d\omega dk \tag{4.1a}$$

$$\lambda_{11} = \int_0^\infty \int_0^\infty \omega k\Phi(\omega,k)d\omega dk \tag{4.1b}$$

$$\lambda_{20} = \lambda_2^{\omega} = \int_0^\infty \int_0^\infty \omega^2\Phi(\omega,k)d\omega dk \tag{4.1c}$$

$$\lambda_{02} = \lambda_2^{k} = \int_0^\infty \int_0^\infty k^2\Phi(\omega,k)d\omega dk \tag{4.1d}$$

The second order moments can be arranged in a 2x2 matrix

$$\vec{\Lambda} = \begin{bmatrix} \lambda_2^{\omega} & \lambda_{11} \\ \lambda_{11} & \lambda_2^{k} \end{bmatrix} \tag{4.2}$$

If the two sided spectral function $\Psi(\omega,k)$ is quadrant symmetric (i.e., if $\Psi(\omega,k)$ satisfies (3.5)), then λ_{11} is zero and $\vec{\Lambda}$ becomes diagonal.

In terms of these moments, the mean rate of upcrossings of threshold b per unit time, $\nu_b^{\omega,+}$, for a given process, is

$$\nu_b^{\omega,+} = \frac{1}{2\pi}\left(\frac{\lambda_2^{\omega}}{\lambda_o}\right)^{1/2} e^{-b^2/2\lambda_o} \tag{4.3}$$

Similarly, the mean rate of upcrossings of threshold b per unit length, $\nu_b^{k,+}$, is given by

$$\nu_b^{k,+} = \frac{1}{2\pi}\left(\frac{\lambda_2^{k}}{\lambda_o}\right)^{1/2} e^{-b^2/2\lambda_o} \tag{4.4}$$

((4.3) and (4.4) are the same as (3.11)). Also, the mean time of excursion $\langle T_b\rangle$ above b, for b/σ large (σ^2 is the variance λ_o), is

$$\langle T_b\rangle = \frac{\sigma}{\sqrt{2\pi}\, b\nu_o^{\omega,+}}\, g\left(\frac{b}{\sigma}\right) \qquad \frac{b}{\sigma} \text{ - large} \tag{4.5}$$

(the same as (3.12)), with g(u) defined by (2.21b). Similarly, the mean length of excursion $\langle X_b \rangle$ above b, for b/σ large, is

$$\langle X_b \rangle = \frac{\sigma}{\sqrt{2\pi}\, b\nu_o^{k,+}} g\left(\frac{-b}{\sigma}\right) \qquad \frac{b}{\sigma} \text{ large} \qquad (4.6)$$

(the same as (3.13)).

Threshold crossings in 2-D occur over some area of parameter space (here space and time). The expression for the mean area of excursion $\langle A_b \rangle$ above b is just

$$\langle A_b \rangle = \frac{2\pi}{b^2} \frac{\lambda_o^2}{|\vec{\Lambda}|^{1/2}} \left[g\left(\frac{-b}{\sigma}\right)\right]^2 \qquad \frac{b}{\sigma} \text{ large} \qquad (4.7)$$

(the same as (3.17)). Also, the mean rate of occurrence of regions of excursion μ_b above b is given by

$$\mu_b = \frac{1}{(2\pi)^{3/2}} \frac{\vec{b}}{\lambda_o^{1/2}} \frac{|\vec{\Lambda}|^{1/2}}{\lambda_o} \frac{e^{-b^2/2\lambda_o}}{g\left(\frac{-b}{\sigma}\right)} \qquad \frac{b}{\sigma} \text{ large} \qquad (4.8)$$

(the same as (3.19)).

The reader may consult sections 2.1, 2.2 and 3.1 of the two previous chapters for the full derivation of these expressions. We will use these formulas to compute the threshold crossing statistics of the SL and SST anomaly fields in Chapter 5.

4.2 SOME RELEVANT ASPECTS OF THE SST AND SL SIGNALS DURING EL NIÑO

The two most extreme oceanic signals, during El Niño events, are certainly observed in the SST and SL equatorial fields. They are also the fields which are better understood, especially SL. Thus, we concentrate

our effort on the extreme anomalies of these two fields which are observed in the equatorial Pacific, during ENSO years.

A - SEA LEVEL

A very rough description of SL along the equatorial Pacific, during non-El Niño years, gives high SL (deep thermocline) at the west, decreasing towards the east (with the thermocline shoaling). This wind setup solution, which balances the wind stress exerted by the Trades with the pressure gradient associated with the sea level slope, drastically changes as the onset of El Niño occurs. A series of maps of SL anomaly in the tropical Pacific for the period 1975-1983 can be seen in Wyrtki and Nakahara (1984) and Wyrtki (1984). This period encompasses the 1976 and 1982/83 events. Two features immediately emerge from those maps: one is the extremely large spatial scales, on the order of several thousand kilometers, with high positive anomalies covering most of the eastern half of the Pacific; the other feature concerns the relatively long time scales, on the order of several months, associated with these anomalies. These two characteristics of the SL anomaly field accompanying El Niño events can be best seen in a time vs. longitude plot, as in Figure 4, adapted from Wyrtki (1983) and relative to the 82/83 El Niño. Anomalies of 20-30 cm were observed during this strong El Niño. It is hard to quantify these anomalies in terms of the standard deviation of the SL field, because of the variability between stations, the scarcity of long records and subtleties in defining a mean annual cycle, just to name a few reasons. The annual variability is weak, with typical values around 5 cm (Wyrtki and Leslie 1980). It is fair to say that an anomaly of twice the annual cycle is significant, and that 2 standard deviations above the mean (including the annual cycle) is a fairly good representation of the large spatial and time scales of the observed El Niño SL signals.

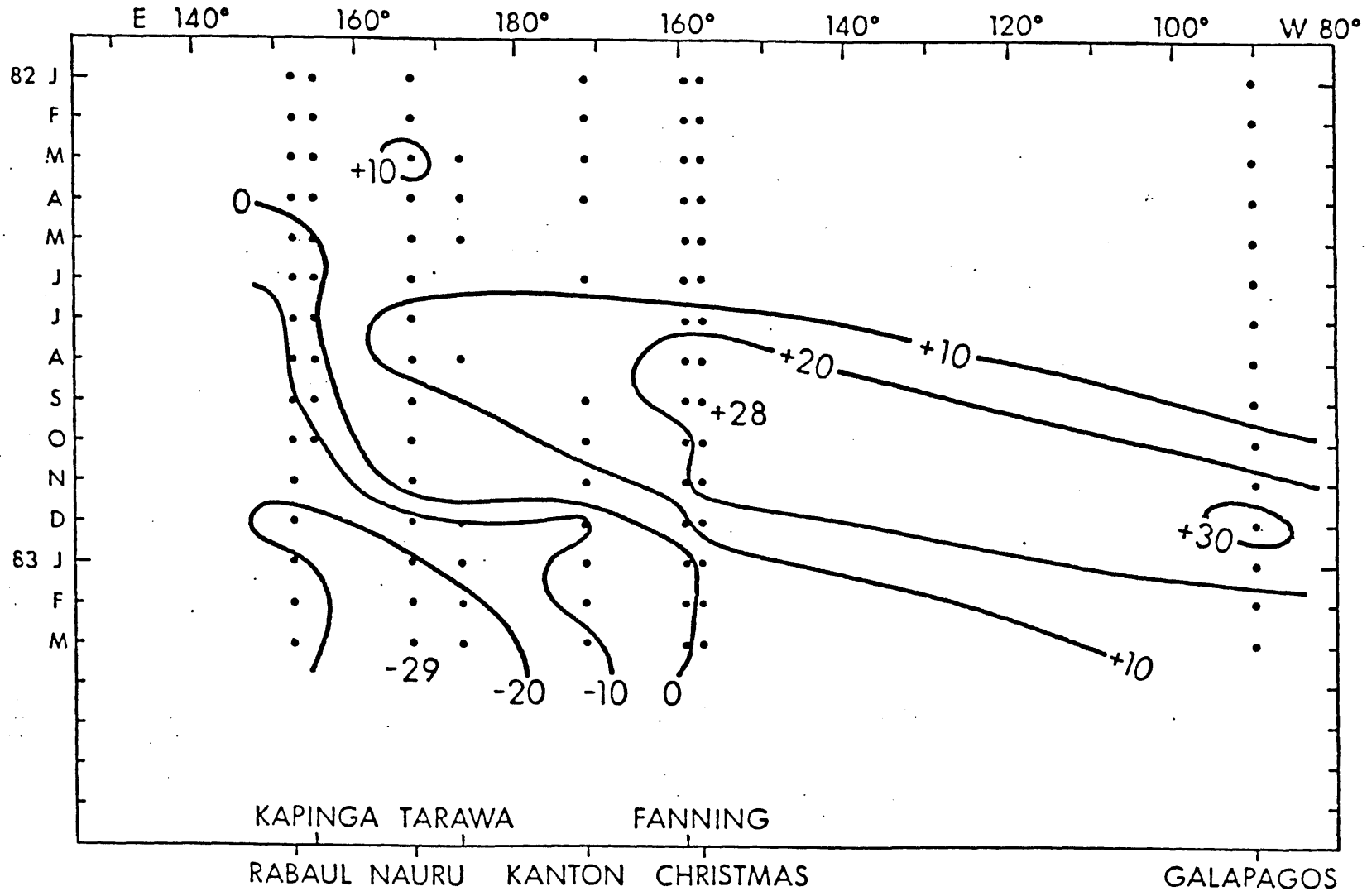

Figure 4. Time-longitude plot of the monthly sea level anomalies (cm) at several near-equatorial stations across the Pacific, for the period January 82 to March 83 (after Wyrtki 1983). Notice the long spatial and temporal scales of these anomalies.

Linear equatorial wave theory (a good review of this theory can be found in Moore and Philander (1978)) has been used quite successfully to model the SL response of the Pacific to wind stress forcing (see, for example, Wunsch and Gill (1976), Eriksen et al. (1983), Cane (1984)). The forced response can be described in terms of the free waves of the system. The dispersion relation for the equatorial wave guide is shown in Figure 5. The low frequency Kelvin and Rossby wave roots are the relevant solutions describing the variability in sea level associated with El Niño. The mixed gravity-Rossby wave has vanishing vertical displacement at the equator and does not contribute to the SL signal there. Short Rossby waves (i.e., large zonal wavenumber k) have wavelengths too small to be excited by the usual wind patterns responsible for El Niño events. They are excited at the western boundary as part of the reflection process, when long Rossby waves hit the coast. Nevertheless, their group speed is very small and they travel a small distance before they decay by frictional processes. Furthermore, the long Rossby waves have relatively small sea level signals at the equator, with the highest amplitudes occurring off the equator, unlike the Kelvin waves (Eriksen et al. 1983). It is therefore reasonable, to expect the Kelvin wave to be the major contributor to SL variance at the equator, at the low frequency range characterizing El Niño phenomena.

The scarcity of long SL records and the poor spatial coverage of the equatorial Pacific, has caused zonal wavenumber-frequency spectral estimates to be virtually non-existent in the literature. The most extensive study of SL spectra I have found is that of Luther (1980). Without dwelling on details irrelevant to this study, the numerous frequency SL spectra, shown in Luther (1980), reveal the redness character

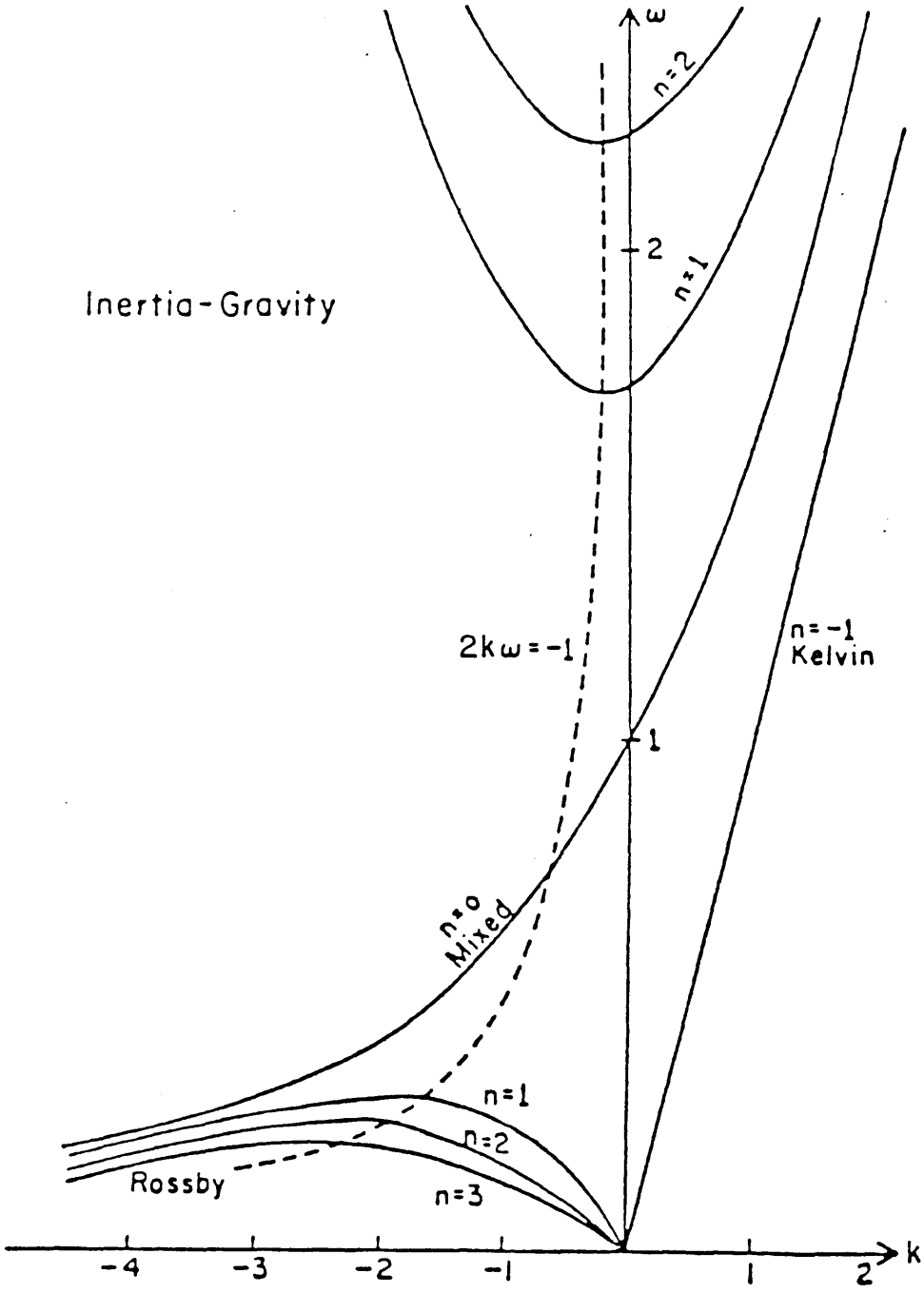

Figure 5. The nondimensional dispersion relation for equatorial waves, where n is meridional mode number. Expressions $k^* = (\beta/c)^{1/2}k$ and $\omega^* = (c\beta)^{1/2}\omega$ give the dimensional wavenumber and frequency respectively, with β and c as defined in section 4.2. Dashed line corresponds to points of zero zonal group velocity (except for n=0) (after Pedloski 1979).

familiar to most geophysical spectra, with frequency dependences, for the range 1 day-1 year, looking like ω^{-p}, with $1 \leq p \leq 2$ (here, ω denotes frequency). For periods longer than 1 year, the ambiguity of the estimates reflects the shortness of the records, but I think it is fair to say that the spectra becomes whiter (flatter).

The important point here is that, from the existent records, the low frequency (periods of 1 year and greater) estimates of the power density of SL have almost no use in assisting on the development of a spectral model, capable of yielding the 2-D (space and time) statistics of extremes we seek in this study.

B - SEA SURFACE TEMPERATURE

The SST variability associated with ENSO events has a fairly similar structure to the SL signal discussed above. The large positive anomalies appear to cover most of the central and eastern Pacific for several months, as is evident from the maps of Rasmusson and Carpenter (1982) or from time-longitude plots of SST anomalies as in Figure 6, adapted from Reynolds (1983) and relative to the 82/83 El Niño. The same large space-time scales have characterized all the SST anomaly records in El Niño years. Anomalies from the composite analysis of Rasmusson and Carpenter (1982) don't exceed 2°C, relative to a long term mean which includes El Niño years. A look at anomaly maps for the 82/83 event brings to evidence the variability between events. During this strong El Niño, temperature anomalies of 5°C were observed (Reynolds 1983).

The difficulty in defining what are the mean and the anomalous SST conditions, makes it hard to specify, with confidence, the departure from normal conditions that the SST fields experience during El Niño. The annual cycle, for example, is highly variable spatially, decreasing in

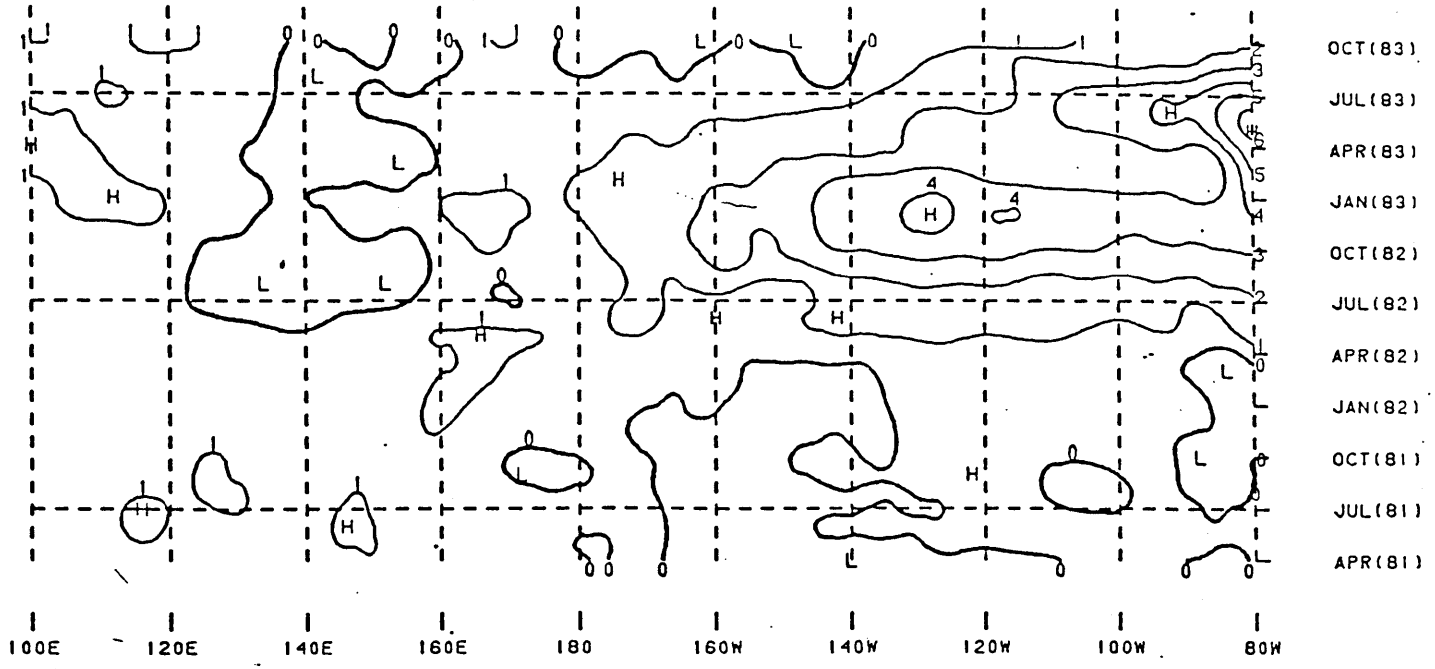

Figure 6. Time-longitude plot of monthly SST anomalies (°C) for the period April 81 to October 83 (after Reynold 1983). The SST anomaly values represent averages over a 10° band of latitude centered on the equator except east of 95°W where it is centered further south (see Reynold (1983) for details).

amplitude westward. Since it will be important to quantify the SST anomalies in terms of the standard deviation, we take as a fair "definition" of El Niño SST anomalies, departures from the mean of 2 standard deviations, as we had done with SL.

Modeling of SST patterns, associated with ENSO variability, have been pursued in the last few years. In general, the ideas of advection and, in a more unsettled way, air-sea interaction processes, are involved in the explanation of SST anomalies, the former being the most important.

A study done by Zebiak and Cane (1983) finds a whole range of advection processes to be important in the complete evolution of SST anomaly fields during El Niño. Remote forcing by wind stress is important in creating anomalies by zonal advection, while local winds can induce variability in the rate of upwelling along the equator (vertical advection) and thus influence the SST anomaly field. Nonlinear advection (e.g., advection of anomalous temperature by anomalous currents) is seen to be important, as well as meridional advection. Even though all these terms are a factor at some time or place, zonal and vertical advection are dominant at the equator while meridional advection is dominant at regions away from the equator. Vertical advection is probably relevant when the collapse of the Trades occur, with the consequent cutting off of the equatorial upwelling, normally driven by the Ekman drift, associated with the Trades. Zonal advection of the mean SST fields at the equator is believed to be responsible for the SST anomalies occurring at the onset of El Niño, at least in the central Pacific, as it has been suggested by Gill (1983) and Harrison and Schopf (1983).

Much of what was said about SL spectra remains even more true, when talking about SST spectra. Most of the frequency spectral estimates

available cover periods of 1 year and shorter. Spectral estimates at longer periods are not possible, due to the shortness of the majority of the records. The frequency SST spectra are generally red at periods of 1 year to a few days, with a frequency dependence ω^{-p}, with $1 < p < 3$ roughly (e.g., Halpern 1984). The ω dependence is not necessarily homogeneous, but no more details can be extracted about the general shapes of SST frequency spectra with confidence. Zonal wavenumber spectral estimates are also nonexistent.

Considering the scenario pictured above and the need for knowing the zonal wavenumber-frequency spectra of SL and SST at the equator, if we are to be able to compute the space and time scales associated with extremes occurring in those fields, the development of an ocean model to obtain those k-ω spectra is needed and shall be pursued next. The model should be aimed at describing the low frequency and large spatial variability of the SL and SST fields typical of El Niño years.

4.3 A MODEL FOR SL AND SST k-ω SPECTRA

The linear theory for the equatorial ocean dynamics has been extensively studied previously. The review by McCreary (1985) summarizes the progress. This theory will be used in order to arrive at model k-ω SL and SST spectra.

Linear, Boussinesq, incompressible equatorial β-plane dynamics are used to describe the dynamical response of a laterally unbounded, flat bottom ocean to wind stress forcing. Only Kelvin waves will be allowed as part of the response of our stratified equatorial ocean. The set of equations governing the dynamical fields of the decribed system is

$$u_t + \frac{p_x}{\rho_o} = \frac{G_z}{\rho_o} \tag{4.9a}$$

$$\beta y u + \frac{p_y}{\rho_o} = 0 \tag{4.9b}$$

$$\rho g + p_z = 0 \tag{4.9c}$$

$$u_x + w_z = 0 \tag{4.9d}$$

$$\rho_t + w\bar{\rho}_z = 0 \tag{4.9e}$$

where the notation is conventional (u and w are perturbation zonal and vertical velocities, respectively; p is perturbation pressure). The basic stratification is denoted by $\bar{\rho}$, while the total density ρ_T can be written as follows

$$\rho_T = \rho_o + \bar{\rho} + \rho \tag{4.10}$$

Also, g is the gravitational acceleration, G denotes the tangential stress acting in horizontal layers, and βy is just the Coriolis parameter. Subscripts indicate partial differentiation. The v field was set equal to zero, to allow only Kelvin waves to be excited.

Equations (4.9a,b) express the zonal and meridional momentum balance respectively. Meridional forcing is left out, because of its relative inefficiency in exciting Kelvin waves, when compared with zonal wind forcing. The zonal perturbation flow is in geostrophic balance with the meridional pressure gradient. Equation (4.9c) is the hydrostatic balance, while (4.9d) is the continuity equation and (4.9e) tells us that local time changes in perturbation density are a result of vertical advection of the basic stratification.

The tangential stress G, which should equal the zonal wind stress τ at the surface, is confined to a surface mixed-layer of depth h_{mix}. Following the standard approach, first used by Lighthill (1969), the wind forcing is

applied as a near-surface body force. In this way, a detailed discussion of the surface boundary layer is avoided. The dependence of G, with depth, in the mixed layer, is more or less arbitrary, provided it goes to zero at the base of the mixed layer, $z = -h_{mix}$. Wunsch (1977) assumes an exponential dependence, while Gill and Clarke (1974) use a linear dependence, invoking some experimental evidence for the uniformity of Ekman currents over the mixed layer. The function G is then given by

$$G = \tau \left(\frac{z}{h_{mix}} + 1\right) \qquad -h_{mix} \leq z \leq 0 \tag{4.11}$$

where τ is the zonal wind stress ($G = \tau$ at the surface $z=0$ and decreases linearly to zero at $z = -h_{mix}$).

The unforced set of equations (put $G = 0$ in (4.9)) can be solved using the standard separation into normal modes, where the u,w,p and ρ fields can be expanded as a sum of vertical modes. Thus, we may write

$$u = \sum_n u_n(x,y,t)\hat{p}_n(z) \tag{4.12a}$$

$$\frac{p}{\rho_o} = \sum_n p_n(x,y,t)\hat{p}_n(z) \tag{4.12b}$$

$$w = \sum_n w_n(x,y,t)\hat{w}_n(z) \tag{4.12c}$$

$$\frac{g\rho}{N^2} = \sum_n h_n(x,y,t)\hat{w}_n(z) \tag{4.12d}$$

where N^2 is the Brunt-Vaisala or buoyancy frequency, defined by

$$N^2 = -\frac{g\bar{\rho}_z}{\rho_o} \tag{4.13}$$

The notation h_n is used because h_n is proportional to the displacement of density surfaces, following Gill and Clarke (1974).

The forced solutions can be found easily by making use of the completeness of the set of eigenfunctions $\hat{p}_n(z)$ (or $\hat{w}_n(z)$) to expand the forcing function as follows

$$\frac{G_z}{\rho_o} = \sum_n X_n(x,y,t)\hat{p}_n(z) \tag{4.14}$$

Using expansions (4.12) and (4.14) in the set of equations (4.9) leads to a separation of the problem into a vertical structure equation

$$\hat{w}_{nzz} + \frac{N^2}{c_n^2}\hat{w}_n = 0 \tag{4.15}$$

and the horizontal equations

$$u_{nt} + p_{nx} = X_n \tag{4.16a}$$

$$\beta y u_n + p_{ny} = 0 \tag{4.16b}$$

$$c_n^2 u_{nx} + p_{nt} = 0 \tag{4.16c}$$

The vertical structure equation (4.15) governs the z dependence of the solutions. It can be solved for general buoyancy frequency profiles, either numerically or by using the WKB method when suitable. For our purposes, N will be taken as constant. The separation constant c_n has dimensions of velocity and gives the phase speed for each Kelvin wave mode. The eigenfunctions $\hat{w}_n(z)$ and eigenvalues c_n are determined by solving (4.15), subject to the conditions that w vanishes at z=0 and z=-D (D is the constant ocean depth). The surface boundary condition (w=0 at z=0) is usually called the rigid lid approximation. Solutions of (4.15) using this approximation are

$$\hat{w}_n(z) = A_n \sin \frac{N}{c_n} z \tag{4.17}$$

with the eigenvalues c_n given by

$$c_n = \frac{ND}{n\pi} \qquad n=1,2,3... \tag{4.18}$$

We have lost from these solutions, the eigenvalue c_o ($c_o = \infty$), which corresponds to the barotropic mode. If we had used a free surface condition, we would have obtained $c_o \simeq (gD)^{1/2}$ for the phase speed of the barotropic mode. The meridional trapping scale associated with this mode is much larger than for the baroclinic modes, making the β-plane approximation invalid. Therefore, treatment of the barotropic mode implies the use of the full spherical equations. Since this mode presumably has a very insignificant sea level signal associated with it (Cane 1984), we will not consider it anymore in our analysis.

It is easy to show that

$$\hat{p}_n(z) = \hat{w}_{nz}(z) \tag{4.19}$$

from which the functions $\hat{p}_n(z)$, describing the vertical structure of the u and p fields, can be computed. The usual normalization procedure for $\hat{p}_n(z)$ is

$$\frac{1}{D}\int_{-D}^{o} \hat{p}_m(z)\hat{p}_n(z)dz = \delta_{mn} \tag{4.20}$$

where δ_{mn} is the Kroenecker delta ((4.20) expresses the orthogonality of the eigenfunctions $\hat{p}_n$). The normalized functions are

$$\hat{p}_n(z) = \sqrt{2}\cos\frac{N}{c_n}z \tag{4.21}$$

We now turn our attention to the horizontal equations (4.16). Combining expressions (4.11) and (4.14) and using orthogonality and the normalization condition (4.20), leads to the following relation between the projection coefficients X_n of the forcing, and the wind stress τ,

$$X_n = b_n\tau(x,y,t) \tag{4.22}$$

where

$$b_n = \frac{1}{\rho_o h_{mix} D} \int_{-h_{mix}}^{o} \hat{p}_n(z)dz \qquad (4.23)$$

The projection factor b_n is in general sensitive to the actual N(z) profile and the mixed layer depth h_{mix}, as first pointed out by Lighthill (1969). Depending on the form of the z-dependence assumed for the surface boundary layer, the integrand in (4.23) may be more complicated.

The horizontal equations (4.16), written in terms of the wind stress $\tau(x,y,t)$ are

$$u_t + p_x = b\tau \qquad (4.24a)$$

$$\beta yu + p_y = 0 \qquad (4.24b)$$

$$c^2 u_x + p_t = 0 \qquad (4.24c)$$

where we have dropped the subscripts n and consider now the equations for a particular mode.

The meridional structure of the solutions can be found from (4.24b), by putting p=uc (this is the free zonally propagating wave solution from (4.24c)). We have for the y dependence then,

$$p \propto e^{-\beta y^2/2c} \qquad (4.25)$$

The Kelvin wave has a Gaussian meridional structure, decaying away from the equator.

We may combine equations (4.24a) and (4.24c) to obtain an equation for perturbation pressure,

$$c^2 p_{xx} - p_{tt} = bc^2 \tau_x \qquad (4.26)$$

The part of the wind stress forcing that will excite Kelvin waves is that which can be projected on the meridional structure given by the basis functions $\exp(-\beta y^2/2c_n)$. Assuming

$$p = P(x,t)\, e^{-\beta y^2/2c} \qquad (4.27)$$

and doing this projection by multiplying (4.26) by the basis function, we obtain

$$c^2 P_{xx} - P_{tt} = \alpha \int_{-\infty}^{\infty} \tau_x(x,y,t) e^{-\beta y^2/2c} \, dy = \alpha F_x(x,t) \qquad (4.28)$$

where α is a constant for each vertical mode, given by

$$\alpha = b \, c^{3/2} \left(\frac{\beta}{\pi}\right)^{1/2} \qquad (4.29)$$

and

$$F(x,t) = \int_{-\infty}^{\infty} \tau(x,y,t) e^{-\beta y^2/2c} \, dy \qquad (4.30)$$

The y dependence in (4.28) has been integrated out and the factor $(c\pi/\beta)^{1/2}$, which results from the integral $\int_{-\infty}^{\infty} \exp(-\frac{\beta y^2}{c}) dy$ performed on the left hand side of (4.28), is absorbed by constant α.

Our goal is to obtain an analytical k-ω spectrum from (4.28). Therefore, we proceed by Fourier transforming the equation in space (zonal coordinate) and time. The forms

$$P(x,t) = \int_{-\infty}^{\infty} \int_{-\infty}^{\infty} \tilde{P}(\omega,k) e^{i(kx+\omega t)} \, dk d\omega \qquad (4.31)$$

and

$$F(x,t) = \int_{-\infty}^{\infty} \int_{-\infty}^{\infty} \tilde{F}(\omega,k) i^{(kx+\omega t)} \, dk d\omega \qquad (4.32)$$

are assumed and used in (4.28) to simply yield

$$\tilde{P}(\omega,k) = \frac{ik\alpha}{(\omega^2 - c^2k^2)} \tilde{F}(\omega,k) \qquad (4.33)$$

The tilde symbol ("~") here stands for the Fourier transform. The expected resonance at values of $\omega = ck$ is present, for at those values, the Kelvin wave dispersion relation is exactly satisfied. In the absence of friction, $\tilde{P}(\omega,k)$ goes to infinity if there is any forcing at ω and k values which

solve $\omega = ck$. This resonant singularity can be very easily removed by the introduction of some type of friction. One simple way of accomplishing this is to let the frequency ω become complex

$$\omega \rightarrow \omega + i\varepsilon \tag{4.34}$$

with ε being some sort of dissipation. Wunsch and Gill (1976) let ε be proportional to the square of the wavenumber, in which case ε represents a sort of Laplacian "pseudofriction" as they call it (pseudo because procedure (4.34) affects also the continuity equation). If we let ε be a constant, the above procedure is equivalent to having Rayleigh friction terms in our beginning equations, as well as Newtonian cooling, with the additional assumption of these two coefficients being equal (see McCreary (1985)). We will follow the later Rayleigh friction representation (ε = constant) in this study.

Making use of the transformation in (4.34), expression (4.33) becomes

$$\tilde{P}(\omega,k) = \frac{ik\alpha}{(\omega^2-\varepsilon^2-c^2k^2+2i\omega\varepsilon)} \tilde{F}(\omega,k) \tag{4.35}$$

where no resonance is now possible.

In order to obtain the ω-k pressure spectrum from (4.35) in terms of the forcing spectrum, we now make the randomization assumption that

$$\langle \tilde{F}(\omega,k)\tilde{F}^*(\omega',k') \rangle = \Phi_F(\omega,k)\delta(\omega-\omega')\delta(k-k') \tag{4.36}$$

with the angular brackets still denoting an ensemble average, * being the complex conjugate, δ being the Dirac delta function and $\Phi_F(\omega,k)$ the zonal wind stress forcing spectrum. The stochastic assumption (4.36) about the wind forcing implies random phases for different ω,k components of the wind field, ruling out the possibility of standing modes. This assumption of stochastic winds simplifies the problem a great deal. Multiplying equation (4.35) by its complex conjugate and using (4.36) quickly yields

$$\Phi_p(\omega,k) = H_p(\omega,k)\ \Phi_F(\omega,k) \tag{4.37}$$

with

$$H_p(\omega,k) = \frac{\alpha^2 k^2}{[(\omega^2-\varepsilon^2-c^2k^2)^2+4\omega^2\varepsilon^2]} \tag{4.38}$$

$\Phi_p(\omega,k)$ is the k-ω spectrum of pressure and the function $H(\omega,k)$, which depends on mode number n, captures the importance of the ocean dynamics in "reshaping" the atmospheric input. The oceanic spectrum is in fact red, in relation to the forcing zonal wind stress spectrum, as we have hinted before.

It is well known that sea level ζ can be obtained from the pressure at z=0, i.e.,

$$\zeta = \frac{p(0)}{g\ \rho_o} \tag{4.39}$$

We thus have, simply

$$\Phi_\zeta(\omega,k) = H_\zeta(\omega,k)\Phi_F(\omega,k) \tag{4.40}$$

with

$$H_\zeta(\omega,k) = \frac{\hat{p}(0)}{g} H_p(\omega,k) \tag{4.41}$$

where $\Phi_\zeta(\omega,k)$ stands for ω-k SL spectrum, and $H_\zeta(\omega,k)$ differs from $H_p(\omega,k)$ by the constant $\hat{p}(0)/g$ ($\hat{p}(0)$ does not change with mode number). Both SL and pressure spectra have the same dependence on mode number.

The k-ω spectrum of the zonal velocity perturbation can be obtained by Fourier transforming equation (4.24c), and using (4.37) to express it in terms of the forcing spectrum $\Phi_F(\omega,k)$. The procedure leads to the expression

$$\Phi_u(\omega\ k) = H_u(\omega,k)\Phi_F(\omega,k) \tag{4.42}$$

with

$$H_u(\omega,k) = \frac{\alpha^2}{c^4} \frac{\omega^2+\varepsilon^2}{(\omega^2-\varepsilon^2-c^2k^2)^2+4\omega^2\varepsilon^2} = \frac{\omega^2+\varepsilon^2}{c^4k^2} H_p(\omega,k) \qquad (4.43)$$

where $\Phi_u(\omega,k)$ is the u spectrum. This spectrum is needed to derive an SST spectrum, as we shall see later.

The frequency spectra $\Phi_\zeta(\omega)$, $\Phi_u(\omega)$ can be obtained by integrating the respective ω-k spectra (expressions (4.40) and 4.42)) with respect to zonal wavenumber k, while $\Phi_\zeta(k)$ and $\Phi_u(k)$ result from integrating (4.40) and (4.42) over frequency, respectively.

It is convenient to keep in mind that, besides the dependence of the H factors on vertical mode number n, in relations (4.40) and (4.42), $\Phi_F(\omega,k)$ also depends on mode number, since it is the spectrum of the projection of the zonal wind stress on the basis functions $\exp(-\beta y^2/2c_n)$, themselves dependent on n. As c_n decreases with increasing mode number n, the integral in (4.28) will tend in general to decrease due to the decreasing decay scale of the exponential. The first baroclinic modes will be the most strongly forced, from this point of view.

Having used linear Kelvin wave dynamics to get a spectrum of p and u in terms of zonal wind stress spectrum, we now turn our attention to the SST problem. A very simple model, based on the findings of Gill (1983) and Harrison and Schopf (1983) as discussed in section 4.2, is adopted here. Anomalous zonal currents produced by our Kelvin wave model advect mean surface temperature fields to produce SST anomalies. Expressing this in mathematical form, we have

$$T'_t = - u \overline{T}_x \qquad (4.44)$$

Here, T' is the SST anomaly and $\overline{T}$ is the prescribed mean surface temperature field, taking to be independent of time. We shall confine our anomalous advection balance equation to be valid only at the equator (i.e. y=0) for

reasons previously cited. The primed and barred temperature fields are to be interpreted in this context. The total surface zonal Kelvin wave induced anomalous velocity is a sum over whatever vertical modes are excited by the wind. For a particular mode, we may write (4.44) as

$$T'_t = -U(x,t)\hat{p}(0)\overline{T}_x \tag{4.45}$$

where we have used the form

$$u_n = U_n(x,t)e^{-\beta y^2/2c_n} \tag{4.46}$$

evaluated at the equator (y=0).

We have disregarded here terms which express the advection of SST anomalies by anomalous currents (i.e., nonlinearities), in addition to vertical and meridional advection terms (obviously with v=0 for Kelvin waves, we can not include the later in our model). Also advection by mean currents is absent, since our basic state ocean is at rest. We will discuss the peculiarities and implications of this oversimplified model later in this thesis.

To arrive at an SST anomaly spectrum, we may Fourier transform the advection equation (4.45), in space and time. Assuming $\overline{T}_x$ to be constant, this transformation is straightforward, yielding

$$i\omega\tilde{T} = -\tilde{U}\,Q \tag{4.47}$$

where we denote the constant $\overline{T}_x\hat{p}(0)$ by Q, for simplicity. If $\overline{T}_x$ is not constant, a convolution of transforms appears on the right hand side. Multiplying (4.47) by its complex conjugate, using the stochastic assumption implied by (4.36) and expression (4.42) for $\Phi_u(\omega,k)$ quickly leads to

$$\Phi_T(\omega,k) = H_T(\omega,k)\Phi_F(\omega,k) \tag{4.48}$$

with

$$H_T(\omega,k) = \frac{Q^2\alpha^2}{c^4}\,\frac{1}{(\omega^2-\varepsilon^2-c^2k^2)^2+4\omega^2\varepsilon^2} = \frac{Q^2}{k^2}\,H_p(\omega,k) \tag{4.49}$$

where $\Phi_T(\omega,k)$ is the SST spectrum. The spectral density is seen to be red in frequency and wavenumber space, in relation to the wind forcing spectra as the form of the dynamic factor $H_T(\omega\ k)$ indicates.

We now have expressions for $\Phi_\zeta(\omega,k)$ and $\Phi_T(\omega,k)$ in terms of the zonal wind stress forcing $\Phi_F(\omega,k)$, from which we can estimate the threshold crossing statistics of the SL and SST anomaly fields we are modeling.

4.4 CONSIDERATIONS ON THE SL AND SST k-ω SPECTRA

Some useful general comments can be made about the spectra derived in the previous section, before discussing the wind field and any reasonable forms $\Phi_F(\omega\ k)$ might take.

A marked difference between the behavior of the dynamical factors H_ζ and H_T at low wavenumber is clearly present ($H_\zeta \to 0$ as $k \to 0$ in contrast with H_T). This fact is not surprising if we realize that SL depends on the zonal derivative of the forcing wind stress. For an unbounded ocean, no Kelvin waves are excited, if the zonal wind stress τ is uniform in x (see equation (4.26)). In contrast, H_T has a maximum at $\omega=k=0$. It is obvious that a constant velocity u would be the largest contributor to the variance of SST anomaly.

All the factors H_ζ, H_u, H_T have a peak along the line $\omega=ck$ on the ω-k plane, corresponding to the resonance which occurs when there is forcing at ω-k points satisfying the Kelvin wave dispersion relation. A large percentage of the SST and SL anomaly variance, is accounted for by these peaks. Along the line $\omega = ck$, the magnitude of the peaks is seen to decrease quickly to zero, as ω (or equivalently k) increases, for the case of H_T, while H_ζ asymptotes to a constant value as ω (or k) get large. This fact can be important when computing statistics of extremes for SL and SST fields,

because of the dependence of those statistics on the high frequency-wavenumber spectral shapes, as we have seen before.

Even though the model spectral Φ_ζ, Φ_T are defined for very large ω, k values, realistically, Kelvin wave dynamics will not be important in determining the spectral shapes of the ζ and u fields at frequencies shorter than a few days. At these high frequencies, gravity waves are more likely to be dynamically important. Different processes have their range of dynamical significance in shaping the spectral functions of u or ζ, and it is not the goal of this study to accomplish a complete and realistic description of Φ_u or Φ_ζ, with only the simple Kelvin wave dynamics. It will be, therefore, necessary, to use some frequency and wavenumber cutoffs, at least at high ω, k, to exclude the unrealistic effects Kelvin waves of periods shorter than a few days would have on the SL and SST extreme value statistics that we seek to extract from our model. The use of these cutoffs will also be necessary to avoid infinite spectral moments (e.g., the variance of SL, as defined by (3.3), is not finite if no cutoffs are used, for $\Phi_F(\omega,k)$ being a constant).

At very low frequencies (i.e., periods greater than a few years), the same motivation exists for introducing frequency and/or wave number cutoffs, although they are not needed to prevent infinite spectral moments. However, defining these cutoff values is more problematic and subtle, therefore we will try to avoid introducing them in our future analysis.

It is important to remember that, due to the pointed differences in the character of H_ζ and H_T, the effect of cutoffs on the computation of extreme value statistics for SL and SST will be drastically different (also depending on the assumed form for $\Phi_F(\omega,k)$).

The complete determination of the oceanic model spectra requires knowledge of $\Phi_F(\omega,k)$, which can introduce several features into Φ_ζ or consequently Φ_T. Any peaks in the forcing spectrum will translate into peaks in the oceanic spectra. Inhomogeneities in the wind spectrum (i.e., different ω or k dependences in different regions in ω-k space) will show up in the oceanic spectra. Despite the simplicity of the ocean dynamics involved, the forcing can produce complicated SL or SST spectral dependences, according to our model, even though we shall restrict ourselves here to simple spectral shapes for $\Phi_F(\omega,k)$. What we know about the zonal wind field in the equatorial regions is discussed next.

4.5 SPECTRAL CHARACTERISTICS OF THE ZONAL WIND STRESS FIELD IN THE EQUATORIAL PACIFIC

The importance of oceanic wind forcing in El Niño events has sparked an extensive effort to try to acquire better knowledge of the tropical Pacific wind field. A substantial number of papers have been published on the subject (e.g., Goldenberg and O'Brien (1981), Rasmusson and Carpenter (1982), Luther and Harrison (1984), Halpern (1985)), using ship, island and buoy wind records in the analysis. The specific details of the zonal wind records are not important, in our context. We may mention, however, some important features of the wind field, associated with ENSO events. The zonal wind anomalies occurring during El Niño years have a pronounced event like character (Luther et al. 1983) and the strongest anomalies occur after the first SST anomalies are observed (Luther and Harrison 1984). There is also an apparent variability of the wind field, if one looks at different El Niño years, at least away from the equator, and attempts to identify major areas of precursor winds, important for every event, are not very successful (Luther and Harrison 1984).

Rather than looking for specific space or time patterns of precursor winds, responsible for the onset of El Niño, our stochastic approach only requires that we know the ω-k spectra, Φ_F, of the forcing winds, especially at the time scales of interest, i.e. at periods longer than a few days. Furthermore, we are only after the rough dependence of Φ_F on ω, k.

A large number of frequency spectra of zonal wind stress have been published in the oceanographic literature. However, only in very few cases do the observations permit spectral estimates at periods greater than 1-2 years. The picture is much worse, when we look for wavenumber or frequency-wavenumber wind stress spectra, which are virtually nonexistent.

The only attempt at estimating the ω-k spectra of zonal wind (not wind stress), to my knowledge, was by Luther (1980). Considering the picture, any attempt to extract unambiguous information from this one case, is doomed to fail. However, something can be gained by being less ambitious and looking at the available ω, k spectral estimates.

There has been a tendency to find no significant interannual peaks in wind spectra, in some studies (e.g., Wyrtki and Meyers 1976). Goldenberg and O'Brien (1981) use ten years of ship wind data and try to see, among other things, whether or not, the ω wind spectra are white at low frequencies. They find this to be the case for periods $\geq$20 months, but their results are limited by the shortness of the records used. In fact, there may be strong aliasing in their spectral estimates because of sparse observations, as suggested by Luther and Harrison (1984).

Zonal wind stress spectra at periods $\lesssim$ 1 year are much more frequent in the literature. They are in general red, with variable ω dependences, but generally close to an ω^{-1} form in the range 1 year-days (e.g., see Luther 1980). A peak at 1 year is generally present in all spectra, showing the

strong annual variability of the tropical regions. It is hard to determine, without ambiguity, where the flattening of the ω spectra occurs, from the situation portrayed above. A reasonable guess seems to point for periods around 1-2 years, where the transition between white and ω^{-1} spectra takes place (Frankignoul and Müller (1979) assume whiteness for periods >10-20 days, in mid and high latitudes).

Estimates of the zonal wavenumber spectrum of the wind stress are extremely rare. Goldenberg and O'Brien (1981) use ship wind data to compute wind stress magnitude power spectra. They find red spectra with no statistically significant peaks, and slopes dependent on latitude and month. Halpern (1985) uses scatterometer data to find kinetic energy spectra with a k^{-2} slope, for wavenumbers between 4 and 60 degrees of longitude. The same dependence is found in mid-latitude atmospheric wavenumber spectra (Frankignoul and Müller 1979), even though a k^{-3} slope seems to be more appropriate for higher latitudes.

The lack of information on the relevant atmospheric spectra $\Phi_F(\omega,k)$ for this study is evident, especially for low frequencies and generally for all wavenumber bands. When picking a particular model for $\Phi_F(\omega,k)$, the scarce information available to us will be used, and some experimenting with different forcing spectra will be needed, in order to explore the uncertainties in the assumed form of $\Phi_F(\omega,k)$.

CHAPTER 5

MODEL SST AND SL EXTREME VALUE STATISTICS

We have developed, until now, the statistical model to deal with extreme values of random fields, and the very simple ocean model to describe the SL and SST anomaly fields in the equatorial region. We shall now put these two models together, in order to study the threshold crossing statistics governing SL and SST anomaly extremes.

5.1 DEFINING RANGE OF VALUES FOR MODEL PARAMETERS (e.g., FRICTION ε, SPECTRAL CUTOFFS)

Before we can assess the time and space scales associated with the extremes of our modeled SL and SST fields, we have to assign some values to a number of parameters arising in our model spectra. Most of these parameters have some definite arbitrariness, when it comes to assigning values to them. Since, as we will find out later, the statistics of extremes will be strongly dependent on the values of parameters such as the Rayleigh friction coefficient ε, we try to limit the most, the range of variation allowed to these parameters, when experimenting with our model. Let us look at each one of these parameters separately.

A - RAYLEIGH FRICTION COEFFICIENT

The constant ε represents the Rayleigh friction in our model, as discussed in section 4.3.

Kelvin waves are seen to propagate all the way from the western Pacific to the eastern boundary, at the normal speeds associated with first baroclinic modes ($\sim$1-3 m/s). Any upper bound on ε should allow for these waves to propagate a distance of 10000 km before decaying. The choice of spindown time (i.e., $1/\varepsilon$) will control the amount of friction in the model.

Gent et al. (1983), for example, take the spindown time to be 1 to 3 years. A spindown of 2 years (i.e., $\varepsilon = (1/2)\ yrs^{-1}$) and horizontal scales on the order of 300 km give horizontal eddy viscosities values around $10^7 cm^2/s$, compatible with the values used in numerical models (e.g., Philander 1981). We will take 3 years as a upper bound for the spindown time, while letting the lower bound be around 6 months. Thus, the range of variation of ε is given by

$$1.057 \times 10^{-8} s^{-1} < \varepsilon < 6.430 \times 10^{-8} s^{-1} \qquad (5.1)$$

B - HIGH FREQUENCY AND WAVENUMBER CUTOFFS

I already mention, in section 4.5, the need for introducing high frequency and wavenumber cutoffs, ω_o and k_o respectively, in order to have finite spectral moments and exclude extrenuous effects on the statistics of extremes, coming from very short time scales which are not damped enough with our frictional scheme. A sort of absolute frequency cutoff for oceanic motions would be the buoyancy frequency N, but we certainly don't want to allow Kelvin waves with periods of a few minutes to be present in our analysis. A better idea is to assume that atmospheric forcing at spatial scales less than the atmospheric Rossby radius will not be important in the generation of Kelvin waves. The atmospheric equatorial Rossby radius takes on values like 600 km-1300 km (Gill 1982). We use these scales in defining the wavenumber cutoff k_o to be

$$5.027 \times 10^{-6}\ rad\ m^{-1} < k_o < 1.068 \times 10^{-5}\ rad\ m^{-1} \qquad (5.2)$$

We may use now the dispersion relation $\omega = ck$ to get a value for ω_o consistent with our choice of k_o. The phase speed c is different for each mode, but a typical value for the first baroclinic mode is $c \sim 2.9$ m/s (see Eriksen et al. (1983) for a table of values of c_n). This value of c yields

$$1.463 \times 10^{-5}\ rad\ s^{-1} < \omega_o < 3.11 \times 10^{-5}\ rad\ s^{-1} \qquad (5.3)$$

equivalent to periods of roughly 2-5 days. The shortest period Kelvin wave allowed in our computations will change in this range. Another look at Table 2 presented in Eriksen et al. (1983) shows that the maximum period for first mode gravity waves is roughly 5 days. So, our assumption about ω_o is consistent with the expectation that, at periods less than a few days, gravity waves will become the most important part of the ocean response.

C - WIND STRESS SPECTRAL PARAMETERS

The available observational evidence suggests that at least in some high frequency range, we should allow for some structure in our forcing spectrum $\Phi_F(\omega,k)$. Using as a remote reason the claim of Frankignoul and Muller (1979), this spectrum could be white down to periods as short as 10 or 20 days. Denoting the transition frequency, at which $\Phi_p(\omega,k)$ changes character, by ω_T, we can take as its extreme upper bound the value corresponding to a period of 30 days. The choice of a lower bound for ω_T is even more arbitrary since there are very few spectral estimates at long periods assisting us on our choice. Even though the spectrum probably becomes white at periods of 1 year or so, we shall take a more conservative value for the lower bound on ω_T, corresponding to a period of 5 years. Thus, we have

$$3.985 \times 10^{-9} \text{ rad s}^{-1} < \omega_T < 2.513 \times 10^{-6} \text{ rad s}^{-1} \qquad (5.4)$$

The wide range of variation of ω_T simply reflects the ambiguity present in the observational evidence we have used and allows us to be on the safe side.

The extremely scarce wavenumber spectral estimates of wind stress strongly constrains our assumptions about $\Phi_F(\omega,k)$. We avoid introducing any k structure in $\Phi_F(\omega,k)$. The possible effects this assumption will have on our computed statistics of extremes will be the subject of speculation and discussion in a later section.

5.2 THRESHOLD CROSSING STATISTICS FOR SEA LEVEL

Before we actually compute the statistics of extremes, as defined in Chapter 2 and 3, for SL anomaly, let us consider some important points in our calculations.

To apply the general theory of statistics of extremes, we have to assume our field to be Gaussian distributed, which seems to be a reasonable assumption. If our random field is not normally distributed, then depending on the assumed pdf, the analysis would be more complicated. With our presumably Gaussian SL field, we may resort to expressions (4.3), (4.4), (4.5) and (4.6) to compute the return period or length and the mean time and distance of excursion of the SL field, above some threshold height, provided we can also compute the spectral moments involved in those expressions.

To calculate the various spectral moments, we need to specify values for the white noise level of $\Phi_F(\omega,k)$ and a number of other constants appearing as part of the dynamical factor H, including the depth of the mixed layer h_{mix} and the full ocean depth D. Instead of doing this, another approach is tried. We take as a definition of an extreme SL anomaly resemblant of El Niño conditions, a value of 2 standard deviations, whatever the actual value of σ might be. Wherever the ratio $b/\lambda_o^{1/2}$ appear on the statistical formulas, we simply replace it by its fixed value. If we do this, we are left with only ratios of moments which only depend on the actual shape of $\Phi_\zeta(\omega,k)$, but not on the constant factors we mentioned above. These factors cancel out of the calculations.

Since our SL spectrum (and in general all the others) is quadrant symmetric, the moment λ_{11} vanishes and the 2-D statistics simplify a little, as outlined in section 3.1 and mentioned in section 4.1. We can then compute the statistics of crossings in time or space, separately, and the

return time and length for zero crossings is given by (4.3) and (4.4) respectively. Because we have fixed the value of the ratio $b/\lambda_o^{1/2}$, the crucial parameter controlling the extreme value statistics is now $\nu_o^{\omega,+}$ and $\nu_o^{k,+}$ (i.e., the ratio of the variance of the derivatives ζ_t and ζ_x to the variance of SL anomaly, which determines the zero crossing statistics). The values of $\nu_o^{\omega,+}$, $\nu_o^{k,+}$ will vary, as we experiment with our spectral parameters (e.g. ε, ω_o, k_o or even spectral shape of $\Phi_F(\omega,k)$), but will be independent of the constants which are absorbed in the factor H_ζ in (4.41).

The SL power spectra specified in (4.40) represents the contribution of only one vertical mode. In general, a number of modes will be part of the ocean response to the forcing winds and they all contribute to the power spectrum. In our model, H_ζ carries a dependence on mode number which suggests a decreasing importance in the contributions of high n modes to the total power. Even the wind power input seems to corroborate this idea, as we have said when discussing the projection of the zonal wind stress onto the meridional basis functions (see equation (4.28)). In practice, only the first few modes are observed to propagate in the ocean. Certainly, the first and second baroclinic modes are predominant in the records (e.g., Eriksen et al. 1983). We will assume that only the first mode is present in our system, for simplicity, without being too unrealistic.

We need now to define a specific form for $\Phi_F(\omega,k)$. From what has been said about wind stress spectrum, we take the following form

$$\Phi_F(\omega,k) = C \qquad \omega < \omega_T \tag{5.5a}$$

$$= C\,\omega_T\omega^{-1} \qquad \omega > \omega_T \tag{5.5b}$$

where C is a constant whose value is not important to us, as we have seen above. The transition frequency ω_T is included in form (5.5b) to allow for continuity of $\Phi_F(\omega,k)$ at ω_T, and its value will vary as defined by (5.4).

Having defined the forcing spectrum $\Phi_F(\omega,k)$, the SL anomaly power spectrum becomes, from (4.40),

$$\Phi_\zeta(\omega,k) = \frac{C\,\hat{p}(0)\alpha^2}{g} \frac{k^2}{[(\omega^2-\varepsilon^2-c^2k^2)^2+4\omega^2\varepsilon^2]} \left(x \frac{\omega_T}{\omega} \text{ for } \omega > \omega_T\right) \qquad (5.6)$$

This spectral function is shown in Figure 7, for specific values of the parameters ε, ω_T and c. The general red character of $\Phi_\zeta(\omega,k)$ is evident, as well as the resonance peak along the line $\omega = ck$ and the decay to zero as $k\to 0$.

If we integrate (5.6) with respect to wavenumber k, we arrive at the frequency SL anomaly spectrum, $\Phi_\zeta(\omega)$, which can actually be compared with actual estimates, briefly discussed in section 4.2. The integration was done numerically for some values of ω, using routines available from NAG Library which are described in the NAG Library Manual (1984). The upper limit of integration, k_o, is chosen according to (5.2), with the lower limit being zero. The obtained SL power spectrum shape is shown in Figure 8. In the frequency range of interest, the structure of $\Phi_\zeta(\omega)$ is seen to be that of Φ_F. The shape of $\Phi_\zeta(\omega)$ is thus strongly dependent on the assumed frequency structure for Φ_F. Figure 8 shows that our spectrum $\Phi_\zeta(\omega)$ is in reasonable agreement with the general aspects of the available spectral estimates mentioned in section 4.2.

We now have to compute the spectral moments $\lambda_o, \lambda_2^\omega$ and λ_2^k to determine the parameters $\nu_b^{\omega,+}$, $\nu_b^{k,+}$ and all the other important statistical parameters involved in characterizing the extreme value patterns of our SL anomaly fields. The moments λ_o, λ_2^ω and λ_2^k, defined by expressions (4.1) or (3.3) will be determined up to a constant.

The double integrations necessary to find the spectral moments were done semi-analytically whenever possible. The first integral was calculated

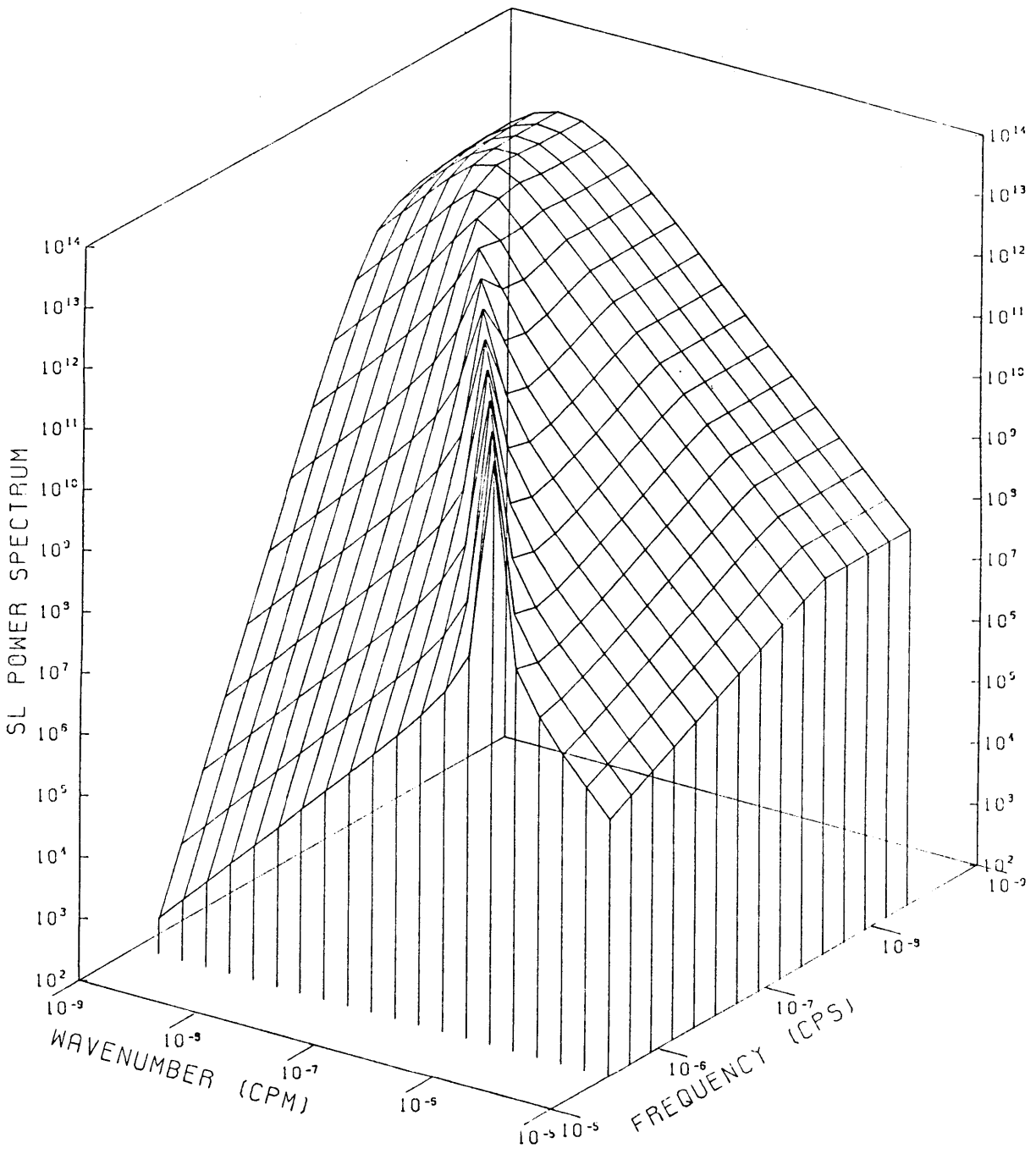

Figure 7. Plot of the analytical SL power spectrum $\Phi_\zeta(\omega,k)$, defined in expression (5.6). The values of $\Phi_\zeta(\omega,k)$ are not important (the constant in (5.6) was arbitrarily set equal to unity), only the shape is relevant. Here, we took $\omega_T \simeq 2\times10^{-7}$ rad s^{-1} (period of 1 year), a spindown time of 1 year and c = 2.91 m/s. Notice the presence of a resonance peak.

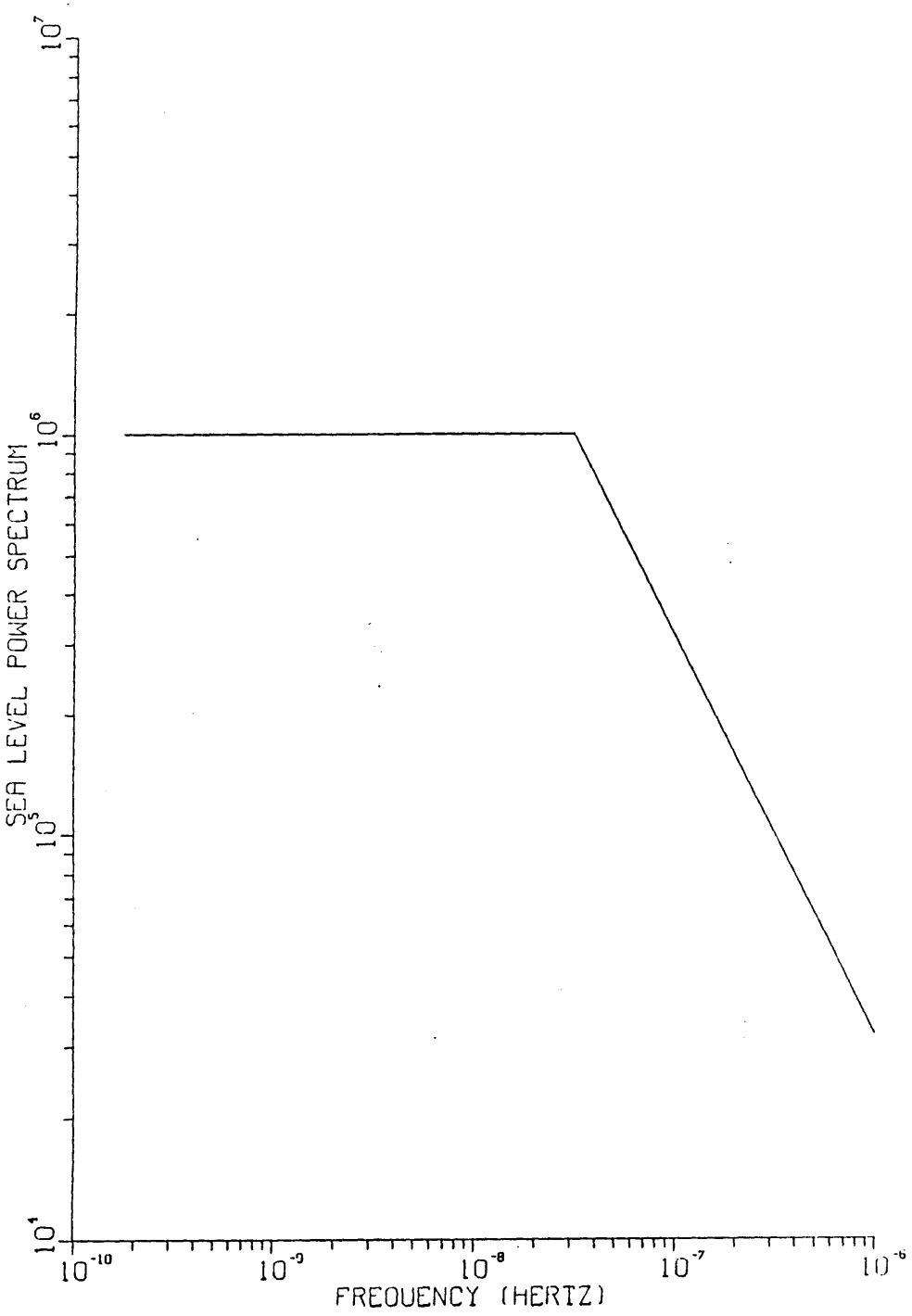

Figure 8. Plot of the analytical SL frequency power spectrum $\Phi_\zeta(\omega)$, obtained by integrating expression (5.6) with respect to k. Values of ω_T, ε and c are the same as in Figure 7. The values of $\Phi_\zeta(\omega)$ are not significant, only the shape is relevant. Notice the correspondence between the shape of Φ_ζ and the assumed shape of the forcing Φ_F, as defined by (5.5).

with the help of integrals in Gradshteyn and Ryzhik (1965), either in ω or k, as suitable. The algebra is tedious and won't be reproduced here. The second integral was computed using numerical integration routines available from NAG Library and described in NAG Library Manual (1984). When calculating λ_2^{ω}, in the range $\omega < \omega_T$, no available analytical formula was found, so double integration was performed using a recursive method (i.e., two one dimensional integration routines were used recursively). The frequency and wavenumber cutoffs, ω_o and k_o, were used as upper limits of integration, with the lower limits being zero in both dimensions. A number of different runs were performed, using different values for ω_o, k_o, ε and ω_T, to explore the ranges over which these parameters were allowed to vary, as expressed in (5.1)-(5.4). A value of c = 2.91 m/s, as given in Eriksen et al. (1983), was used in the calculations. This is a typical value for the phase speed of the first baroclinic Kelvin mode in the equatorial Pacific (see, e.g., Wunsch and Gill (1976)).

Once the spectral moments λ_o, λ_2^k and λ_2^{ω} were computed, finding the statistics of extremes for the SL anomaly field was straightforward. Values for the mean period for a zero upcrossing, $1/\nu_o^{\omega,+}$, and the mean period for an upcrossing of the 2 standard deviation (2σ) threshold, $1/\nu_{2\sigma}^{\omega,+}$, are obtained using the general expression (3.11) or the equivalent expression (4.3). The values for the mean distance between a zero upcrossing, $1/\nu_o^{k,+}$, and the mean distance between upcrossings of the 2σ threshold, $1/\nu_{2\sigma}^{k,+}$, are similarly obtained using (3.11) or (4.4). Expressions (3.12) and (3.13) or the equivalent expressions (4.5) and (4.6) easily give the mean time and the mean distance that SL will stay above the 2σ level, i.e., $\langle T_{2\sigma} \rangle$ and $\langle X_{2\sigma} \rangle$ respectively. A value of g(2) = 0.8429 is used, as tabulated in Vanmarcke (1983). Because λ_{11} vanishes in our case, the 2-D statistics are trivially

obtained from the 1-D time and space results. The mean area of excursion above the 2σ level, $\langle A_{2\sigma}\rangle$ is given by (3.14) or (4.7). Once $\langle A_{2\sigma}\rangle$ is known, the mean number of local maxima above 2σ per unit time, per unit distance, $\mu_{2\sigma}$, can be obtained from (3.18) with approximation (2.21) in place of $F^c(b)$ or from expression (4.8).

The results are presented in Table I, for different values of ω_o, k_o and ω_T. The parameters describing the temporal and spatial statistics of extremes are mean quantities defined as averages over infinite time and space coordinates. The real ocean has north-south boundaries and hence a finite zonal extent. Therefore, in practice, a perfect comparison of our spatial results with statistics computed from ocean records could never be realized, due to the inherent finiteness of the space domain. In reality, the same occurs when talking about the time statistics, since the available data always covers only a finite interval of time. The important difference is that the time domain can always be extended in practice by collecting data over longer periods of time, while that is not possible in the space domain. This fact is relevant when analyzing our statistical results. The interpretation of the spatial statistics is less reliable, especially if the expected values yielded from the theory are large compared with the spatial extent of the ocean (roughly 10000 km for the Pacific). We shall only use in our discussions the parameter $\langle X_{2\sigma}\rangle$, even though all 3 parameters dealing with the spatial statistics are given in Table I, for completeness.

Only results obtained with spindown time of 1 year are shown, since varying ε did not significantly change the results. This simply reflects the fact that the dependences of λ_o and λ_2^{ω} or λ_2^{k} on ε are roughly the same, thus rendering the values of $\nu_o^{k,+}$, $\nu_o^{\omega,+}$ rather independent of the value used for ε, at least within the limits specified in (5.1).

TABLE I

Statistics of extremes for SL, for spindown time of 1 year and various values for ω_T, ω_o and k_o

a) $\omega_o = 1.463 \times 10^{-5} s^{-1}$
$k_o = 5.027 \times 10^{-6} m^{-1}$

	Time			Space			2-D	
$2\pi/\omega_T$ (months)	$1/\nu_o^+$ (days)	$1/\nu_{2\sigma}^+$ (days)	$\langle T_{2\sigma} \rangle$ (days)	$1/\nu_o^+$ (km)	$1/\nu_{2\sigma}^+$ (km)	$\langle X_{2\sigma} \rangle$ (km)	$\langle A_{2\sigma} \rangle$ (km-days)	$\mu_{2\sigma}$ (km^{-1} day^{-1})
60	18.5	137	3.12	1351	9986	227	708	3.212×10^{-5}
30	17.6	130	2.96	1364	10081	229	678	3.354×10^{-5}
12	16.2	120	2.73	1388	10253	233	637	3.572×10^{-5}
2	13.1	97	2.21	1482	10949	249	550	4.136×10^{-5}

b) $\omega_o = 3.11 \times 10^{-5} s^{-1}$
$k_o = 1.068 \times 10^{-5} m^{-1}$

	Time			Space			2-D	
$2\pi/\omega_T$ (months)	$1/\nu_o^+$ (days)	$1/\nu_{2\sigma}^+$ (days)	$\langle T_{2\sigma} \rangle$ (days)	$1/\nu_o^+$ (km)	$1/\nu_{2\sigma}^+$ (km)	$\langle X_{2\sigma} \rangle$ (km)	$\langle A_{2\sigma} \rangle$ (km-days)	$\mu_{2\sigma}$ (km^{-1} day^{-1})
60	9.2	68	1.54	631	4661	106.1	164	1.387×10^{-4}
30	8.8	65	1.47	636	4696	106.9	157	1.449×10^{-4}
12	8.2	60	1.37	644	4757	108	148	1.537×10^{-4}
2	6.8	50	1.14	674	4977	113	130	1.75×10^{-4}

The dependence of the results on ω_T is also very weak, but because the range of variation of ω_T is large (see (5.4)), substantial changes occur on the results and thus, we have given in Table I, the statistics obtained for different values of ω_T. A 30-fold change in ω_T results in a less than 1.5-fold change in the computed statistics. In general, the time statistics are more affected by ω_T than the space statistics, an expected feature since ω_T directly controls the shape of $\Phi_\zeta(\omega)$ at high frequencies, as seen in Fig. 8, while its effect on $\Phi_\zeta(k)$ is more spread out. This leads to a stronger dependence of $\overset{\omega}{\lambda}_2$ on ω_T than $\overset{k}{\lambda}_2$ and thus, to the different behavior of the space and time statistics, when ω_T is varied. Notice that an increase in ω_T causes $1/\overset{\omega,+}{\nu}_o$ to decrease, while $1/\overset{k,+}{\nu}_o$ increases. Since all the moments λ_o, $\overset{k}{\lambda}_2$ and $\overset{\omega}{\lambda}_2$ increase with ω_T, we conclude that the most affected by changes in ω_T is $\overset{\omega}{\lambda}_2$, with the least affected being $\overset{k}{\lambda}_2$.

The important parameters which seem to have a stronger effect on our results are the frequency and wavenumber cutoffs, ω_o and k_o, respectively. The cutoffs are crucial in determining the second order moments, but not so influential in the calculation of the variance λ_o. This differential dependence of the spectral moments on ω_o, k_o is what makes these parameters important in this context. The statistical results clearly suggest that $\overset{k,+}{\nu}_o$, $\overset{\omega,+}{\nu}_o$ go roughly as $(\omega_o k_o)^{1/2}$ for the ω_o and k_o ranges defined by (5.2) and (5.3).

The dependences of the statistical results discussed above can not be generalized to different areas of parameter space (i.e., k_o, ω_o, ε, ω_T) because of the complex, nonlinear, interdependence of all these parameters. For example, the importance of cutoffs ω_o, k_o on the moment calculations is dependent upon the redness of our spectrum, which is a function of ω_T. In

general, this complexity increases in proportion to the number of parameters and the irregularity of the spectral shapes.

The time and space scales of SL anomaly excursions above 2σ emerging from the computed statistics presented in Table I, are somewhat shorter than the scales usually associated with ENSO events and discussed in section 4.2. The return times for crossings of the 2σ threshold are at most 5 months, while the frequency of El Nino events is more like one every 4 years. The mean time SL will stay above this 2σ threshold is at most roughly 3 days in contrast with persistence of SL anomalies of that magnitude over a few months when El Nino happens. Similarly the distances over which SL anomaly exceeds 2σ, of the order of 200 km, are an order of magnitude smaller than what is observed during ENSO in the equatorial region. Assumption of any higher threshold (e.g., 3σ or 4σ) would yield much longer return periods. In fact, the return period $1/\nu_b^{\omega,+}$ increases in an exponential fashion, like the term $\exp\{b^2/2\sigma^2\}$. However, the time and space scales, $\langle T_b \rangle$ and $\langle X_b \rangle$, as defined in (4.5) and (4.6), would only get smaller.

The 2-D statistical parameters $\langle A_{2\sigma} \rangle$ and $\mu_{2\sigma}$ simply reflect the nature of the extremes for the unidirectional space and time processes. Their interpretation is clear. If, for example, we take the case where $2\pi/\omega_T$ = 60 months and ω_o, k_o are smallest, since every 9986 km we expect to see the SL signal above the 2σ level and each excursion will take 3.12 days, in the mean sense, we should expect one excursion region for an area (9986)(3.12) km-day. The inverse of this is just the value of $\mu_{2\sigma}$. The mean area of excursion $\langle A_{2\sigma} \rangle$ is 708 km-day. Even though this does not say whether the excursions take place over 10 km-70 days or over 700 km-1 day, we know from the values of $\langle T_{2\sigma} \rangle$ and $\langle X_{2\sigma} \rangle$ that the most probable situation will be one

in which the excursion will occur for a few days and over a distance of the order of 200 km, which is the rough magnitude of $\langle X_{2\sigma} \rangle$. We should keep in mind that all the results given by the theory refer to mean values and it is in this sense that they should be interpreted.

At any rate, we have a SL anomaly field which crosses the 2σ threshold much more frequently than the observed El Niño signal, with each event lasting only a few days and spanning only a few hundred kilometers, in the mean, contrasting with El Niño conditions. The clustering effect discussed in section 2.3 could be responsible for these effects, if the crossings occurred in tightly packed clusters. This does not seem to be the case here, since our SL spectrum is fairly wide-band, nor does the observational evidence support a narrow-band SL signal, despite the scarcity of data.

5.3 THRESHOLD CROSSING STATISTICS FOR SST

We now analyze our model SST anomaly spectra, in light of what we have just done for the SL anomaly field. Much of the strategy used in the previous section when computing extreme value statistics of our SL field, can be applied here.

The assumption of normality of the SST field is still made, with no particular evidence on the contrary. Most of the SST records available do not allow for a representative test of normality, because of the very few independent points provided to test the normal hypothesis.

We still fix the value of b/σ to be 2, and let the various parameter ranges be defined as in section 5.1. We may expect their influence on the SST statistics to be different than in the previous section by the simple fact that the SST spectrum is different from $\Phi_\zeta(\omega,k)$. Maintaining the same forms (5.5a,b) for the power density of the forcing, $\Phi_F(\omega,k)$, then from (4.48) and (4.49), the SST spectrum $\Phi_T(\omega,k)$ is given by

$$\Phi_T(\omega,k) = \frac{C\ Q^2\alpha^2}{c^4} \frac{1}{(\omega^2-\varepsilon^2-c^2k^2)^2+4\omega^2\varepsilon^2} \left(x \frac{\omega_T}{\omega} \quad \text{for} \quad \omega > \omega_T\right) \quad (5.7)$$

This function is shown in Figure 9. The resonance peak is still present as in the case of $\Phi_\zeta(\omega,k)$ (Fig. 7), but now the redness character is much more pronounced in wavenumber as expected if we compare the forms of (5.6) and (5.7). The flattening of $\Phi_T(\omega,k)$ at low k, ω differs markedly from the decaying behavior of $\Phi_\zeta(\omega,k)$, as $k \to 0$.

Integration of (5.7) over k can be done analytically, with the help of integrals given in Gradshteyn and Ryzhik (1965), to obtain the SST frequency spectrum $\Phi_T(\omega)$, which is shown in Figure 10. The spectral function $\Phi_T(\omega)$ also compares reasonably well with the general characteristics present in available spectral estimates of $\Phi_T(\omega)$, which were briefly discussed in section 4.2, just as it was found with our analytical form for $\Phi_\zeta(\omega)$.

Having defined the function $\Phi_T(\omega,k)$ we can proceed to compute the SST statistics of extremes. The constant factor appearing in (5.7) is not important in our calculations, just as in the SL computations. We will take again only the contribution of the first baroclinic mode to the power density, with the value of c = 2.91 m/s.

The spectral moments, λ_o, $\overset{\omega}{\lambda_2}$ and $\overset{k}{\lambda_2}$, of $\Phi_T(\omega,k)$ were computed semi-analytically. Either the integration over k or over ω was performed with the help of integrals given in Gradshteyn and Ryzhik (1965). The remaining integral was calculated numerically using the available routines described in the NAG Library Manual (1984). The moments were used to detemine the different statistical parameters of interest. Several runs were done to explore the dependence of the SST statistics on parameters ε, ω_T, ω_o and k_o.

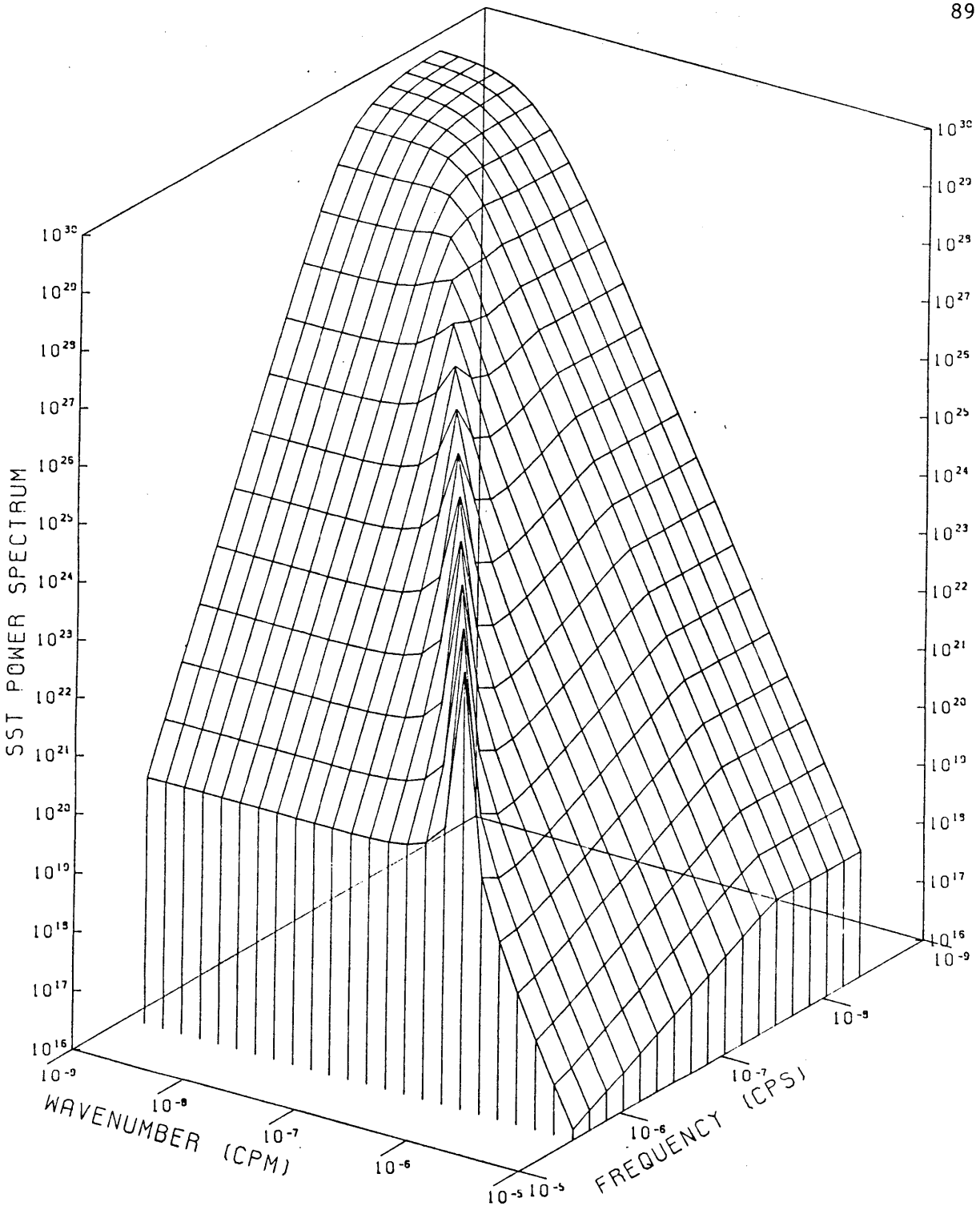

Figure 9. Plot of the analytical SST power spectrum $\Phi_T(\omega,k)$, defined in expression (5.7) (as in Fig. 7). Notice the presence of a resonance peak and the flattening at low ω,k.

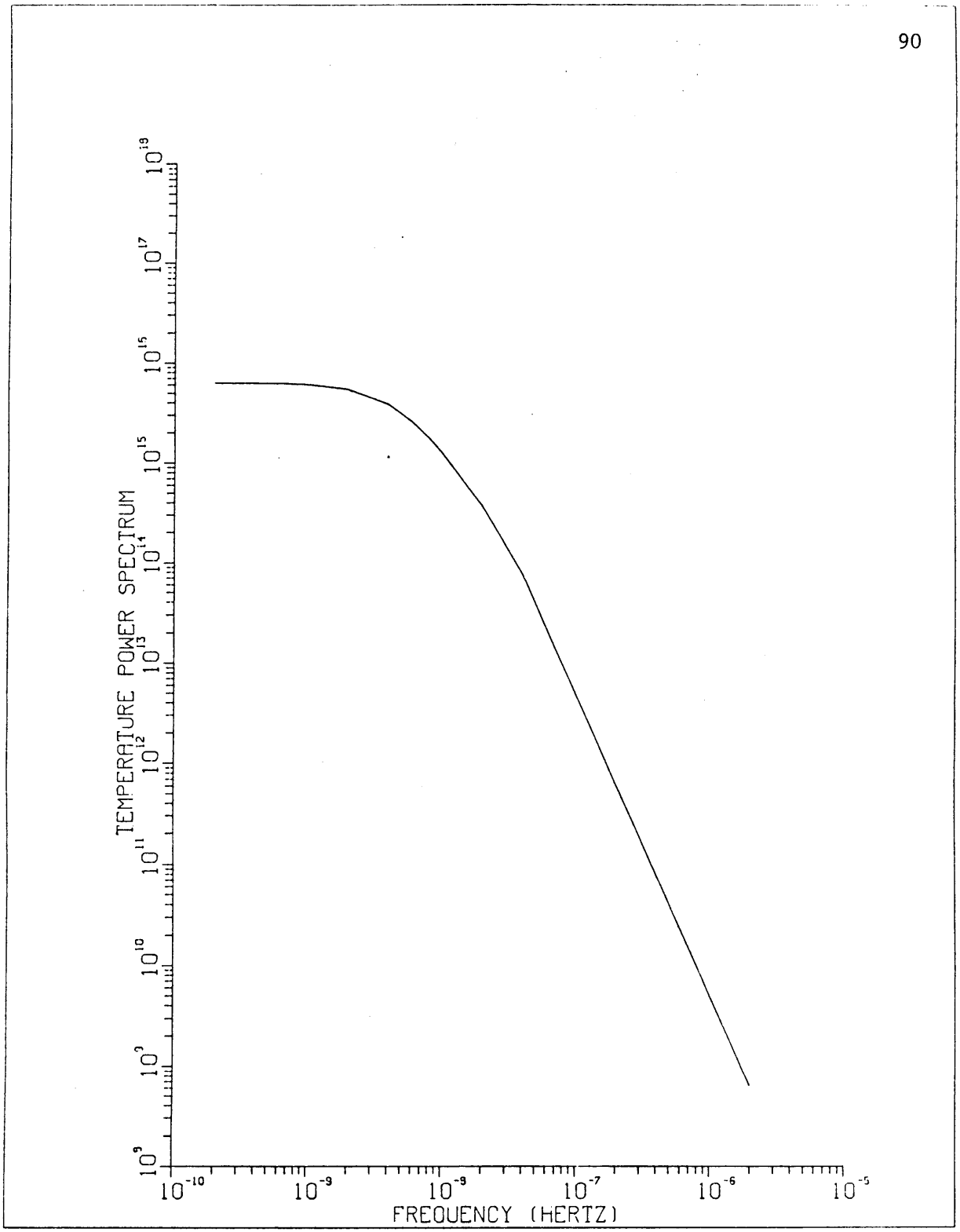

Figure 10. Plot of the analytical SST frequency power spectrum $\Phi_T(\omega)$, obtained by integrating expression (5.7) with respect to k. Values of ω_T, ε, and c are as in Figure 7. Only the shape of the spectrum is significant.

Table II summarizes the obtained SST extreme value statistics. In contrast with the SL case, changes in cutoffs ω_o and k_o had negligible effects on the statistics and therefore, only results for cutoffs at wavelengths of 600 km and periods of roughly 2 days are shown in Table II. This relative irrelevance of ω_o and k_o to the statistics is expected due to the redder character of $\Phi_T(\omega,k)$ when compared with $\Phi_\zeta(\omega,k)$.

The dependence of the statistical results on parameters ε and ω_T is strong and highly visible from Table II, since these parameters are allowed quite a bit of variation. The frequency ω_T now controls more effectively the values of $\overset{k}{\lambda}_2$ and $\overset{\omega}{\lambda}_2$. This is easily seen if we notice that as ω_T increases, both $1/\nu_o^{\omega,+}$ and $1/\nu_o^{k,+}$ decrease, which together with the fact that all the moments increase with ω_T, leads to the conclusion that ω_T affects more the moments $\overset{k}{\lambda}_2$ and $\overset{\omega}{\lambda}_2$ than λ_o. Similar reasoning may be used to see that the friction coefficient ε is more influential in determining λ_o. The ratio $\overset{k}{\nu}_o/\overset{\omega}{\nu}_o \sim \overset{k}{\lambda}_2/\overset{\omega}{\lambda}_2$ is observed to decrease as ω_T increases, therefore meaning a stronger effect of ω_T on $\overset{\omega}{\lambda}_2$, which is expected since ω_T affects the frequency structure of $\Phi_T(\omega,k)$ directly.

The time and space SST statistical results shown in Table II (and other results not presented here) suggest a dependence on ω_T and ε which is less then linear. Again, different regions of parameter space may yield different dependences, but at least in our range, the values of $\nu_o^{k,+}$ and $\nu_o^{\omega,+}$ vary as ω_T^p and ε^p, with $p < 0.5$ in general.

The time and space scales for crossings of the 2σ threshold by our model SST anomaly field are much larger than our SL results from the previous section. There is also a bigger spread in scales arising from the sensitivity of the SST statistics to the factors ω_T and ε which are allowed to change significantly. As a general trend, the shorter the spindown time

TABLE II

Statistics of extremes for SST, with $\omega_o = 1.463 \times 10^{-5} s^{-1}$ and $k_o = 5.027 \times 10^{-6} m^{-1}$. Units are the same as in Table I

a) $\varepsilon = 6.342 \times 10^{-8} s^{-1}$ (spindown ~6 months)

	Time			Space			2-D	
$2\pi/\omega_T$ (months)	$1/\nu_o^+$ (days)	$1/\nu_{2\sigma}^+$ (days)	$\langle T_{2\sigma} \rangle$ (days)	$1/\nu_o^+$ (km)	$1/\nu_{2\sigma}^+$ (km)	$\langle X_{2\sigma} \rangle$ (km)	$\langle A_{2\sigma} \rangle$ (km-days)	$\mu_{2\sigma}$ (km^{-1} day^{-1})
60	610	4511	102	1.4×10^5	1×10^6	2.3×10^4	2.3×10^6	9.7×10^{-7}
30	491	3626	83	1.1×10^5	8.4×10^5	1.9×10^6	1.6×10^6	1.4×10^{-6}
12	350	2584	59	8.4×10^4	6.2×10^5	1.4×10^4	8.3×10^5	2.7×10^{-6}
2	174	1289	29	4.3×10^4	3.2×10^5	7.3×10^4	2.1×10^5	1.1×10^{-5}

b) $\varepsilon = 1.057 \times 10^{-8} s^{-1}$ (spindown ~3 years)

	Time			Space			2-D	
$2\pi/\omega_T$ (months)	$1/\nu_o^+$ (days)	$1/\nu_{2\sigma}^+$ (days)	$\langle T_{2\sigma} \rangle$ (days)	$1/\nu_o^+$ (km)	$1/\nu_{2\sigma}^+$ (km)	$\langle X_{2\sigma} \rangle$ (km)	$\langle A_{2\sigma} \rangle$ (km-days)	$\mu_{2\sigma}$ (km^{-1} day^{-1})
60	1665	1.2×10^4	280	4.1×10^5	3×10^6	6.8×10^4	1.9×10^7	1.2×10^{-7}
30	1254	9263	211	3.1×10^5	2.3×10^6	5.2×10^4	1.1×10^7	2.1×10^{-7}
12	863	6373	145	2.2×10^5	1.6×10^6	3.6×10^4	5.2×10^6	4.3×10^{-7}
2	426	3146	72	1.1×10^5	7.9×10^5	1.8×10^4	1.9×10^6	1.8×10^{-6}

(i.e., the bigger ε) and the whiter the SST spectrum (i.e., the bigger ω_T), the smaller the space and time scales become and vice versa. Physically, stronger friction (Rayleigh type) in the system effectively drives the variance down, while a white spectrum enhances the importance of rapid (short period or short wavelength) fluctuations on the excursions above high thresholds. These two effects combine to give the lowest values for the mean period or distance between zero upcrossings. With spindown time around 6 months and the wind stress spectrum white down to periods of 2 months, excursions over the 2σ level occur every 3 to 4 years and last for a month over distances on the order of 7000 km. This is a typical situation during El Niño. In contrast, for a spindown time of 3 years and $\Phi_F(\omega,k)$ white down to periods of 5 years only, it would take 32 years in the mean for an "event" to take place, lasting over 9 months and covering a distance of 18000 km. As a naive comparison with ENSO conditions, we would say that our "events" occur less frequently but last longer than the observed records in the equatorial Pacific, generally speaking.

The frequency of occurrence of crossings above some threshold is critically dependent on whether our threshold is two or any other number of standard deviations. On the other hand, $\langle T_b \rangle$ and $\langle X_b \rangle$ are not so sensitive to our assumption about the crossing threshold. Thus, these later values are in a sense more reliable than the computed return times.

5.4 COMPARISON OF SL AND SST EXTREME VALUE STATISTICS

The discrepancy between the space and time scales for the extreme values of our SL and SST fields is readily seen by comparing results presented on Tables I and II. This discrepancy is more or less implicit in the different forms the spectral densities Φ_ζ and Φ_T take. For example, the sharp peak at the origin $\omega=0$, $k=0$ which is a dominant feature of Φ_T is not

present in Φ_ζ, for reasons related to the dynamical factors H, as discussed in section 4.4. This difference is likely to affect the values obtained for the variance λ_o, since this moment is very sensitive to what goes on at the low ω, small k region of the spectrum, for the case of generally decaying (red) spectral shapes. The SST variance λ_o will be larger than for SL, relatively speaking, and the ultimate effect of this is to drive the extreme value space and time scales up for the case of SST. In essence, the shapes of Φ_ζ and Φ_T imply that the ratio of the power present at low ω-small k to the power present at higher ω and k is bigger for the case of SST than for SL (see Fig. 7 and 9). This is even more clear if we recall what was said before about the different behavior of the factors H_ζ and H_T (see (4.41) and (4.49)), as we move along the line $\omega = ck$ in ω-k plane, which defines the resonant peaks (see section 4.4). The fact that H_ζ asymptotes to a constant value as ω (or k) gets large along that line enhances the power present at high ω-k regions of the spectrum, while the decay of H_T under the same conditions leads to the opposite effect. An obvious effect of this spectral feature is to increase the variance of the derivative processes in general. A more "wiggly" process (SL in our case) is certainly expected to cross any high threshold more often than a smoother (smaller λ_2^k, λ_2^ω) process, with smaller excursion areas associated with each event in general.

The considerations stated above make us think whether the discrepancy in the extreme value scales of SL and SST is only the result of some artificial assumption we have made or whether it is a result of any intrinsic feature of the SL and SST spectrum which we have reproduced correctly with our analytical model. Actually, no such major differences in the SL and SST signals associated with El Niño events are observed in the equatorial Pacific and, despite the poor area coverage at some regions, it

is hard to believe that a finer observational network should reveal a much different picture from what is known today in this respect. Thus we are led to consider the effects of our basic assumptions which differentially affect the spectra Φ_ζ and Φ_T.

It is obvious that the model used for the forcing spectrum $\Phi_F(\omega,k)$ is crucial in determining the overall shape of Φ_ζ and Φ_T. The form (5.5) chosen for Φ_F is certainly quite arbitrary, especially in relation to the lack of structure in wavenumber k. Some of the sharp differences in the SL and SST results can actually be accounted for by this less realistic feature of our stochastic forcing model. The importance of the strong peak at k=0, ω=0, present in Φ_T, can be severely attenuated by assuming for example that no forcing is available at wavelengths longer than a certain cutoff value. Frankignoul and Müller (1979), for example, assume a k^2 dependence of $\Phi_F(\omega,k)$ for $k < k_L$ and a k^{-2} dependence for $k > k_L$ in modeling wind forcing at mid-latitudes, based on actual estimates of the wind stress spectrum. We may expect any of these modifications to affect the previous SL and SST results in a much different way due to the different character of the dynamical factors H_ζ and H_T.

Let us illustrate the sensitivity of SST statistics to a simple change in the k structure of Φ_F. We shall take the same form (5.5) for Φ_F but now we don't have any forcing for $k < k_L$, where k_L is our cutoff. We may take k_L to be equivalent to a wavelength on the order of the perimeter of the earth at the equator, which is roughly equal to 40000 km. Thus, we have

$$k_L = 2 \times 10^{-7} \text{ m}^{-1}$$

A more conservative estimate could be taken if we disregarded forcing at spatial scales longer than the width of the equatorial Pacific basin (~10000 km).

The statistical results for SST, computed using the slightly different Φ_F, are shown in Table III. Only the parameters $\langle T_{2\sigma} \rangle$ and $\langle X_{2\sigma} \rangle$ are presented this time. A comparative look at Table II reveals the importance of the modification of Φ_F to the SST extreme value statistics. The mean time and mean distance spent above threshold 2σ are roughly an order of magnitude smaller than the values computed before. We may also notice that now the parameter ω_T is not critical in determining the SST statistics as it was found before. It appears to become slightly more important at its higher ranges. Similarly, parameter ε is not so important in the statistical results. These dependences of SST statistics on ω_T and ε resemble the situation found for SL in section 5.2.

The modification introduced in Φ_F here has little effect on SL statistical results not only because $\Phi_\zeta(\omega,k) \to 0$ as $k \to 0$ even if we don't use any lower wavenumber cutoff in the forcing spectrum, but also because the statistics are less sensitive to what happens at the low ω,k parts of the spectrum $\Phi_\zeta(\omega,k)$ in general. The SST scales shown in Table III are more consonant with the SL scales in Table I and the large discrepancy observed before is simply accounted for by making the wind forcing more realistic. Obviously, this is done at the cost of bringing a new parameter k_L into the analysis. The arbitrariness of k_L and the extreme sensitivity of the model SST results to its assumed value is a rather unfortunate combination. We thus have to be cautious when interpreting our results. Results in Table III stand more like an example, to show the delicacy actually involved in our assumptions about $\Phi_F(\omega,k)$.

TABLE III

Statistics of extremes for SST, with no forcing at $k < 2\times10^{-7}m^{-1}$ (values of ω_o, k_o and units are as in Table II)

a) $\varepsilon = 6.342\times10^{-8}s^{-1}$

$2\pi/\omega T$	$\langle T_{2\sigma}\rangle$	$\langle X_{2\sigma}\rangle$
60	12	2735
30	11.6	2691
12	11.1	2625
2	8.4	2063

b) $\varepsilon = 1.057\times10^{-8}s^{-1}$

$2\pi/\omega T$	$\langle T_{2\sigma}\rangle$	$\langle X_{2\sigma}\rangle$
60	10.5	2593
30	10.4	2583
12	10.3	2570
2	8.3	2082

5.5 INTERPRETATION OF THE MODEL SL AND SST STATISTICS IN THE LIGHT OF OCEANIC CONDITIONS DURING EL NIÑO

We have seen that, for reasonable forms of $\Phi_F(\omega,k)$, the time and space scales for SL and SST excursions above the 2σ threshold obtained with our model can vary a great deal, but are in general smaller than El Niño scales, observed to be on the order of a few months and several thousand kilometers. Our "events" occur more frequently than the mean 3 to 4 year spacing between El Nino happenings. The reliability of these results is weak. Had we looked at events defined by a ratio $b/\sigma = 3$ instead of $b/\sigma = 2$, the return times would grow by a factor of 12, while the values of $\langle T_b \rangle$ and $\langle X_b \rangle$ would be reduced by 2/3.

Assuming that the SL and SST fields are really Gaussian processes, our statistical results can only be changed by modifying the spectral density functions which we have used in computing our extreme value statistics. This can be done in two ways, either by changing the ocean model dynamics and/or thermodynamics or by changing the forcing wind spectrum. The effects of any such modifications on the SL statistics may be very different than the effects on the SST statistics.

There is a certain appeal for using our simple ocean model, discussed in section 4.3, in conjunction with the form (5.5) for the forcing spectrum $\Phi_F(\omega,k)$, as we have argued previously. In fact, the model yields reasonable forms for $\Phi_\zeta(\omega,k)$ and $\Phi_T(\omega,k)$, as shown in Figures 7 and 9. Furthermore, the model SL and SST frequency spectra, shown in Figures 8 and 10, compare reasonably well with available estimates. However, there is still a lot of room for different dynamics, thermodynamics and forcing spectra to be tried.

Although our dynamical and thermodynamical model tries to capture some of the basic ingredients which actually make an El Niño event happen, it is

by no means complete, and its results have to be interpreted accordingly. Some of the important, realistic elements left out of our simple ocean model are discussed in a later section, even though their effects on the shapes of Φ_ζ and Φ_T are subtle.

Turning to the possible changes in the forcing wind spectra, a lot more experimenting with spectral forms of Φ_F could have been tried, namely to include some wavenumber dependence of the form k^{-p} (p is arbitrary), instead of only introducing the cutoff k_L. As an easy illustration, consider the following form for the forcing function

$$\Phi_F(\omega,k) = C\, k^{-2} \qquad \omega < \omega_T,\ k > k_L \qquad (5.8a)$$

$$= C\, k^{-2}\omega_T\omega^{-1} \qquad \omega > \omega_T,\ k > k_L \qquad (5.8b)$$

We have just introduced a k^{-2} dependence for $k > k_L$ and set $\Phi_F(\omega,k) = 0$, for $k < k_L$, with k_L and ω_T defined as in section 5.3. A k^{-2} dependence is reasonable in light of what has been previously said about the known spectral estimates of the wind stress. With this forcing spectrum, the expression for $\Phi_\zeta(\omega,k)$ becomes identical to the form $\Phi_T(\omega,k)$ used to compute SST results given in Table III, i.e., the SL statistics for Φ_F given by (5.8) are the same as the statistics given in Table III. A considerable increase in the space and time scales of SL statistics results from using (5.8) instead of (5.5) in the statistical calculations, and even though we did not compute the new SST statistics using (5.8), we would expect the SST values of $\langle T_{2\sigma}\rangle$ and $\langle X_{2\sigma}\rangle$ to go up in a similar manner. We may say that the general effect of having $\Phi_F \sim k^{-p}$ for some range of wavenumbers is to increase the spatial and temporal scales for the excursions. Such a redder wind stress spectrum would primarily limit the power at high wavenumbers, driving the values of λ_2^k (and also λ_2^ω indirectly) down and therefore increasing the values of $1/\nu_o^{\omega,+}$ and $1/\nu_o^{k,+}$, if the variance λ_o were not

affected much (true where most of the variance is contained in the low ω, small k part of the spectrum). Again, the differential dependence of λ_o and λ_2^k and λ_2^ω on the spectral shape is what matters here and it can be fairly complicated for general spectra.

There is also room for trying different ω dependences for Φ_F. An ω^{-2} shape for $\omega > \omega_T$ is certainly very reasonable considering the observational evidence available, but the general trend for increasing $\langle T_{2\sigma} \rangle$ and $\langle X_{2\sigma} \rangle$ is still true.

Introducing more redness in the forms of $\Phi_F(\omega,k)$ leads undoubtedly to increased values for the parameters $\langle T_{2\sigma} \rangle$ and $\langle X_{2\sigma} \rangle$ for both SL and SST. How red should the spectra Φ_ζ and Φ_T be in order to give extreme value statistics compatible with El Niño observations? Using the same ocean model which yielded the forms (4.41) and (4.40) for Φ_ζ and Φ_T respectively, it seems reasonable to say that a forcing spectrum of the form (5.8) would be sufficient to make the results more compatible with El Niño observations. However, we should keep in mind that the use of (5.8) instead of (5.5) would make $\Phi_\zeta(\omega)$ and $\Phi_T(\omega)$ redder than as shown in Figures 8 and 10, leading to disagreement with most of the available estimates of these two frequency spectra. This constraint, provided by observational evidence on the shapes of $\Phi_\zeta(\omega)$, $\Phi_T(\omega)$, is important when experimenting with different spectral shapes of Φ_ζ and Φ_T.

5.6 A POSSIBLE REINTERPRETATION OF OUR SL AND SST STATISTICAL RESULTS

In light of our previous findings, we offer in this section a reinterpretation of our statistical results.

Even though small by El Niño standards, the values of $\langle X_{2\sigma} \rangle$ and $\langle T_{2\sigma} \rangle$ obtained here and presented in Tables I and III are still significant. The model's ability to produce extensive SST anomalies is apparent. There is a

marked tendency for the spatial scales of excursions to more closely resemble El Niño conditions, especially for SST. This is in fact important, if we bring into consideration feedback effects between the atmosphere and the ocean. These air-sea interaction processes are thought to have a strong role in prolonging the SST and SL extreme conditions during El Niño. The massive collapse of the trades over the central and western Pacific is usually associated with the weakening of the Walker circulation, which occurs when the normal east-west mean SST gradient (cold in the east and warm in the west) is disturbed by appearance of warm SST anomalies in the east. The strongest anomalies in the zonal winds take place after the advent of SST anomalous conditions (Luther and Harrison 1984). The forcing of tropical atmospheric wind anomalies by SST patterns has been found to be important in the theoretical studies of Gill (1980) and Zebiak (1984). In light of this, our stochastically forced SST anomalies may represent the right conditions to trigger a longer event by feedback mechanisms. Anomalies of 2σ over regions of 2000 km and for periods of 10 days seem to be enough large scale to induce significant disruptions in the wind field. Randomly forced SST anomalies may be crucial in triggering El Niño events by feedback mechanisms.

5.7 IMPORTANT MISSING ELEMENTS OF OUR MODEL

The ocean model which we have used here for the purpose of studying the large scale SL and SST signal in the equatorial Pacific is obviously oversimplified. A lot of important features of the real ocean are grossly represented in our model or totally absent in most cases.

The absence of meridionally oriented coasts in our unbounded ocean is very convenient to simplify the dynamics. The effect of coasts is generally two-fold: it adds the reflected waves to the dynamical fields; and it

eliminates from the signal the waves which would be forced in the "outside" regions and propagate into the basin. The reflection of equatorial trapped waves off meridional coasts is contemplated by Moore and Philander (1978). It requires the full set of available equatorial wave motions, to satisfy the boundary conditions of no flow at the coasts. A Kelvin wave model is insufficient to treat this problem. Coasts can support east-west SL gradients and make the oceanic response to constant winds very different from an unbounded ocean. They may be a factor in intensifying the anomalies close to the boundaries as it is generally seen, for example, in Wyrtki's maps of SL anomaly (Wyrtki and Nakahara 1984, Wyrtki 1984). Coastal upwelling normally occurring at the Peruvian coast is certainly important for the pattern of SST anomalies in the eastern Pacific, but the inclusion of this process can not be considered in any simple model. It is hard to tell the effect that coasts would have in the model SL and SST statistics (i.e., in the shapes of $\Phi_\zeta(\omega,k)$ and $\Phi_T(\omega,k)$).

The equatorial current system is fairly complicated and strongly differs from the resting basic state one normally assumes. The mean state of these currents (south and north equatorial currents, equatorial countercurrent and the undercurrent) is disturbed by the equatorially trapped waves propagating in the Pacific, but other effects can produce departures from the mean state, like changes in the curl of the wind stress. These effects are not captured in a wave model. The advection processes seen to be involved in creating SST anomalies are probably more complicated in presence of the mean currents, even though the onset stages of warm SST anomalies in the central Pacific are well explained by simple advection of mean temperature gradients by anomalous currents, which is the mechanism used in this study.

There is a full range of thermodynamical processes left out of our model. Vertical and meridional advection are important at some time. Obviously, no meridional advection is associated with Kelvin waves (v=0) but the inclusion of Rossby waves in the dynamics makes this process possible. The effects of Ekman drift in the upwelling rate at the equator are also overlooked in our model, where no vertical advection is considered. The decrease in upwelling at the equator associated with wind anomalies typical of El Niño conditions, is likely to intensify and prolong the SST anomalous conditions. Feedback processes are also not contemplated in this study. Their major influence in the surface winds was discussed at the end of the previous section.

Nonlinearities are completely excluded from our model. They may have important effects in various ways. Nonlinear dynamics may lead to different propagation velocities for the equatorial trapped waves usually considered and intensification of the dynamical fields of these waves at the crests. Cane (1984) suggests that an enhancement of the sea level response occurs as the Kelvin waves slow down and steepen, when they approach the Peruvian coast, because of nonlinear effects much like waves inciding on a sloping beach. The theoretical work of Boyd (1980) suggests that nonlinear effects may even cause Kelvin waves associated with El Niño conditions to break, which would have dramatic effects in the propagation of signals from the western to the eastern Pacific. Concerning the thermodynamical processes, the effects of nonlinearities are better established. Nonlinear advection terms (e.g. $u'T'_x$) left out of the thermodynamic equation (4.44) may play a role at some point during El Niño, as found by Zebiak and Cane (1983).

The ultimate effect of all the missing dynamical and thermodynamical processes mentioned above on the spectral shapes of Φ_ζ and Φ_T, and

consequently on the SL and SST statistics of extremes, may be very complicated. Such a complex model is beyond the scope of this study. However, we do believe that the spectra Φ_ζ and Φ_T which have been obtained from a much simpler model and used in computing our statistical results, are fairly realistic in their general forms, even though extremely simple in structure.

The statistical model used to compute SL and SST extremes is sensitive to some of its uncertainties. The statistical assumption about the pdf governing the SL and SST fields is critical. Statistics of extremes for Gaussian fields are very different from statistics of extremes for fields obeying an arbitrary pdf (see, e.g., Vanmarcke 1985). If SL and SST fields are not Gaussian, the results would be in general different. There is no reason to believe that this is so.

Although with all these shortcomings, the model used is believed to include enough essential features so that the results yielded are significant in interpreting the large scale oceanic SL and SST anomalies associated in some way with El Niño occurrences.

CHAPTER 6

SUMMARY AND CONCLUSIONS

We have attempted to investigate the possibility of stochastic wind forcing being an important mechanism in generating El Niño like conditions in the equatorial ocean. Our analysis has been simplified by a variety of assumptions. We have considered the linear response of a continuously stratified equatorial β-plane ocean to zonal wind stress forcing. Our ocean has a flat bottom and is unbounded laterally. The zonal velocity field yielded by these dynamics was used to advect a mean zonal SST gradient to produce SST anomalies at the equator. Rayleigh friction was used to prevent infinite response at resonance. The solutions were obtained in the form of zonal wavenumber-frequency SL and SST spectra, valid at the equator. The zonal winds were assumed to be stochastic and various forms for the spectral shape of the wind stress forcing were used. Extreme value statistics of our anomalous SL and SST fields were computed from their analytical spectra, using the theoretical statistical tools presented in Chapters 2 and 3. The SL and SST fields were taken to be Gaussian in calculating the mean return period for excursions above the 2σ threshold and the mean time or distance these fields will stay above this level once they cross it. Excursions above the 2σ level were taken to be representative of El Niño conditions in general.

We find from our statistical results that stochastic forcing by the wind may be important in generating El Niño events, even though other effects like feedback between the atmosphere and the ocean may be responsible for the long duration of anomalous conditions in the tropical regions occurring during El Niño years. Randomly forced SST anomalies have significant spatial extent (on the order of 1000 km) and last for periods on

the order of 10 days. The need for better knowledge of the k-ω zonal wind stress spectrum in the tropical regions is of primary importance in corroborating our suggested results. To be specific, more estimates of the k structure of the wind spectrum are necessary to assist in choosing a forcing spectrum in our model. The statistics are sensitive to the ω and k dependence of $\Phi_F(\omega,k)$. In general, any redder form for $\Phi_F(\omega,k)$ than what has been assumed here will tend to give longer time and space scales for extreme excursions of SL and SST fields. Available spectral estimates of SL and SST frequency spectra may be used as a constraint on the possible shapes our model spectra can take, without becoming unrealistic.

The estimates of the mean return period, $1/\nu_b^{\omega,+}$, are extremely dependent on the definition of El Nino conditions, taken here to be anomalies in SL and SST on the order of 2σ. Longer records, especially for SST, may be needed to better determine, for example, what the value of σ really is. It would also be nice if we could be more certain about the pdf underlying the SL and SST anomaly fields. If reliable estimates of the spectra $\Phi_\zeta(\omega,k)$ and $\Phi_T(\omega,k)$ were available, extreme value statistics could be computed directly from them, but there will always be a certain ambiguity on spectral estimates at very low frequencies. Without reliable estimates of the mean return period, $1/\nu_b^{\omega,+}$, it is speculative to try to say how often we do expect stochastically forced El Nino events. Our results may indicate that at least some events may be triggered by random winds, but I think a more quantitative statement on this issue is disallowed by the uncertainty of some of our assumptions and the sensitivity of the value of $1/\nu_b^{\omega,+}$ to them.

The implication of our stochastic assumption on the predictability of El Nino events is clear. There is no way we can forecast with confidence an event until it is actually underway, i.e., the triggering effect is not

deterministic in this study and thus impossible to predict. The results don't rule out the obvious importance of processes which can be better understood from a deterministic point of view. In fact, our model is itself deterministic in a sense. The random element comes from the forcing, but a certain degree of predictability is added by the deterministic ocean dynamics, as expressed in the redder character of the ocean response spectra when compared with the forcing spectra (a white spectra corresponds to no predictability in this interpretation).

Further investigation is needed in order to refine some of our critical assumptions made about the wind forcing and the SL and SST pdf. Only then a better grasp of the importance of the stochastic element in causing ENSO events can be obtained. A more sophisticated ocean model may also be a reasonable thing to try, even though the model SL and SST spectra used here are not unrealistic.

REFERENCES

Barnett, T.P., Prediction of El Niño of 1982-83, see Witte 1983, pp. 169-178, 1983.

Boyd, J.P., The nonlinear equatorial Kelvin wave, J. Phys. Oceanogr. 10, 1-11, 1980.

Busalacchi, A.J. and J.J. O'Brien, The seasonal variability in a model of the tropical Pacific, J. Phys. Oceanogr. 10, 1929-1951, 1980.

Busalacchi, A.J., K. Takeuchi, and J.J. O'Brien, On the interannual wind-driven response of the tropical Pacific Ocean, in Hydrodynamics of the Equatorial Ocean, 155-195, Amsterdam: Elsevier, 1983.

Cane, M.A., Oceanographic events during El Niño, Science 222, 1189-1195, 1983.

Cane, M.A., Modeling sea level during El Niño, J. Phys. Oceanogr. 14, 1864-1874, 1984.

Cane, M.A. and S.E. Zebiak, A theory for El Niño and the Southern Oscillation, (to be published), 1985.

Cramer, H., On the intersections between trajectories of a normal stationary stochastic process and a high level, Arkiv. Mat. 6, 337, 1966.

Cramer, H., and M.R. Leadbetter, Stationarity and Related Stochastic Process, Wiley, New York, 1967.

Eriksen, C.C., M.B. Blumenthal, S.P. Hayes, and P. Ripa, Wind-generated equatorial Kelvin waves observed across the Pacific Ocean, J. Phys. Oceanogr. 13, 1622-1640, 1983.

Feller, W., An Introduction to Probability, Theory, and Its Application, Vol. I, 2nd edition, Wiley, New York 1957.

Frankignoul, C. and K. Hasselman, Stochastic climate models, Part II. Application to sea surface temperature anomalies and thermocline variability, Tellus 29, 289-305, 1977.

Frankignoul, C. and P. Muller, Quasigeostrophic response of an infinite β-plane ocean to stochastic forcing by the atmosphere, J. Phys. Oceanogr. 9, 104-127, 1979.

Gent, P.R., O'Neill, K., and M.A. Cane, A model of the semiannual oscillation in the equatorial Indian ocean, J. Phys. Oceanogr. 13, 2148-2160, 1983.

Gill, A.E., Some simple solutions for heat-induced tropical circulation, Q.J.R. Met. Soc. 106, 447-462, 1980.

Gill, A.E., Atmosphere-Ocean Dynamics, Academic Press, Inc., New York, 1982.

Gill, A.E., An estimation of sea-level and surface-current anomalies during the 1972 El Niño and consequent thermal effects, J. Phys. Oceanogr. 13, 586-606, 1983.

Gill, A.E., and A.J. Clarcke, Wind-induced upwelling, coastal currents and sea-level changes, Deep-Sea Res. 21, 325-345, 1974.

Goldenberg, S.B., and J.J. O'Brien, Time and space variablity of tropical Pacific wind stress, Mon. Wea. Rev. 109, 1190-1207, 1981.

Gradshteyn, I.S., Ryzhik, I.M., Table of Integrals, Series and Products, 4th ed. Academic Press, 1086 pp., 1965.

Gumbel, E.J., Statistics of Extremes, Columbia University Press, New York, 1958.

Halpern, D., Comparison between in situ SST measurements and the NMC SST analysis in the eastern equatorial Pacific before and during the

1982-83 El Niño, in Proceedings of the Eighth Annual Climate Diagnostics Workshop, 17-21 October 1983, Toronto, Ontario, 1984.

Halpern, D., Variability of the surface wind field in the eastern and central equatorial Pacific ocean, (to be published), 1985.

Harrison, D.E., and P.S. Schopf, Kelvin wave-induced anomalous advection and the onset of SST warming in El Nino events, Mon. Wea. Rev. 112, 923-933, 1984.

Horel, J.D., and J.M. Wallace, Planetary scale atmospheric phenomena associated with the Southern Oscillation, Mon. Wea. Rev. 109, 813-829, 1981.

Inoue, M., and J.J. O'Brien, A forecasting model for the onset of a major El Niño, see Witte 1983, 159-167, 1983.

Lighthill, M.J., Dynamic response of the Indian Ocean to the onset of the southwest monsoon, Phil. Trans. Roy. Soc. London, Ser. A, 265, 45-92, 1969.

Longuet-Higgins, M.S., On the statistical distribution of the height of sea waves, J. Mar. Res. 11, 246-266, 1952.

Luther, D.S., Observations of long period waves in the tropical oceans and atmospheres, Ph.D. Thesis, MIT-Woods Hole Oceanographic Institution Joint Program in Oceanography, 1980.

Luther, D.S., Harrison, D.E., and R.A. Knox, Zonal winds in the central equatorial Pacific and El Niño, Science 222, 327-330, 1983.

Luther, D.S., and D.E. Harrison, Observing long-period fluctuations of surface winds in the tropical Pacific: initial results from island data, Mon. Wea. Rev. 112, 285-302, 1984.

Lyon, R.H., On the vibration statistics of a randomly excited hard-spring oscillator II, J. Acoust. Soc. Am. 33, 1395, 1961.

McCreary, J.P., Modeling equatorial ocean circulation, Ann. Rev. Fluid Mech. 17, 359-409, 1985.

Moore, D.W. and S.G.H. Philander, Modelling of the tropical ocean circulation, in The Sea, 6, 319-361, New York: Wiley-Interscience, 1978.

NAG Library Manual (Fortran), Mark 11, Numerical Algorithms Group 1984.

O'Brien, J.J., Busalacchi, A., and J. Kindle, Ocean models of El Nino, in Resource Management and Environmental Uncertainty: Lessons From Coastal Upwelling Fisheries, M.H. Glantz and J.D. Thompson, Eds., Wiley-Interscience 159-212, 1981.

Pedloski, J., Geophysical Fluid Dynamics, Springer-Verlag, Berlin and New York, 1979.

Philander, S.G.H., The response of equatorial oceans to a relaxation of the Trade Winds, J. Phys. Oceanogr. 11, 176-189, 1981.

Rasmusson, E.M., and T.H. Carpenter, Variations in tropical sea surface temperature and surface wind fields associated with the Southern Oscillation/El Nino, Mon. Wea. Rev. 110, 354-384, 1982.

Rasmusson, E.M. and J.M. Wallace, Meteorological aspects of the El Nino/ Southern Oscillation, Science 222, 1195-1202, 1983.

Reynolds, R.W., The sea surface temperaturs during the 1982-83 El Nino event, see Witte 1983, 19-24, 1983.

Rice, S.O., Mathematical analysis of random noise, Bell System Tech. J., 23, p. 282, 1944, p. 26, 1954. Also reprinted in N. Wax, Selected Publications on Noise and Stochastic Processes. Dover, New York, 1954.

Schopf, P.S., and D.E. Harrison, On equatorial waves and El Nino, I: Influence of initial states on wave-induced currents and warming, J. Phys. Oceanogr. 13, 936-948, 1983.

Shepard, F.P., Submarine Geology. 2nd edition, Harper & Row, New York, Evanston and London, 1963.

Vanmarcke, E.H., First passage and other failure criteria in narrow-band random vibration: a discrete state approach, Research Report No. R69-68 MIT Dept. of Civil Eng., Cambridge, Mass., 1969.

Vanmarcke, E.H., On the distribution of the first passage time for normal stationary random processes, J. Appl. Mech., Trans. ASME, 42, 215-220, 1975.

Vanmarcke, E.H., Random Fields: Analysis and Synthesis. MIT Press, Cambridge, Mass. and London, England, 1983.

Vanmarcke, E.H., Extreme value statistics compatible with random field theory, Proceedings of IUTAM Symposium on Probabilistic methods in the mechanics of solids and structures, Springer-Verlag, Berlin 1985.

Witte, J.M., ed., Papers from 1982/83 El Niño/Southern Oscillation Workshop held at AOML/NOAA, Miami, Florida, November 3-4, 1983, Reg. No. 4: Gov. Print. Office, 1983.

Wunsch, C.I., Response of an equatorial ocean to a periodic monsoon, J. Phys. Oceanogr. 7, 497-511, 1977.

Wunsch, C.I. and A.E. Gill. Observations of equatorially trapped waves in Pacific sea level variations, Deep-Sea Res. 23, 371-390, 1976.

Wyrtki, K., El Niño - The dynamic response of the equatorial Pacific ocean to atmospheric forcing, J. Phys. Oceanogr., 5, 572-584, 1975.

Wyrtki, K., Sea level during the 1972 El Niño, J. Phys. Oceanogr. 7, 779-787, 1977.

Wyrtki, K., The response of sea surface topography to the 1976 El Niño, J. Phys. Oceanogr. 9, 1223-1231, 1979.

Wyrtki, K., Sea level during the 1982-83 El Niño, see Witte 1983, 25-32, 1983.

Wyrtki, K., Monthly maps of sea level in the Pacific during the El Niño of 1982 and 1983, in Time Series of Ocean Measurements, IOC Tech. Ser. No. XX, Vol. 2 (in press) 1984b.

Wyrtki, K. and W. Leslie, The mean annual variation of sea level in the Pacific Ocean, Univ. Hawaii, Re. HIG-80-5, 1980.

Wyrtki, K., and G. Meyers, The trade wind field over the Pacific Ocean, J. Appl. Meteor. 15, 698-704, 1976.

Wyrtki, K. and S. Nakahara, Monthly maps of sea level anomalies in the Pacific 1975-1981, Univ. Hawaii, Ref. HIG-84-3, 1984.

Zebiak, S.E., A simple atmospheric model of relevance to El Niño, J. Atmos. Sci. 39, 2017-2027, 1982.

Zebiak, S.E., Tropical atmosphere-ocean interaction and the El Niño/Southern Oscillation phenomenon, Ph.D. Thesis, MIT, 261 pp., 1984.

Zebiak, S.E. and M.A. Cane, Modelling of sea surface temperature during El Niño, see Witte 1983, 223-229, 1983.

APPENDIX A

RELATION BETWEEN SPECTRAL MOMENTS OF A PROCESS AND THE VARIANCES OF THE PROCESSES AND ITS DERIVATIVES

To derive relations between the spectral moments of a process X(t) and the variance of the process itself and its derivatives X'(t), X"(t), $X^n(t)$, we may use the concept of a transfer function $H(\omega)$. This function $H(\omega)$, defined in the frequency domain, is associated with the response of a linear system to a unit impulse input function.

If we hit a linear system with a Dirac delta function at t', then the response function h(t-t') is called the unit impulse response function. Its Fourier transform is called the transfer function $H(\omega)$ and completely characterizes the system.

A relation between input and output can be defined in terms of $h(\tau_\ell)$ or $H(\omega)$. In the time domain, a well known result is that the output O(t) is given by the convolution of the impulse response function with the input I(t), which in mathematical terms can be expressed as follows

$$O(t) = h(t)*I(t) \tag{A.1}$$

where the symbol * stands for the convolution operation. The convolution theorem clearly gives then

$$\tilde{O}(\omega) = \tilde{H}(\omega)\tilde{I}(\omega) \tag{A.2}$$

where ~ stands for the Fourier transform operation.

Multiplication by the complex conjugate gives the input-output relation in the frequency domain

$$\Phi_O(\omega) = |H(\omega)|^2\Phi_I(\omega) \tag{A.3}$$

Here, $\Phi(\omega)$ is the power density function and subscripts O, I stand for output, input respectively.

Now consider a linear system which differentiates the input signal, i.e.,

$$O(t) = \frac{dI(t)}{dt} \tag{A.4}$$

From (A.2) the transfer function is simply

$$\tilde{H}(\omega) = i\omega \tag{A.5}$$

and using, (A.3) we obtain

$$\Phi_O(\omega) = \omega^2 \Phi_I(\omega) \tag{A.6}$$

We now define the spectral moments λ_j as

$$\lambda_j = \int_0^\infty \omega^j \Phi(\omega) d\omega \tag{A.7}$$

Taking j=2 in this definition and using (A.6), we have

$$\lambda_2 = \int_0^\infty \omega^2 \Phi_O(\omega) d\omega = \sigma_O^2 \tag{A.8}$$

We know that the autocorrelation function $B(\tau_\ell)$ is just equal to the Fourier transform of the power density. Consequently, the variance σ^2 which is just the value of the autocorrelation function at zero lag, is given in general by

$$\sigma^2 = B(0) = \int_0^\infty \Phi(\omega) d\omega \tag{A.9}$$

Combining (A.8) and (A.9) finally yields

$$\lambda_2 = \int_0^\infty \Phi_O(\omega) d\omega = \sigma_O^2 \tag{A.10}$$

The second spectral moment of process I(t) is just the variance of the derivative process O(t).

In terms of the autocorrelation function

$$\lambda_2 = \int_0^\infty \omega^2 \Phi(\omega) d\omega = \left| \frac{d^2 B}{d\tau_\ell^2} \right| (\tau_\ell = 0) \tag{A.11}$$

The second spectral moment is equal to the absolute value of the second derivative of the autocorrelation function evaluated at zero.

The relations derived above can easily be extended to establish the equivalence between higher spectral moments of a process X(t) and the variances of the derivative processes $X^n(t)$. A relation of particular use in this study is

$$\lambda_4 = \int_0^\infty \Phi_X''(\omega)\, d\omega = \sigma_{X''}^2 \qquad (A.12)$$

In words, the variance of process X"(t) is given by the fourth spectral moment of $\Phi(\omega)$.

Appendix B List of Figures

Appendix C List of Tables

Appendix D. List of Symbols

a_b	constant determining rate of decay of $L_b(0)$ with time
A_b	area of excursion above b
$A_{b,R}$	area of excursion above b by envelope R
B	autocorrelation function
b	threshold level
b_n	projection factor
C	white noise level of forcing spectrum
c_n	separation constant
D	ocean depth
f_R	pdf of envelope R
f(x)	probability density function
$F^c(x)$	complementary cumulative distribution function
$F_U(u)$	standard normal cumulative distribution function
G	tangential stress
g	gravitational acceleration
H	dynamic factor
h_{mix}	depth of mixed layer
k	zonal wavenumber
k_o	high wavenumber spectral cutoff
k_L	low wavenumber spectral cutoff
$L_b(t_o)$	probability that first crossing of b occurs after time t_o (reliability function)
$\langle N_b \rangle$	expected value of clump size (valid for both narrow and wide band processes)
N	buoyancy frequency
P	perturbation pressure (function of x and t only)
p	perturbation pressure

R	envelope of some random process
r_b	mean clump size (narrow band processes)
T'	surface temperature anomaly
$\overline{T}$	mean surface temperature
T_b	time spent above b
T_b'	time spent below b
$T_{b,R}$	time spent above b by envelope R
$T_{b,T}$	time spent above b by X_T
t	time coordinate
u	perturbation zonal velocity
w	perturbation vertical velocity
x	space (zonal) coordinate
X_b	length of excursion above b
X_T	local average process
y	latitudinal distance from equator
Z	Bernoulli variable
α	constant (defined in (4.29))
βy	Coriolis parameter
$\vec{\Delta}$	matrix of 2nd order bandwidth coefficients
δ	2nd order measure of bandwidth of the spectral density function
δ^k	2nd-order bandwidth measure (space process)
δ^ω	2nd-order bandwidth measure (time process)
ε	friction coefficient
Φ	one sided power density function
Φ_F	forcing spectrum
Φ_p	sea pressure spectrum
Φ_T	SST spectrum

Φ_ζ	sea level spectrum
ϕ	random phase angle
$\gamma(t)$	variance function
Γ	4th order measure of bandwidth of the spectral density function
$\vec{\Lambda}$	2x2 matrix of second order spectral moments
λ_{jn}	spectral moment of j-th order with respect to ω and n-th order with respect to k
λ_j^k	spectral moment of zeroth order with respect to ω and j-th order with respect to k
λ_n	n-th spectral moment
λ_j^ω	spectral moment of zeroth order with respect to k and j-th order with respect to ω
μ_b	mean rate of occurrence of regions of excursion above b
$\mu_{b,R}$	mean number of crossings per unit area for R
$1/\nu_b^+$	return time
ν_b	mean value for the rate of crossing of threshold b
ν_b^+	mean value for the rate of upcrossings of threshold b
ν_b^-	mean value for the rate of downcrossings of threshold b
$\nu_{b,m}$	mean rate of occurrence of local maxima above threshold b
ν_m	mean rate of occurrence of local maxima
$\nu_{b,R}$	mean rate of occurrence of crossings of b by envelope R
$\nu_{b,R}^+$	mean rate of upcrossings of b by envelope R
$\nu_{b,T}^+$	mean rate of upcrossings of b by process X_T
$\nu_b^{k,+}$	mean rate of upcrossings in space above b

$\nu_b^{\omega,+}$	mean rate of upcrossings in time above b
ω	angular frequency
ω_m	mid-band frequency
ω_o	high frequency spectral spectral cutoff
ω_T	transition frequency
Ω_j	j-th characteristic frequency
Ψ	two-sided spectral density function
ρ	perturbation density
$\overline{\rho}$	basic stratification
ρ_T	total density
σ	standard deviation
σ_r	standard deviation of envelope process
$\sigma_{r'}$	standard deviation of derivative of envelope process
σ_{r_x}	standard deviation of space derivative of envelope R
σ_{r_t}	standard deviation of time derivative of envelope R
σ_t	standard deviation of time derivative of Y(x,t)
σ_T	standard deviation of process X_T
$\sigma_{x'}$	standard deviation of derivative process X'(t)
$\sigma_{x''}$	standard deviation of 2nd derivative process X"(t)
σ_x	standard deviation of space derivative of Y(x,t)
Θ	scale of fluctuation
τ	zonal wind stress
τ_ℓ	time lag
$\vec{\tau}_\ell$	lag vector
ζ	sea level
$\hat{}$	function of z only
$\sim$	Fourier transform